MASTERARBEIT | MASTER'S THESIS

Titel | Title

Towards Toxicity Risk Assessment of environmental samples applying biological Barriers in vitro models

verfasst von | submitted by

Sylvia Bekhit BSc

angestrebter akademischer Grad | in partial fulfilment of the requirements for the degree of

Magistra pharmaciae (Mag. pharm.)

Wien | Vienna, 2026

Studienkennzahl lt. Studienblatt | Degree programme code as it appears on the student record sheet:	UA 066 605
Studienrichtung lt. Studienblatt | Degree programme as it appears on the student record sheet:	Masterstudium Pharmazie
Betreut von | Supervisor:	Dipl.-Ing. Dr. Winfried Neuhaus Privatdoz.

Eidesstattliche Erklärung

Ich erkläre eidesstattlich, dass ich die Arbeit selbständig angefertigt, keine anderen als die angegebenen Hilfsmittel benutzt und alle aus ungedruckten Quellen, gedruckter Literatur oder aus dem Internet im Wortlaut oder im wesentlichen Inhalt übernommenen Formulierungen und Konzepte gemäß den Richtlinien wissenschaftlicher Arbeiten zitiert, durch Fußnoten gekennzeichnet bzw. mit genauer Quellenangabe kenntlich gemacht habe.

Wien, am _____

Unterschrift der / des Studierenden

Abstract

There is an increasing concern that smaller plastic particles could spread more easily and pose greater health and environmental risks than larger particles. It has been reported, that plastic particles can enter the human body through several primary routes: ingestion**,** inhalation, and dermal absorption (Wu *et al.,* 2022), making them a possible threat to human's health. A recent study has detected 6ppd-Quinone, a salmon-toxic compound derived from car tires, in human urine, serum, and cerebrospinal fluid, indicating the need to investigate its potential human toxicity. (Yi *et al.,* 2025)

In this context, the project examined how nanopolystyrene particles of varying sizes and surface chemistries, as well as 6PPD-quinone, affect the viability of key cells of the neurovascular unit, in particular endothelial cells and microglia, and how "real life" indoor dust extracts influence both neurovascular and lung cells. The project used brain endothelial (hCMEC/D3) and lung A549 cells in a Transwell model to examine the effect of selected undefined airborne compound and particle mixtures. On Barrier integrity and cell viability following an extenstive extract screen of over 120 samples.

The findings demonstrated that high doses (greater than 300 μg/L or 100 μg/L) of the Nanoplastics resulted in reduced cell viability. The most toxic particles, were the unstained PS carboxylated 50 nm and unstained PS aminated 50 nm, proving that both size and zeta potential influence the cell toxicity of nanopolystyrene, with smaller particles having stronger effects. 6ppd-quinone also exhibited toxic effects, especially in brain endothelial cells, with cell viability dropping below 50% at the highest tested concentration. Lastly, exposure to selected undefined airborne dust extracts in the Transwell model increased the metabolic activity of brain endothelial cells (hCMEC/D3) in the basolateral compartment, with some samples causing activity levels up to 168% of the control. This suggested that the extracts, triggered elevated mitochondrial or metabolic activity, likely due to cellular stress, rather than actual cell proliferation. However, transepithelial electrical resistance (TER) measurements indicated no significant impact on lung barrier integrity after 48 hours of exposure.

Zusammenfassung

Kleinere Plastikpartikel stehen zunehmend im Fokus der Forschung, da sie sich leichter in der Umwelt verbreiten und potenziell größere Gesundheitsrisiken darstellen als größere Partikel. Mikro- und Nanoplastik kann über Inhalation, Nahrungs- und Wasseraufnahme und dermale Aufnahme in den menschlichen Körper gelangen (Wu *et al.,* 2022). Zudem wurde kürzlich 6PPD-Chinon, ein aus Autoreifen stammendes toxisches Abbauprodukt, in menschlichen Körperflüssigkeiten nachgewiesen, was die Untersuchung möglicher gesundheitlicher Auswirkungen erforderlich macht (Yi *et al.,* 2025).

In dieser Arbeit wurde untersucht, wie Nanopolystyrolpartikel unterschiedlicher Größe und Oberflächenchemie sowie 6PPD-Chinon die Zellviabilität von Zellen der neurovaskulären Einheit, insbesondere Endothelzellen und Mikroglia, beeinflussen. Darüber hinaus wurden die Effekte "realitätsnaher" Luftfilter-Extrakte auf neurovaskuläre und pulmonale Zellen analysiert. Hierzu wurden zerebrale mikrovaskuläre Edothelzellen (hCMEC/D3) und Lungenepithelzellen (A549) in einem Transwell-Modell eingesetzt, um Zellviabilität und Barriereintegrität nach Exposition gegenüber definierten Nanopartikeln und über 120 undefinierten Luftfilter-Extraktproben zu untersuchen.

Die Ergebnisse zeigten, dass hohe Konzentrationen von Nanoplastikpartikeln zu einer deutlichen Reduktion der Zellviabilität führten, wobei insbesondere 50-nm-Polystyrolpartikel mit carboxylierten oder aminierten Oberflächen die stärksten toxischen Effekte aufwiesen. Auch 6PPD-Chinon zeigte ausgeprägte zytotoxische Effekte, insbesondere in zerebralen mikrovaskulären Endothelzellen. Die Exposition gegenüber ausgewählten Luftfilter-Extraktproben führte zu einer erhöhten metabolischen Aktivität der zerebralen mikrovaskulären Endothelzellen, was auf eine stressbedingte Reaktion hindeuten könnte, während keine signifikanten Veränderungen der Lungenbarriereintegrität festgestellt wurden.

Acknowledgments

I would like to express my sincere gratitude to all those who made this work possible and contributed to its development and completion.

First and foremost, I would like to express my sincere gratitude to Prof. Dr. Dipl.-Ing. Winfried Neuhaus for his invaluable expertise and continuous support throughout this project. His guidance and clear vision shaped every stage of this thesis, from research to writing. My appreciation also extends to the AIT, Austrian Institute of Technology GmbH for providing an excellent research environment and outstanding facilities, that made the realization of this thesis possible in the first place. I would also like to extend my gratitude to Dr. Andreas Brachner, scientist at AIT, for his scientific support and practical involvement during multiple phases of my study.

Furthermore, my sincere thanks go to Adrian Klepe, a PhD student at AIT. His unwavering support in shaping my experiments, overcoming challenges, and providing thoughtful guidance, combined with his expertise and kind spirit, was essential to the successful progress of my research.

From the bottom of my heart, I thank my family. I am deeply grateful for their encouragement, and loving support throughout my life, especially for believing in me as I undertook the demanding journey of my pharmacy studies and my research at the AIT, two of the most challenging yet profoundly rewarding experiences of my life. Their faith in me gave me the strength to persevere and succeed in both.

Table of content

1 Introduction 1

1.1 The Blood-brain barrier 1
1.1.1 Blood-brain barrier *in vitro* models 3
1.2 The Lung 5
1.2.1 Lung *in vitro* models 7
1.3 Passage of fine particles from the lung into the brain 10
1.4 Plastic 11
1.4.1 Polystyrene 12
1.5 Routes of Human Exposure to Plastics 13
1.6 Health risks and potential toxicity of (Nano)plastic 14
1.7 6ppd-quinone 15

2. Aim of the thesis 18

3 Materials and Methods 19

3.1 Materials 19
3.2 Cell culture 23
3.2.1 Cell lines 23
3.2.2 Cell maintenance and seeding 24
3.2.3 Solutions 26
3.3 Preparation of nanoparticles 28
3.3.1 Staining of particles with AttoDye 29
3.4 Cell cultivation in 96-well plates/ Experimental setups 30
3.4.1 Experimental setup of hCMEC/D3 and nanoplastic 30
3.4.2 Experimental setup of HMC3 and NP 32
3.4.3 Experimental setup of hCMEC/D3 and 6ppd-Q 34
3.4.4 Experimental setup of HMC3 and 6ppd-Q 35
3.5 Exposure of filtered indoor particles on human lung cells A549 35
3.5.1 Sampling process in Barcelona 36
3.5.2 Extraction process 38
3.5.3 Screening process with A549 cells 39
3.5.4 Sampling Overview 40
3.5.5 Establishment of culture conditions for A549/D3 Transwell® model 41
3.5.6 Experimental procedure 42

4 Particle characterization 44

5 Assays 47

5.1 MTT Assay 47

6 Statistical analysis 49

6.1 MTT Assay for cell viability 49
6.2 TER 49

7 Results 50

7.1 NTA Particle characterization and fluorescence measurement of Nanoplastics . 50
7.2 Effects of potential environmental toxins on cell viability 52
7.2.1 Effects of 6ppd-Q on cell viability..... 52
7.2.2 6ppd-Q and hCMEC/D3 cells..... 53
7.2.3 6ppd-Q and Microglial (HMC3) cells..... 54
7.3 Effects of stained nanoplastic particles on cell viability of hCMEC/D3 55
7.4 Effects of unstained nanoplastics on cell viability of HMC3..... 57
7.5 Effects of Air filter dust extracts on lung cell proliferation 63
7.6 NTA data correlation to cell viability of the extract screening 66
7.7 Optimization of the A549/D3 co-culture Transwell® model..... 70
7.8 TEER Results of A549/D3 Transwell® model..... 74
8 Discussion 77
8.1 Effects on cell viability..... 77
8.2 Pilot experiment: A549 screening Monoculture and A549/hCMEC/D3 co-culture Transwell® model 79
8.2.1 Model limitations and future improvements 81
9 Conclusion.....83
Bibliography..... 85
List of Figures.....100
List of Tables 102
Abbreviations list.....103

1 Introduction

1.1 The Blood-brain barrier

The blood-brain barrier (BBB) is a semipermeable and extremely selective barrier, that separates blood from the brain's extracellular fluid (Alahmari *et al.,* 2021) and thus preventing extravasation of blood products into the brain to protect neural tissue and preserve an internal homeostatic environment (McConnell & Mishra, 2022).

It is primarily formed by a layer of specialized endothelial cells lining the brain's capillaries, which are tightly sealed together through complex junctional structures known as tight junctions (Appelt-Menzel *et al.,* 2017).

Surrounding and supporting the BBB is the neurovascular unit (NVU), an intricate network of various cell types, including pericytes, astrocytes, microglia, and neurons, that collectively interact to regulate neuroimmune responses, vascular permeability, cerebral blood flow (CBF), and maintain a homeostatic CNS environment (McConnell & Mishra, 2022).

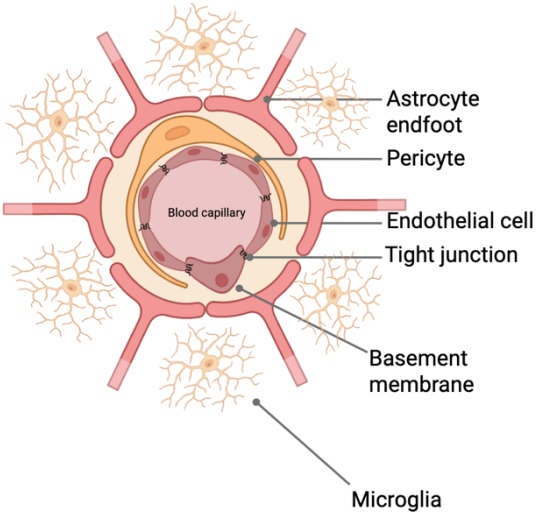

Figure 1: Schematic representation of BBB's cellular structures. Figure made using Biorender, 2026.

BBB formation starts during embryonic development as endothelial cells enter the central nervous system (CNS) and initiate vessel growth. Their tight junctions are formed by a complex of transmembrane proteins, including occludin and claudins, as well as cytoplasmic adaptors such as zonula occludens protein 1 (ZO-1), establishing a paracellular barrier against molecular and ionic transport. They also recruit pericytes, which wrap around the vessels, supporting their maturation, stabilizing the vascular

structure, and contributing to the development of a functional and selective barrier (Chen *et al.*, 2017).

Microglia, are a kind of neuroglia, distributed all across the brain and spinal cord. They account for roughly 5-20 percent of the overall glial cell population (Alahmari *et al.,* 2021). These microglia cells are derived from the yolk sac early in development, (McConnell and Mishra, 2022) and they have two main functional roles: immune defense and CNS maintenance (Ginhoux *et al.,* 2013). In adults, microglia serve as the brain's resident immune cells, constantly monitoring their environment and responding to injury or changes by shifting between pro- and anti-inflammatory states. When inflammation occurs, their role extends beyond defence, they help to limit damage to the CNS and promote healing and structural restoration (Ginhoux *et al.,* 2013). In this activated state, they to help clear debris, communicate with peripheral immune cells, and regulate astrocyte activity (McConnell and Mishra, 2022). On the other hand, research shows that microglial cells help to regulate how neurons grow, develop, and connect with each other, thus influencing the blood-brain barrier (BBB), either supporting or disrupting it depending on injury context (McConnell and Mishra, 2022).

Astrocytes, which closely surround brain capillaries, play a key role in forming the basement membrane and maintaining homeostasis (Fernando *et al.,* 2023). They link neurons to vessels and help coordinate microvascular responses through junctional signaling (Sato *et al.,* 2022). Additionally, astrocytes shape immune activity in the brain by releasing both pro- and anti-inflammatory cytokines and chemokines, affecting microglia and macrophage behavior (Sato *et al.,* 2022).

Pericytes exhibit features of both macrophages and smooth muscle cells (Kim et al., 2006). They are essential for blood vessel development, blood-brain barrier maintenance, restricting immune cell infiltration into the CNS, and regulating cerebral blood flow (Armulik *et al.,* 2010). Additionally, pericytes contribute to clearing toxic metabolites through phagocytosis and possess multipotent stem cell capabilities (Nakagomi *et al.,* 2015). In cell culture studies, microglia, astrocytes, and neurons have been shown to engage in complex signaling with one another, a process that seems to intensify in the presence of neurological disorders or other pathological conditions (Abbott *et al.,* 2006).

1.1.1 Blood-brain barrier *in vitro* models

In vitro models of the blood-brain barrier (BBB) are essential for examining its function and underlying mechanisms. In addition to that, they replace animal models and study the BBB in the context of neurotoxicology and neurological diseases. (Madorran *et al.*,2020).

Among the different models, the immortalized human brain cerebral microvascular endothelial cell line (hCMEC/D3) is the mostly used cell line and has the potential to be used for a standardized *in vitro* BBB model, offering advantages such as reproducibility, homology and low cost (Qi *et al.*, 2023). A major advantage of the hCMEC/D3 cell line is its stable, easily cultured human microvascular cerebral endothelial cell (CEC) population that perserve a normal BBB phenotype. This model is well suited for drug uptake, active transport studies, and investigating brain endothelium responses to pathogens and inflammation (Weksler *et al.,* 2013).

The human microglial cell line, HMC3, has also become a widely used model to explore how different cells and molecules interact within the neurovascular unit, especially regarding inflammation (Lepiarz and Olajide, 2019). HMC3 cells are important for studying immune functions in the brain. They release cytokines and can engulf particles, mimicking the activity of microglia *in vivo.* This makes them useful for exploring immune aspects in the CNS (Dello Russo *et al.,* 2018).

To evaluate how substances influence the integrity of the blood-brain barrier, hCMEC/D3 cells can be employed in transwell systems where barrier permeability is monitored. One key method involves measuring the transendothelial electrical resistance (TEER), which provides insight how ion permeability might be restricted by tight junctions between endothelial cells. Variations in TEER values can describe the extent to which a compound compromises the structural integrity of the BBB (Helms *et al.,* 2016).

The hCMEC/D3 and HMC3 cells together are reliable cell lines to explore how different substances affect the brain's barrier. By examining structural damage, immune reactions, and changes in gene regulation, researchers can better understand how these compounds may disrupt the BBB.

Table 1. Most common *in vitro* BBB models

Cell line	Immortality origin	References	First publication
hCMEC/D3	Transduction with hTERT and SV40 large T antigen	Poller *et al.,* (2008)	Weksler *et al.,* 2005
hBMEC hBMEC-60	Transduction with SV40 large T antigen (Stins *et al.,*1997) Transduction with the human papillomavirus (HPV)16 E6/E7 genes (Rood *et al.,* 2000)	Bowman *et al.,* 1983	Stins *et al.,*1997 Rood *et al.,* 2000
TY10	Conditionally immortalized (proliferation controlled in a temperature sensitive mechanism)	Maeda *et al.,* 2013	Sano *et al.,* 2010
BB19	Transformation with HPV E6 and E7 genes and Transduction with SV40 large T antigen	Kusch-Poddar *et al.,* 2005	Prudhomme *et al.,* 1996
SV-HCEC	Transfection with SV40 large T antigen	Bähr et al., 2003	Muruganandam *et al.,*1997
HMC3 (ATCC CRL-3304)	Transfection with SV40 large T antigen (CHME3 clone)	Dello Russo *et al.,* 2018	Janabi et al.,1995
HMO6	Transduction with v-myc Retrovirus	Narantuya *et al.,* 2010	Nagai et al., 2001
C20	Transduction with hTERT + SV40	Alvarez-Carbonell *et al.,* 2019	Garcia-Mesa *et al.,* 2017

1.2 The Lung

Micro- and Nanoplastics have been detected in the air, identifying inhalation as a relevant human exposure pathway to plastic particles (Wright *et al.,* 2020). A recent study has revealed that inhalation of Polystyrene Nanoplastics may cause inflammation in lung tissue because of oxidative stress. (Wu *et al.,* 2023).
Another study revealed that inhaling these particles, may induce lung fibrosis damage and chronic obstructive pulmonary disease (COPD)-like lesions in rodents (Yang *et al.,* 2024) A more recent study indicates that Polystyrene Nanoplastics induce oxidative stress triggering the expression of inflammatory cytokines, such as IL-6, IL-1β and TNFA in mice, thus leading to lung injury (Wang *et al.,* 2025).

The primary role of the lung is to facilitate the exchange of gases, supplying the body with oxygen needed for aerobic metabolism and eliminating carbon dioxide, the waste product generated during this process (Miller *et al.,* 2017). To enable this, the lung has the largest epithelial surface, forming a complex network of tube-like epithelial branches known as the conducting airway. This structure, composed of surfactant, epithelial and endothelial cells, and a shared basal lamina, is optimized for gas exchange but leaves lung tissue vulnerable to airborne toxins, particles, and microbes (Miller *et al.,* 2017).

The lung is unique in possessing two circulatory systems: the pulmonary circulation, which facilitates gas exchange and accommodates the entire cardiac output at low pressure, and the bronchial circulation, which supplies oxygenated blood to the airways and vessel walls (Suresh and Shimoda, 2016). The pulmonary endothelium forms a continuous barrier, actively maintaining fluid homeostasis (Suresh and Shimoda, 2016). However, inflammation or infection can disrupt this barrier, increasing permeability and leading to oedema (Suresh and Shimoda, 2016).

The lung employs multiple defense mechanisms to protect itself against airborne particles and pathogens (LeMessurier *et al.,* 2020). The epithelium forms a tightly sealed physical barrier through intercellular junctions, while the mucosal epithelium traps inhaled microorganisms within a secreted mucus layer. Pathogens held back in the mucus are removed by the mucociliary escalator via coordinated ciliary beating. In

parallel, epithelial cells express pattern-recognition receptors that enable early detection of invading agents and initiation of immune responses (Vareille *et al.,* 2011). Surfactant reduces surface tension thus maintaining alveolar stability, while resident immune cells, including alveolar macrophages and dendritic cells eliminate pathogens (LeMessurier *et al.,* 2020). Additional immune protection is provided by phagocytic cells that engulf and degrade invading pathogens (Martin & Frevert, 2005).

The alveolar epithelium consists primarily of two specialized cell types: type I and type II alveolar epithelial cells. Type 1 cells exhibit a complex morphology characterized by extensive cytoplasmic leaflets that line most of the alveolar surface, forming the extensive interface required for efficient gas exchange (Weibel, 2015). Type 2 cells serve as progenitor cells for type 1 and are responsible for the secretion of pulmonary surfactant. (Weibel, 2015). Pulmonary surfactant is composed predominantly of phospholipids, including 1,2-dipalmitoyl-sn-glycero-3-phosphocholine (DPPC) and phosphatidylglycerol, alongside neutral lipids such as cholesterol and surfactant proteins A–D (Nkadi *et al.,* 2009).

Nanoparticles, also known as ultrafine particles, typically measure between 1 and 1000 nanometres in diameter. While they are a component of ambient air pollution, they are also intentionally engineered for a wide range of applications, including medical applications (Malaviya *et al.,* 2020). As an example, DNA-modified nanoparticles have been synthesized for applications such as nanobarcoding and DNA sensing (Samanta *et al.,* 2016).

Several independent studies have demonstrated that particle size and surface area are critical factors influencing the extent of pulmonary damage. Fine (≤2.5 μm) and ultrafine particles (≤0.1 μm) (Kumar *et al.,* 2021), due to their ability to penetrate deep into the respiratory tract and lodge within the alveoli, where up to 50% may remain in the lung parenchyma, are particularly potent in triggering inflammatory and oxidative responses (Valavanidis *et al.,* 2008). Depending on their chemical makeup and physical properties, they have the potential to induce acute inflammation, which may eventually lead to pulmonary fibrosis. (Malaviya *et al.,* 2020)

1.2.1 Lung *in vitro* models

Among the different lung derived cell types used for two-dimensional (2D) cell cultures, are A549, Calu-3, BEAS2B or hAELVI cells to investigate basic respiratory functions, drug transport, and cytotoxicity. Calu-3 cells originate from the submucosal gland of a human cancer patient and exhibit high levels of goblet cell markers. When grown at the air-liquid interface (ALI), they differentiate into various cell types, making them valuable for investigating mucus production and mucociliary dysfunction. In contrast, A549 cells, which are frequently used as a model for the alveolar epithelial barrier, come from type 2 pneumocytes. These cells primarily have a secretory role and play a minimal part in forming the epithelial barrier (Forbes & Ehrhardt, 2005). Therefore, alternative alveolar cell models that accurately represent the barrier-forming type 1 pneumocytes are more appropriate for experiments involving permeability, diffusion, or barrier disruption. Currently, the only cell line available for modeling alveolar type 1 pneumocytes is the hAELVi cell line (Kuehn *et al.,* 2016). While these 2D *in vitro* models are cost-effective and reproducible, they lack the complex architecture and cellular diversity of native lung tissue. (Kühl *et al.,* 2023).

Air-liquid interface (ALI) airway culture models can replicate the characterisric features of the respiratory tract *in vitro* (Chiok *et al.,* 2024). In ALI systems, primary airway epithelial cells are cultured on permeable supports, exposing the apical surface to air and the basal surface to nutrient media. This setup promotes differentiation into an epithelium with ciliated and mucus-producing cells, making ALI cultures valuable for studying mucociliary clearance, barrier function, and respiratory infections (Miller *et al.,* 2017). According to Kühl et al., a key limitation of ALI cultures is their limited lifespan, once fully differentiated, the cells gradually lose viability, making them less suitable for prolonged or high-throughput studies (*Kühl et al.*, 2023).

Advancements in stem cell technology have led to the creation of three-dimensional (3D) lung organoids. These structures, derived from human pluripotent stem cells, self-organize into miniaturized versions of lung tissue, recapitulating key aspects of lung development and disease. Lung organoids have been instrumental in modeling conditions such as cystic fibrosis, pulmonary fibrosis, and viral infections, providing a platform for drug testing and personalized medicine (Kühl *et al.*, 2023).

In contrast to cellular cell models, organoids represent fully differentiated 3D tissue structures. Lung organoids are derived from human induced pluripotent stem cells (iPSCs), *ex vivo* adult stem cells (ASCs), or embryonic stem cells, and can be cultured at the air–liquid interface (ALI) or within hydrogels (Choi *et al.,* 2020). Three-dimensional organoid systems cultured in hydrogels were initially established to explore lung development (Franzdóttir *et al.,* 2010). However, more recently, these models have been extended to a broader range of applications, including the investigation of respiratory disorders, viral infections, and the assessment of drug-induced toxicity (Barron *et al.,* 2021).

Precision-cut lung slices (PCLSs) offer a three-dimensional experimental model that closely reflects the native lung environment. Conventional cell cultures and organoid systems depend on long differentiation processes, whereas PCLSs retain intact tissue architecture and distinct macrophage subsets. However, the availability of human PCLSs is restricted, and their viability in culture is limited to approximately one week, in contrast to air–liquid interface (ALI) cultures, which can be maintained for 21–28 days. Consequently, PCLSs are not well suited for long-term exposure studies *(Barron et al.,* 2021).

Table 2. Most common *in vitro* respiratory models

Model type	***In vitro* example of host pathogen interaction**	**Cell types used**	**Reference**
Submerged cell line culture	Respiratory syncytial virus	Bronchial cell line (BEAS- 2B); Primary human and bronchial epithelial cells	Becker *et al.,* 1992
ALI cultures	SARS- CoV	Primary human alveolar type 2 cells (ALI monoculture) Calu-3 cell line (ALI co-culture)	Qian *et al.,* 2013
Organoids	Parainfluenza	iPSCs, ASCs, human embryonic stem cells	Porotto *et al.,* 2019
PCLS	Influenza	Healthy lung slices from cancer patients undergoing lung resection	Wu *et al.,* 2010

1.3 Passage of fine particles from the lung into the brain

Air pollution continues to pose a significant global threat to public health. Over the past several decades, extensive epidemiological and experimental research has identified the lungs and cardiovascular system as the primary organs affected by exposure to polluted air (Qi *et al.,* 2022).

Exogenous fine particles and nanoparticles are capable of entering the human brain through the lung–blood–brain pathway. (Qi *et al.,* 2022) Once inhaled, cellular toxicity is size dependant, meaning that nanoplastics have a greater ability to penetrate biological systems than microplastics (Liu *et al.,* 2021).

Upon inhalation, fine and ultrafine particles deposit on the surfactant film at the air–liquid interface of the alveoli. Surface forces can displace these particles, allowing them to interact with primary target cells. Ultrafine particles, due to their small size of ≤ 100 nanometers in diameter, can penetrate through lung tissue compartments, reaching capillaries and entering the bloodstream. This systemic circulation enables their distribution to various organs, including the liver, spleen, kidneys, heart, and brain (Peters *et al.,* 2016).

This translocation can occur even in the absence of apparent damage to the BBB however, exposure to such particles frequently leads to compromised structural integrity and deformation of the blood vessels of the BBB (Qi *et al.*, 2022).

Recent findings establish a strong connection between air pollution or occupational exposure and the accumulation of particles in brain tissue, a phenomenon that may play a role in the development of neurological disorders. Notably, in this study the brain retains these particles for a longer duration than other organs, suggesting the potential for sustained toxic effects within the CNS (Qi *et al.,* 2022).

1.4 Plastic

Plastic has become an integral part of modern life, yet its widespread use has raised significant concerns about its impact on human health and the environment.

In 2017, more than eight million tons of plastics entered the oceans, this amount is >33 times as much as that of the total plastics accumulated in the oceans by 2015. (Li *et al.,* 2023). There are many different types of plastics including polypropylene (PP), polyethylene (PE), polyethylene terephthalate (PET), polystyrene (PS), polyurethane (PU), polyvinyl chloride (PVC), and polycarbonate (PC) (Geyer *et al*. 2017). Polyethylene (PE) is the most widely produced plastic in the world. It accounts for approximately 36% of all non-fiber plastic ever made (Geyer *et al*. 2017).

Most plastics are produced from non-renewable petroleum sources. Their incineration releases toxic substances such as CO_2, dioxins, and mercury, posing environmental and health risks (Verma *et al.,* 2016). Recycling plastic remains economically unattractive, as virgin plastic is cheaper to produce, its cost influenced by natural gas prices and global politics. Current recycling methods mainly target uniform, high value plastic waste (Merrington *et al.,* 2017). Despite these facts, plastic quickly gained widespread popularity, not only because of its low production cost, but also due to its lightweight nature, versatility, and excellent performance (Geyer *et al.,* 2017). Its remarkable durability and resistance to biodegradation have even led scientists to name the current geological epoch, the Plasticene Age (Reed, 2015).

Because of their durability, these plastic wastes undergo continuous fragmentation through “aging” processes such as exposure to ultraviolet radiation, temperature fluctuations, mechanical wear, and biological activity (Dawson *et al.,* 2018).

When broken down into particles smaller than 5 mm, they were classified as microplastics (MPs), with particles under 1 µm further categorized as nanoplastics (NPs). MPs are divided into two types based on their origin: primary MPs, which are deliberately produced for use in cosmetic products, and secondary MPs, which result from the degradation and weathering of larger plastic items like textiles and tires (Wright and Kelly, 2017).

Plastic particles have been detected in aquatic organisms, including oceans, sediments, rivers and soil (Wright *et al.,* 2013), and surprisingly food items such as salt, sugar, honey, beer and plastic bottles also feature these particles (Banerjee *et al.,* 2021; Brachner *et al.,* 2020; Prata et al., 2020, Wright & Kelly, 2017).

Microplastics are detected from the south to Antarctica (Aves et al., 2022), north to the Arctic, (Bergmann *et al.,* 2022), even up to the peak of Mount Everest (Napper *et al.,* 2020) Plastic is the largest part of marine garbage (Rellan *et al.,* 2023).

Plastic particles the environment can enter the human body through different ways, such as contaminated air or ingestion via water or food, as mentioned before. These particles can also interact with the skin, via contact with contaminated dust, clothing, or other contaminated products (Prata *et al.,* 2020). Additionally, plastic particles may enter the human body through parenteral routes (Banerjee and Shelver, 2021; Weis *et al.,* 2015). Plastic particles were also reported to be seen in the human blood (Leslie *et al.,* 2022).

The widespread use of these polymers leads to an omnipresent source of contamination, through contact with or intake of food, water, or air. All of this illustrates the diverse forms and sources of micro- and nanoplastics in the environment and, consequently, the potential human exposure to plastic particles in everyday life.

1.4.1 Polystyrene

The focus in this study was on polystyrene nanoplastics. Polystyrene (PS) is a widely used plastic polymer found in packaging materials, disposable cutlery, and foam products. Due to its low biodegradability and high fragmentation potential, polystyrene contributes significantly to microplastic pollution. Studies have shown that polystyrene micro- and nanoplastics can induce oxidative stress, inflammation, and cellular toxicity in BEAS-2B cells *in vitro* and thus potentially in humans upon exposure (Dong *et al.*, 2020). The toxicity of polystyrene particles largely depends on their size, shape, and surface chemistry, which influence their interaction with biological systems (Banerjee and Shelver, 2021).

1.5 Routes of Human Exposure to Plastics

Plastic particles can enter the human body through several primary routes: ingestion, inhalation, and dermal absorption (Wu *et al.,* 2022).

Ingestion and inhalation are the two major exposure pathways. An adult may consume approximately 5.1×10^3 microplastic particles from table salts and up to 4.1×10^4 microplastic particles via drinking water annually (Wu *et al.,* 2022). Plastic in bottled drinking water was found to be from the caps and could have long-term exposure implications (Choudhary *et al.,* 2020). Particles have also been found in beer, energy drinks and other soft drinks (Kosuth *et al.,* 2018; Shruti *et al.,* 2020) and more recently microplastics have been found within the flesh of fruit (especially Apples) and vegetables (especially carrots) (Oliveri Conti *et al.*, 2020). Meanwhile, inhalation intake ranges from 0.9×10^4 to 7.9×10^4 microplastic particles per year (Wu *et al.,* 2022). The airborne micro- and nanoplastic have their origin mostly in urban dust that contains textile fibres, wear particles from tire and road materials, like paint (Goßmann *et al.,* 2022; Prata, 2018). The intake of these particles would be further distributed in different tissues and organs of humans depending on their sizes.

Although all three routes contribute to human exposure to microplastics and nanoplastics, particles in the environment represent an important pathway of exposure. This is due to long-term weathering of polymers, leaching of polymer chemical additives, residual monomers, exposure to pollutants and pathogenic microorganisms all being active in these environments (Li *et al.,* 2018; Viršek *et al.,* 2017).

1.6 Health risks and potential toxicity of (Nano)plastic

A major issue when determining the risks of microplastics to human health is the lack of information on human exposure. Adequate analytical tools to sample, isolate, detect, quantify, and characterize small microplastics, especially nanosized plastic particles, are urgently needed (Vethaak & Legler, 2021). There's also the issue of standardization of analytical approach. It is missing, thus researchers face a lack of reference materials, experimental design and official definitions (Brachner *et al.,* 2020).

The first atmospheric measurements of larger-sized, predominantly fibrous microplastics indicate that plastic particles are a relevant component of fine dust, with, for example, deposition rates in central London ranging between 575 and 1008 microplastic particles per square meter per day (Wright *et al.,* 2020).

Nanoplastic exposure raises more concern, due to their small size, there are potential risks to the respiratory tract, as ultrafine and nanoparticles are known to penetrate to the alveolar regions of the lungs, potentially impairing their functions (Michelini *et al.,* 2025).

In vitro experiments have demonstrated that nanoplastics can induce oxidative stress, inflammatory responses, and cytotoxicity in lung epithelial cells, raising concerns about respiratory health (Prata, 2018; Rodrigues *et al.,* 2025). Animal studies further suggest that ingested or inhaled microplastics can translocate to multiple organs, including the liver, kidneys, and brain, potentially disrupting immune function and causing oxidative damage (Garcia *et al.,* 2023).

Two other research groups have recently checked the toxicity of NPs in lung and bronchial cells. Xu and colleagues found that polystyrene nanoplastics (25 and 70 nm) impaired viability and upregulated nuclear factor (NF)-κB as well as some pro-inflammatory cytokines at concentrations of 50 μg/mL and above in the human alveolar epithelial line A549 (Xu *et al.,* 2019).

While larger microplastics are mostly excreted via feces, nanoplastics may cross the intestinal barrier and enter the bloodstream, because of their small size. Although acute intestinal toxicity is unlikely under realistic exposure levels, persistent low-level accumulation of these particles in the gut could pose unknown risks (Wright *et al.,* 2017).

In general, it must be noted that all these effects and the associated toxicity can vary greatly among different types of plastics, meaning that the harmfulness mainly depends on the type of plastic and the related particle characteristics (Banerjee and Shelver, 2021).

1.7 6ppd-quinone

N'-(1,3-Dimethylbutyl)-N'-phenyl-p-phenylenediamine (6PPD), a commonly used antioxidant in rubber manufacturing, has attracted worldwide concern, because its environmental oxidation product, 6PPD-quinone (6PPD-Q), poses significant toxicity and eventual health risks. (Yi *et al.,* 2025)

The compound 6PPD-quinone was first identified as the cause of acute toxicity in coho salmon (Oncorhynchus kisutch). For decades, unexplained mass die-offs of coho salmon were observed in urban streams following rainstorms in the U.S. Pacific Northwest. Despite numerous investigations, the cause remained elusive. To uncover the culprit, a dedicated research team in Canada formed a task force. After five years of intensive study, they successfully pinpointed 6PPD-quinone as the responsible agent in 2020 (Tian *et al.,* 2021).

Although awareness of 6PPD-quinone as an environmental contaminant is growing, there is still a substantial lack of comprehensive knowledge regarding its behavior, transformation, and effects across different environmental compartments. Its transformation mechanisms, degradation rates, and interactions with co-occurring pollutants remains not fully understood. (Hassan Kazmi *et al.,* 2024)

According to Greer et al., exposure with 6PPD-quinone leads to transcriptional alterations in pathways associated with vascular permeability, compromising the integrity of cell-cell adhesions and impairing endothelial junctions (Greer *et al.,* 2023). These physiological effects manifest in a set of symptoms collectively termed "urban runoff mortality syndrome," (Yi *et al.*, 2025) which includes signs such as disorientation, loss of equilibrium, and ultimately death. Alarmingly, the compound's acute lethal concentration (LC50) for coho salmon is just 95 ng/L,- well below levels commonly detected in the environment (Greer *et al.*, 2023).

Investigations into other fish species have demonstrated a wide range of sensitivity to 6PPD-quinone. Brook trout and rainbow trout, for instance, are significantly less sensitive than coho salmon but still experience mortality at environmentally relevant concentrations. In contrast, species like sockeye salmon, zebrafish, and Atlantic salmon showed apparent behavioural effects or mortality under similar exposure conditions (Greer *et al.,* 2023).

In mice studies it was shown that both 6PPD and its transformation product, 6PPD-quinone, may possess hepatotoxic properties. These compounds were found to accumulate in the liver and contribute to disruptions in lipid metabolism, indicating a potential risk for liver dysfunction (Fang *et al.,* 2023).

As tire wear particles (TWPs) are continuously released into the environment, 6PPD-quinone (6PPD-Q) has become widely dispersed across air, water, soil, and biological systems, where it bioaccumulates through the food chain. Significantly, 6PPD-Q has been identified in human urine, serum, and cerebrospinal fluid, and its link to abnormal α-synuclein aggregation in the brains of individuals with Parkinson's disease highlights its potential neurotoxicity. (Yi *et al.,* 2025)

In the atmosphere, 6PPD reacts with ozone under light and high temperature conditions to form 6PPD-Q. (Yi *et al.,* 2025) Both 6PPD and 6PPD-Q are widely found in indoor and outdoor dust at ng/g levels, of 1.7–223 for 6PPD and 0.33–82 ng/g for 6PPD-Q posing exposure risks through ingestion, inhalation, and skin contact. Infants in particular, show higher intake levels compared to adults (Zhu et al., 2024). Fang et al. demonstrated in 2023 that exposure to 6PPD-Q may increase the liver weight and the triglyceride level, and also may alter the hepatic metabolism in mice (Fang *et al.,* 2023).

In humans, higher concentrations of 6PPD-quinone (6PPD-Q) detected in the follicular fluid of women with polycystic ovary syndrome (PCOS) have been associated with a range of reproductive disruptions. These include prolonged menstrual cycles, elevated serum levels of testosterone and anti-Müllerian hormone (AMqiH), an increased luteinizing hormone (LH) to follicle-stimulating hormone (FSH) ratio, a decrease in the rate of high-quality embryo development, and reduced levels of growth differentiation factor 9 (GDF9) within the follicular fluid (Yu *et al.,* 2024).

A chinese biomonitoring study detected the presence of 6PPD-quinone in human urine, with concentrations exceeding those of its parent compound, 6PPD. The analysis, based on 150 urine samples from various demographic groups, revealed that pregnant women exhibited the highest average levels of both substances: 0.068 ng/mL for 6PPD and 2.91 ng/mL for 6PPD-quinone (Du B *et al.,* 2022). In another study, 6PPD-Q was quantified at 0.40, 0.076, and 2.91 ng/mL in the urine samples of adults, children, and pregnant women, respectively, with detection frequencies ranging from 60% to 100%. Additionally, experiments conducted on mice have indicated that 6PPD exhibit a higher likelihood of bioaccumulation in the liver of mice in comparison to 6PPD-Q (Fang *et al.,* 2024).

In another study, Patients with Parkinson's disease revealed elevated levels of 6PPD-quinone in their cerebrospinal fluid, averaging 11.18 ng/mL, compared to 5.07 ng/mL in a healthy control group. The findings indicate that 6PPD-quinone may contribute to neurodegenerative processes, as it was shown to promote the formation of Lewy neurites at environmentally relevant concentrations and to induce mitochondrial dysfunction in primary dopaminergic neurons (sourced from C57BL/6 mice) using an α-synuclein preformed fibril (PFF) seeding model (Fang *et al.,* 2023).

The results indicate that broader investigations of 6PPD-quinone effects in human cells are required to assess potential health risks.

2. Aim of the thesis

The aim of this thesis is to explore the potential health risks posed by environmental particle exposure, focusing on both well-characterized plastic-related substances and complex airborne materials. This investigation is structured around three distinct yet complementary approaches using *in vitro* cell culture systems. Firstly, the study should assess the effects of synthetically produced and chemically defined plastic particles on cells of the central nervous system (CNS), including their impact on the blood–brain barrier (BBB). Secondly, the toxicity of 6PPD-quinone (6PPD-Q), a small molecule derived from tire wear particles, which has demonstrated aquatic toxicity and is now tested here for its neurotoxic potential on mammalian cells should be examined. Thirdly, the thesis should investigate complex, undefined airborne dust extracts collected from school classrooms in Spain during both winter and summer seasons. These samples, which reflect realistic environmental exposure scenarios, should be applied to the human alveolar epithelial cell line A549 to evaluate their impact on lung cells and assess seasonal variation in potential toxicity. While the defined nanoplastic particles and 6PPD-Q should be tested using CNS-related models, the school air samples should be screened using a respiratory model, acknowledging the lungs as the primary site of airborne particle exposure. Through this comparative approach, the study also aims to evaluate the applicability of *in vitro* models as reliable tools for monitoring particle-induced toxicity and health risks.

3 Materials and Methods

3.1 Materials

Table 3. Polystyrene Nanoparticles

Name	Company	Catalogue No.	Concentration mg/mL
Polybead Microspheres 0.1 µm	Polysciences	00876-15 ml	26.0
Polybead Carboxylate Microspheres 0.1 µm	Polysciences	16688-15 ml	27.0
Polybead Amino Microspheres 0.1 µm	Polysciences	16586-5 ml	26.3
Polybead Microspheres 0.05 µm	Polysciences	08691-10ml	26.0
Polybead Carboxylate Microspheres 0.05 µm	Polysciences	15913-10ml	27.0
DiagPoly amine polystyrene particles 0.05 µm	CD Bioparticles	DFO-L027	10.0

The particles purchased from Polysciences /CD Bioparticles. According to the product data sheet, particles produced by CD Bioparticles are stored in deionized water containing a small amount of surfactant, and 2 mM sodium azide.

Table 4. Devices

Name	Company
CellDrop FLTM	DeNovix Inc.
Enspire: 2300 Multilabel Reader	Perkin Elmer
EVOM3- Trans Epithelial Electrical Resistance (TEER) meter	World Precision Instruments
Grant SUB Aqua Pro : SAP 12	Grant Instruments
Herasafe KS 18 Laminar Air Flow	Thermo Fisher Scientific
Incubator (MCO-170A/C)	Panasonic
Mikroskop: Olympus BX43 FCKX41	Olympus Austria GmbH
NTA: ZetaView Quatt 4 – Laser System	Particle Metrix GmbH
pH-Meter Mettler	Mettler toledo Seven Direct SD50
Ultrasonic bath	VWR, USC-TH
UV Lamp 15 W, Germicidal	Osram
Vortex: Genie 2	Scientific Industries

Table 5. Consumables

Name	Company	Catalogue Npo.
24-well cell culture plate	Greiner Bio-One	662641
96-well cell culture plate	Greiner Bio-One	655 180
96-well cell culture plate – Nunclon Delta Surface	Thermo Fisher	167425
HPLC vials N11, flat, crimp neck, 1.5 ml, 11.6x32 mm, clear	Macherey-Nagel	702 01HP
Microplate 96-well, F-bottom, chimney well, black	Greiner Bio-One	655096
Microplate 96-well, F-bottom, transparent	Greiner Bio-One	655101
Parafilm 10.2 cm x 38.1 m roll	LabShop	PM-996
Petri dishes, 100 x 15 mm	Kord Valmark	877-877-9680
Pipette tips, safeseal SurPhobsterile tips (10µL 100 µL, 200 µL 1000 µL)	Biozym	VT0200,VT0230,VT0240
Serological pipettes (5 mL, 10 mL, 25 mL)	Sarsted	861.253.001 861.254.001 861.685.001
Syringe 1 mL Inject F-Solo	VWR/B.Braun	720-2561
Syringe 10 mL Inject Luer Solo	VWR	4606108V
T25 cell culture flask with filter	Greiner Bio-One	690175
T75 cell culture flask with filter	Greiner Bio-One	658175
ThinCerts™ inserts for 24-well plates, pore size 0.4 µm, transparent	Greiner Bio-One	662641 LOT: 23180116
ThinCerts™ inserts for 24-well plates, pore size 0.1 µm,transparent	Greiner Bio-One	662610 LOT:23180134

Table 6. Chemicals

Name	Company	Catalogue Npo.
Ascorbic acid (AA)	Sigma-Aldrich	A4544
Bovine Serum Albumin (BSA)	Roth	8076.2
Calibration beads for the ZetaView – fluo640, DR-660 – 200 nm	Particle Metrix	120-0104
Calibration beads for the ZetaView – scatter, PS beads – 100 nm	Particle Metrix	110-0020
Collagen IV	Sigma-Aldrich	C5533-5mg
DMEM	Sigma-Aldrich	D5796 – 500mL
DMSO (Dimethylsulfoxid)	ThermoFisher Scientific	D2438-50ML
Dulbecco's Phosphate Buffered (DPBS)	Gibco	14190-094
EBM-2 medium, 1 L	Lonza, Szabo-Scandic	LON190860
EGTA	Sigma-Aldrich	E3889
FBS: Fetal bovine serum	Sigma-Aldrich	F9665 LOT:19A124
Gelatine	Sigma	22,151.02
hbFGF	Sigma- Aldrich	P0291-2506
HEPES solution, 1M pH 7.0-7.6, sterile filtered	Life Technologies Sigma Aldrich	15630-080/ H0887
L-Glutamine (200 mM)	Sigma Aldrich	G7513
MEM Non-Essential Amino Acids Solution (MEM NEAA)	Gibco	11140-035
MTT (Thiazolyl Blue Tetrazolium Bromide)	Sigma-Aldrich	M2128
Penicillin/Streptomycin; solution stabilized with 10 000 units of penicillin and 10 mgstreptomycin/ml	Sigma- Aldrich	15140-122/ 15630-080
Trypsin/EDTA	Pan Biotech	P10-023100
Vasculife basal medium (475 mL)	CellSystems	LM-0002

3.2 Cell culture

All cell culture work was performed in a sterile laminar flow hood. The cells were cultured in an incubator at 5% CO_2 (atmospheric air), 37°C, and 95% humidity. Before each procedure involving the cells (such as medium change, seeding, or experiments), the cells were examined under a microscope for appearance, density, and morphology, as well as for the absence of contamination.

3.2.1 Cell lines

Three human cell lines were used in experiments: the human brain microvascular endothelial cell line hCMEC/D3, human microglial cell line HMC3 and human lung adenocarcinoma cell line A549.

The hCMEC/D3 cell line originates from microvessels of the human temporal lobe, obtained from surgical samples collected during an epilepsy treatment procedure from an adult female epilepsy patient. The initial cell population was enriched for cerebral endothelial cells (CECs) (Weksler *et al.,* 2005). To achieve immortalization, cells underwent sequential transduction with lentiviral vectors encoding the catalytic subunit of human telomerase (hTERT), which extends telomeres, and the SV40 large T antigen, which inhibits tumor suppressor pathways (Weksler *et al.,* 2005; Poller *et al.,* 2008). Immortalized CECs were then selected through limiting dilution cloning, and the resulting clones were thoroughly validated for their brain endothelial characteristics (Poller *et al.,* 2008).

HMC3 human microglial cells are transformed human microglial cells that retain the properties of primary microglial cells. The HMC3 cell line was established through SV40-dependent immortalization of a human fetal brain-derived primary microglia culture (Dello Russo *et al.,* 2018). Resting HMC3 cells exhibited strong positivity for the microglia/macrophage marker IBA1 and expressed the endotoxin receptor CD14, while showing no expression of the astrocyte marker GFAP. Markers indicative of microglial activation, including MHCII, CD68, and CD11b, were not expressed in resting HMC3

cells, but their expression was significantly upregulated following activation with IFN-gamma (10 ng/mL for 24 hours) (Li *et al.,* 2009).

A549 cells are adherent epithelial cells derived from a human alveolar basal epithelial adenocarcinoma. The cell line was established in 1972 from the lung tissue of a 58-year-old Caucasian male (Giard *et al.,* 1973). A549 cells are widely used as a model of alveolar epithelial function and lung-related toxicity or drug delivery studies. They exhibit key epithelial features, such surfactant production, and are known to retain a functional p53 pathway (Lieber *et al.,* 1976; Foster *et al.,* 1998).

3.2.2 Cell maintenance and seeding

hCMEC/D3 cells were passaged every Wednesday at a 1:3 ratio with a seeding cell number of 40.000 cells/ cm^2 and required a gelatine-coated surface for proper attachment. Gelatine (Sigma) coating of T25 flask was performed by applying sterile 0.5% gelatine solution to the flask (2 mL for T25 flask), distributing it on the surface of the flask and incubating for minimum 30 minutes at room temperature. The cells were grown in EBM-2 medium, supplemented by 10mM HEPES, 5% of FBS Fetal Bovine Serum (Sigma), 1% of Penicillin/Streptomycin (Sigma), 5µg/ml of Ascorbic acid (Sigma) and 1ng/ml of hbFGF (Sigma). The medium change followed a strict, weekly schedule where the medium was changed every Monday, Wednesday and Friday.

For the monoculture experiment the hCMEC/D3 cells were passaged, by detaching them by washing the T25 flask twice with 3mL of DPBS, adding 700 µL of Trypsin-EDTA solution to the flask and tilting the flask to distribute the solution on the surface. The flask was then incubated for 3 minutes in the incubator. Detachment of cells was verified by eye or in the microscope. The detached cells were resuspended in 5.3 mL of complete growth medium, the cell suspension was homogenized and singularized by pipetting up and down 5 times, using a 5 mL serological pipette and transferred to separate Falcon tubes for each condition. A new culture flask was prepared by coating it with 2 mL of 0.5% gelatin solution and incubating it at room temperature for 30 minutes. After aspirating the 0.5% gelatin solution, 3 mL of complete EBM-2 medium were added to the new flask as well as 2mL of cell suspension to achieve a splitting ratio of 1:3.

Cell counting was done with the automated cell counter (CellDropFL). Cell count was done three times per every condition, by applying 10 µL of cell suspension to the cell counter device for every count. Having measured 3 times, cell number was averaged. The cell suspension was calculated accordingly to obtain the needed amount required for each seeding.

The HMC3 cells were grown in basal EMEM growth medium (Sigma) supplemented with 10% of FBS Fetal Bovine Serum (Sigma), 1% of Penicillin/Streptomycin (Sigma), 1mM of Na- Pyruvate (Sigma), 1mM of MEM NEAA Non Essential Amino Acids (Gibco), 2mM of L-Glutamine (Gibco), (EMEM 5+). HMC3 cells were passaged once a week with seeding a cell number of 40.000 cells/cm^2. These cells were seeded in the same way the hCMEC/D3 were seeded, but the medium change followed a different protocol, where the medium used was EMEM 5+ and it was changed every Monday, Wednesday, Friday and Sunday.

A549 cells were passaged twice a week with seeding a cell number of 10.000 cells/cm^2 for inserts and 36.000 cells/cm^2 for the wells of 96 well plate. Cells were grown in basal Dulbecco's Modified Eagle Medium DMEM, supplemented by 10% of FBS Fetal Bovine Serum (Sigma) and 1% of Penicillin/Streptomycin (Sigma).

The lung cells were passaged, by detaching them by washing the T25 flask twice with 3mL of DPBS, adding 700 µL of Trypsin-EDTA solution to the flask and tilting the flask to distribute the solution on the surface. The flask was then incubated for 3 minutes in the incubator. The detached cells were resuspended in 7.3 mL of DMEM medium, supplemented with10% fetal bovine serum (FBS; Sigma) and 1% penicillin/streptomycin (Sigma) The cell suspension was homogenized and singularized by pipetting up and down 5 times, using a 5 mL serological pipette and transferred to separate Falcon tubes for each condition. No gelatin solution was needed for coating the new flask. 7mL of DMEM ++ medium were added to the new flask as well as 1mL of cell suspension to achieve a splitting ratio of 1:8. The medium change followed a strict, weekly schedule where the medium used was DMEM ++ and changed every Monday, Wednesday and Thursday.

All cell lines were grown in their respective medium and incubated at 37°C, 5% CO2, 95% air atmosphere, 95% humidity.

For the co-culture experiment, 24-well plates (Greiner) and ThinCerts® with a pore size of 0.4 µm (Greiner, transparent) were used. The basolateral side of the inserts (the wells) were filled with 900 µL complete EBM-2 medium. The apical side of the inserts were filled with 300 µL of DMEM++ medium. On Day 2 and Day 4 the medium was changed. For this the inserts were moved to an empty plate so the basolateral medium could be aspirated and replaced by 900 µL of complete EBM-2. The inserts were flipped over a Petri dish using forceps to remove the old medium. The inserts were then moved back to the original plate with fresh medium and 300 µL of complete DMEM++ was added to the apical side. On Day 7, the procedure was repeated but instead of complete EBM-2 medium the old medium was replaced with serum reduced EBM-2 (0.25% FBS) (refer to chapter 3.5.6 Experimental procedure).

3.2.3 Solutions

1 mg/mL Ascorbic acid:

The end concentration of ascorbic acid solution added up to 1 mg/mL: Total volume of solution - 20 mL: 20 mg of ascorbic acid was dissolved in 20 mL basal EBM-2 and sterile filtered (0.22 µm). The solution was aliquoted in 1.5 mL Eppendorf vials and stored at -20°C.

0.5 % gelatine for coating:

1 L of 0.5% gelatine solution (w/v) was prepared by dissolving 5 g of gelatine powder in 1L deionized water in a glass bottle at 55-60°C. The solution was then autoclaved at 120°C for 30 minutes, cooled down, and stored at room temperature.

hbFGF:

hbFGF was dissolved in 0.1% BSA at 100 µg/mL to make a stock solution. This stock solution was then diluted to 200 ng/mL in 0.1% BSA for EBM-2 medium. Solutions were sterile-filtered, aliquoted, and stored at –20 °C, with in-use aliquots of 5 mL kept at 4 °C.

MTT Stock Solution

MTT (3-(4,5-dimethylthiazol-2-yl)-2,5-diphenyltetrazolium bromide): 5 mg

(Concentration: 5 mg/mL)

The MTT stock solution was prepared by dissolving 50 mg MTT in 10 mL PBS (phosphate-buffered saline) and subsequently sterile-filtered with a syringe filter with a por size of 0.22 µm. The stock solution was stored in a 15 mL tube (made of polypropylene, PP) at 4 °C. The solution was stored in the dark at 4 °C and used within 4 weeks.

EBM-2 Complete Medium:

The following final concentrations were used (dissolved in EBM-2):

– Ascorbic acid: 5 µg/mL

– HEPES: 10 mM

– FBS: 5%

– Pen/Strep: 1%

– hbFGF: 1 ng/mL

The prepared complete EBM-2 medium (without hbFGF) was stored in a 50 mL polypropylene tube at 4 °C and warmed to 37 °C before use. This medium was used within one week of preparation. The growth factor hbFGF was added immediately before use to reach a final concentration of 1 ng/mL (e.g., for 50 mL of EBM-2 complete medium, 250 µL hbFGF). Once the hbFGF was added the medium was used up on the same day.

EMEM 5+

The growth medium for HMC3 cells was EMEM 5+. The following final concentrations were used (dissolved in EMEM)

–Natrium Pyruvate: 1mM

– NEAA: 0,5 mL

– FBS: 10%

– Pen/Strep: 1%

–L-Glutamine: 2 mM

The prepared complete medium was stored in a 50 mL polypropylene tube at 4 °C and warmed to 37 °C before use. The solution was used within one week of preparation.

3.3 Preparation of nanoparticles

Nanoparticle suspensions were transferred into 1.5 mL HPLC glass vials, sealed with parafilm, and sonicated for 10 minutes in an ultrasound bath without heating. Under a laminar flow hood, spectroscopic glass cuvettes were rinsed with water and then with ethanol. Approximately 10% more nanoparticle solution than required was pipetted into each cuvette. The prepared cuvettes were then positioned in the laminar flow cabinet as shown in Figure 2 (green circle).

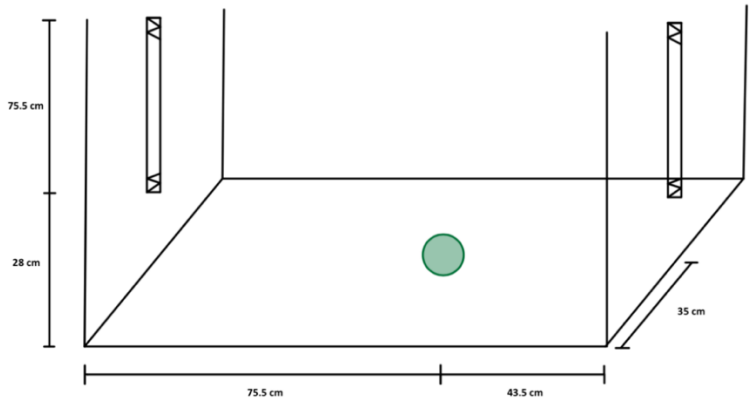

Figure 2: Laminar flow cabinet used for UV radiation of nanoplastic. Green circle represents the area where the glass spectroscopical cuvettes were placed. (Chmielewska, 2023)

The laminar flow cabinet was closed and the UV lamps were turned on for 30 minutes. Then, the samples were collected in 1.5 mL Eppendorf tubes. Different nanoparticle concentrations in basal cell culture media were achieved via partial serial dilution. The scheme of the performed serial dilutions can be seen in Figure 3.

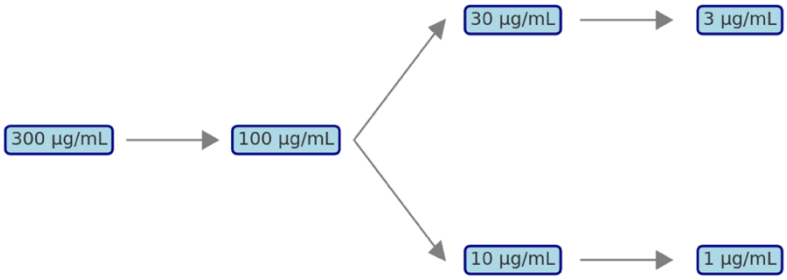

Figure 3: Serial dilution – concentrations of nanoparticles (adapted from Chmielewska, 2023.

Each dilution was adjusted to match the water content of the highest concentration. Before application to the cells, dispersions were vortexed and mixed with a micropipette.

3.3.1 Staining of particles with AttoDye

To prepare the dye solution, 1 mg of Atto665 dye was dissolved in 1 mL of sterile-filtered (0.22 µm) deionized water in a 1.5 mL HPLC vial.

For the nanoplastic particle preparation, 5–7 drops from the stock solutions of nanoplastic particles were added to 1.5 mL HPLC glass vials. (refer to Table 3 in chapter 3.1). The samples were then sonicated for 10 minutes without heat to ensure proper dispersion. Following sonication, the solutions were transferred to 2 mL glass vials.

To achieve a final dye concentration of 6 µg/mL, 24 µL of the Atto665 stock solution was added to each Nanoplastics sample. For Polystyrene carobxylated 50 nm, 100 nm and Polystyrene aminated 100nm, 1902 µL Milli-Q water and 74 µL of each nanoplastic stock solution was added to the 24 µL of the Atto665 dye. For Polystyrene pristine 50nm and 100nm, 1900 µL Milli-Q water and 76 µL of it's nanoplastic stock solution was added to the 24 µL of the Atto665 dye. And lastly for Polystyrene aminated 50nm, 1778,4 µL Milli-Q water and 197,6 µL of its nanoplastic stock solution was added to the 24 µL of the Atto665 dye. The mixtures were then vortexed to ensure homogeneity. 1.5 mL of each sample was transferred into 2 mL glass vials (two vials per sample), sealed with parafilm and aluminum foil, and incubated for 2 hours at room temperature at 100 rpm. The incubation was conducted in a non-transparent box with a lid to prevent interference from UV light.

During the staining process, 5 Litre beakers were filled with 2 Litre of Milli-Q water in preparation for dialysis. Once staining was complete, the samples were transferred into a dialysis tube and subjected to dialysis with daily water changes for a period of five days.

After dialysis, the samples were collected in 1.5 mL HPLC glass vials for further analysis. Fluorescence measurements were performed using a plate reader, followed by nanoparticle tracking analysis (NTA). The size, the zeta potential, and the number of fluorescent particles of the nano plastic particles were established on the ZetaView NTA device.

3.4 Cell cultivation in 96-well plates/ Experimental setups

3.4.1 Experimental setup of hCMEC/D3 and nanoplastic

hCMEC/D3 endothelial cells were seeded on pre-coated (0.5% gelatin in deionized water, 100 µL/well, 30 minutes , room temperature) 96-well plates. Two plates were used for each experiment. Gelatin was removed using a multichannel pipette immediately before cell seeding. Cells were seeded into 11 out of 12 columns; the 12th column served as a blank, containing only medium without cells, to allow for background correction during absorbance measurements. The total volume of the cell suspension or medium (blank column) was 200 µL per well.

The seeding density was 40,000 cells/cm^2. Cells were washed the twice with 3mL of DPBS, and then detached using 700 µL Trypsin-EDTA, incubated briefly, and subsequently neutralized with complete EBM-2 medium. After resuspension, cell concentration was determined using an automated cell counter. Based on the surface area of the 96-well plate, which was 0,336 cm^2 and the desired seeding density, the required volume of cell suspension was calculated and mixed with an appropriate volume of EBM-2 medium supplemented with fibroblast growth factor (FGF). The resulting cell-medium mixture was thoroughly homogenized before use. After thorough mixing with a serological pipette, the suspension was transferred to a Petri dish and seeded into the pre-coated 96-well plates using a multichannel pipette. The plates were then incubated at 37 °C, 5% CO_2, 95% air atmosphere, and 95% humidity.

On Day 2 post-seeding, a complete medium change was performed using fresh EBM-2 supplemented with hbFGF. On Day 5, the medium was replaced with EBM-2 containing 0,25% FBS to slow down proliferation and support the formation of a stable endothelial monolayer.

On Day 6, cells were exposed to fluorescently labeled polystyrene nanoparticles (NPs):

- PS P100 (pristine, 100 nm)
- PS A100 (aminated, 100 nm)
- PS C50 (carboxylated, 50 nm)

All NPs had been previously stained and stored at 4 °C in 1.5 mL HPLC glass vials. On the day of treatment, they were sonicated in an ultrasonic water bath for 10 minutes (without heating) to ensure proper dispersion. Glass cuvettes were washed with MilliQ water followed by 70% ethanol, filled with 100 µL of each NP stock solution and UV-sterilized under a UV hood for 30 minutes. (see chapter 2.3 Preparation of Nanoparticles) After UV exposure, the sterilized NP dispersions were transferred into new sterile vials, sealed with parafilm and aluminum foil, and labeled accordingly.

Dilutions were prepared in Vasculife medium from 1000 µg/mL NP stock solutions to the following final concentrations: 100, 30, 10, 3, and 1 µg/mL. To prepare these concentrations:

- 100 µg/mL: 1800 µL Vasculife + 200 µL stock
- 30 µg/mL: 1800 µL Vasculife + 60 µL stock + 140 µL MQ water
- 10 µg/mL: 1800 µL Vasculife + 20 µL stock + 180 µL MQ water
- 3 µg/mL: 1940 µL VL/MQ (9.9 mL VL + 0.1 mL MQ H_2O) + 60 µL of 100 µg/mL stock
- 1 µg/mL: 1980 µL VL/MQ + 20 µL of 100 µg/mL stock

Remaining VL/MQ solution was used for control wells.

Immediately before NP treatment, the wells were washed once with Vasculife medium. The NP dispersions were vortexed and pipette-mixed to ensure homogeneity. All procedures were carried out in the stem cell laminar flow hood under dark conditions to protect fluorescent dyes from photobleaching (hood lights off, aluminum foil used)

Design of Plates:

Plate 1:

Column 1-5 (Polystyrole pristine)	Column 6-10 (Polystyrole aminated)	Column 11	Column 12 (Blanks)
Column 1: 100 µg/mL Column 2: 30 µg/mL Column 3: 10 µg/mL Column 4: 3 µg/mL Column 5: 1 µg/mL	Column 1: 100 µg/mL Column 2: 30 µg/mL Column 3: 10 µg/mL Column 4: 3 µg/mL Column 5: 1 µg/mL	Vasculife + MQ H_2O	VL + MQ H_2O

Plate 2:

Column 1-5 (Polystyrole carboxylated)	Column 6-10	Column 11	Column 12 (Blanks)
Column 1: 100 µg/mL Column 2: 30 µg/mL Column 3: 10 µg/mL Column 4: 3 µg/mL Column 5: 1 µg/mL	Columns 6-8: only Vasculife Columns 9-10: Vasculife + fresh sterile filtered H_2O	Vasculife + MQ H_2O	VL + MQ H_2O

After NP application, the plates were incubated for 48 hours at 37 °C, 5% CO_2, 95% air atmosphere, and 95% humidity before further analysis.

3.4.2 Experimental setup of HMC3 and NP

HMC3 cells were similarily seeded on 96 well plates in 11 out of 12 columns, but without any coating. Equally as hCMEC/D3 the 12th column served as blank which was later subtracted from the absolute absorption values obtained from other wells. The total volume of the cell suspension or medium (blank column) was 200 µL. Cells were cultured in complete EMEM medium supplemented with 10% fetal bovine serum (FBS; Sigma), 1% penicillin/streptomycin (Sigma), 1 mM sodium pyruvate (Sigma), 1 mM non-essential amino acids (MEM NEAA; Gibco), and 2 mM L-glutamine (Gibco). HMC3 cells were maintained under standard incubation conditions (37 °C, 5% CO_2, 95% air, 95% humidity) and were passaged once per week at a seeding density of 40,000 cells/cm^2. After seeding, the medium was changed every second day, including weekends. The cells used were kept between passage 19 – 35.

Cells were washed the twice with 3mL of DPBS, and then detached using 700 µL Trypsin-EDTA, neutralized with complete EMEM, and resuspended. Cell concentration was determined using the automated cell counter, CellDrop FL. A calculated volume of the suspension was combined with fresh growth medium and mixed thoroughly. The mixture was transferred to a Petri dish and seeded into the wells using a multichannel pipette.

On the treatment day with NP, cells were washed once with basal EMEM (without supplements). Unstained polystyrene nanoparticles (NPs) were used, including:

- PS P100: pristine polystyrene, 100 nm
- PS P50: pristine polystyrene, 50 nm
- PS C100: carboxylated polystyrene, 100 nm
- PS C50: carboxylated polystyrene, 50nm
- PS A100: aminated polystyrene, 100nm
- PS A 50nm: animated polystyrene 50nm

Nanoplastic stock solutions were vortexed thoroughly before dilution in basal EMEM. All treatments were performed under sterile conditions in a laminar flow hood. NP dispersions were freshly prepared on the day of application and applied directly to the cells.

The following conditions were applied for the plate treated with carboxylated PS C50 nanoparticles:

- Columns 1–2: Basal EMEM (untreated control)
- Column 3: EMEM supplemented with 10% FBS and additives (positive control)
- Columns 4 & 11: Basal EMEM + sterile MilliQ H_2O
- Columns 5–10: Basal EMEM containing PS C50 at concentrations of 300, 100, 30, 10, 3, and 1 µg/mL, respectively
- Column 12: Basal EMEM (blank; no cells)

Plates were incubated for 48 hours post-treatment at 37 °C, 5% CO_2, and 95% humidity before analysis.

3.4.3 Experimental setup of hCMEC/D3 and 6ppd-Q

hCMEC/D3 cells were seeded onto 96-well plates pre-coated with 3mL 0.5% gelatin dissolved in deionized water, incubated at room temperature for 30 minutes. After removal of the coating solution, wells were washed twice with PBS and allowed to equilibrate under the laminar air hood. Cells were seeded in 11 out of 12 columns; one column was left blank (medium only, no cells) and later used for background subtraction in absorbance-based assays. Each well was filled with 200 µL of cell suspension with EBM-2 medium. The plates were incubated at 37°C, 5% CO_2, and 95% humidity.

As mentioned in the chapter 3.2.2 , the medium change with completed EBM-2 was done weekly every Monday, Wednesday and Friday. On Day 5, the medium was replaced with EBM-2 containing 0,25% FBS to slow down proliferation and support the formation of a stable endothelial monolayer.

On the day of treatment (Day 6), cells were washed once with pre-warmed EBM-2 medium. For the treatment 6PPD-quinone (6PPD-Q) solutions were prepared freshly in two steps under sterile conditions inside the laminar air hood:

A 10 mg/mL stock solution of 6PPD-Q was used to prepare a serial dilution in DMSO. The following intermediate concentrations were generated through stepwise dilution:

3 mg/ml: 3,3 µL of 10 mg/mL stock 6ppd-quinone bottle and 6,7 µL DMSO

1mg/ml: 1 µL of 10 mg/mL stock 6ppd-quinone bottle & 9 µL DMSO

300 µg/ml: 3,3 µL of 1 mg/mL solution and 6,7 µL DMSO

100 µg/ml: 1 µL of 1 mg/mL solution and 9 µL DMSO

30 µg/ml: 3,3 µL of 100 µg/mL solution and 6,7 µL DMSO

10 µg/ml: 1 µL of 100 µg/mL solution and 9 µL DMSO

Each DMSO dilution was sterile filtered using a 0.22 µm syringe filter and stored in sterile 1,5 mL Eppendorf tubes until further use. From the intermediate DMSO stocks, working concentrations were prepared by diluting them into EBM-2 medium at a 1:1000 ratio (e.g., 2 µL DMSO 6ppd-Q stock solution solution into 1998 µL EBM-2). This resulted in the

following final concentrations: 10,000 µg/mL, 3,000 µg/mL, 1,000 µg/mL, 300 µg/mL, 100 µg/mL, 30 µg/mL and 10 µg/mL.

Just before application, solutions were vortexed to ensure homogeneity. Cells were then exposed to the treatment media for 24 hours under standard culture conditions.

After the 24-hour incubation, cell viability was assessed using the MTT assay**.** 10 µL of the 12 mM MTT stock solution was added to each well. Following reagent incubation for 10 minutes at 37°C and solubilization, absorbance at 570 nm was measured using a microplate reader.

3.4.4 Experimental setup of HMC3 and 6ppd-Q

HMC3 cells were used following the same experimental setup, with the only changes being the use of EMEM medium and no gelatin coating of the 96-well plates. Cells were seeded with one column left blank for background subtraction, and all other steps, including incubation, detachment, seeding, treatment, and viability assays, were performed as described in chapter 3.2.2 Cell maintenance and seeding.

3.5 Exposure of filtered indoor particles on human lung cells A549

In the next set of experiments, the focus was set on analyzing air filter samples collected from schools in Barcelona, to assess the extracts and their potential impact on lung cells. Specifically, filters were obtained from six different schools and five houses across Barcelona, with samples collected during both the winter and summer seasons. This seasonal comparison allowed for the investigation of potential variations in particle load due to environmental or behavioral changes throughout the year. In total, 124 samples were analyzed. Each filter was extracted, which were then characterized for extracted particles using Nanoparticle Tracking Analysis (NTA) to determine their size distribution, particle concentration, and zeta potential. These parameters provide insights into the physical properties of the particles, such as their surface charge, which can influence their interaction with biological membranes. To evaluate the biological effects of these extracts, a cell viability test (MTT assay) was conducted using cultured lung cells. To assess the potential cytotoxic effects of the extractions, an initial screening was performed using the A549 lung epithelial monoculture model as described in chapter 3.2.2 Cell maintenance and seeding.

The MTT assay measures mitochondrial metabolic activity as an indicator of cell health and viability, thus enabling the assessment of potential cytotoxic effects caused by particle exposure. In addition, transepithelial electrical resistance (TEER) measurements were done to evaluate the integrity of the epithelial barrier. TEER provides a quantitative measure of tight junction function and is a key indicator of whether particles compromise the protective barrier of lung epithelial cells.

Together, these methods provided a comprehensive approach to understanding both the physicochemical characteristics and the possible biological impact of airborne extracts from dust collected from indoor environments commonly occupied by children.

3.5.1 Sampling process in Barcelona

The sampling campaign was conducted in Barcelona between February and July 2024, covering both a winter and a summer season. Indoor particulate matter (PM 2.5) samples were collected from five schools and five residences. At each site, sampling was performed for one week, typically resulting in 10 samples per location (5 filters in winter and 5 in summer). In some cases, school holidays reduced the number of collected filters to three or four.

To minimize noise during operation, the sampling equipment was enclosed in a large metal box containing a smaller plastic box lined with sound insulation. At each sampling location, one SKC Leland Legacy Pump was installed and connected to a personal environmental monitor (PEM) sampler equipped with a pre-muffled quartz filter (47 mm). The PEM sampler was specifically designed for the collection of PM 2.5.

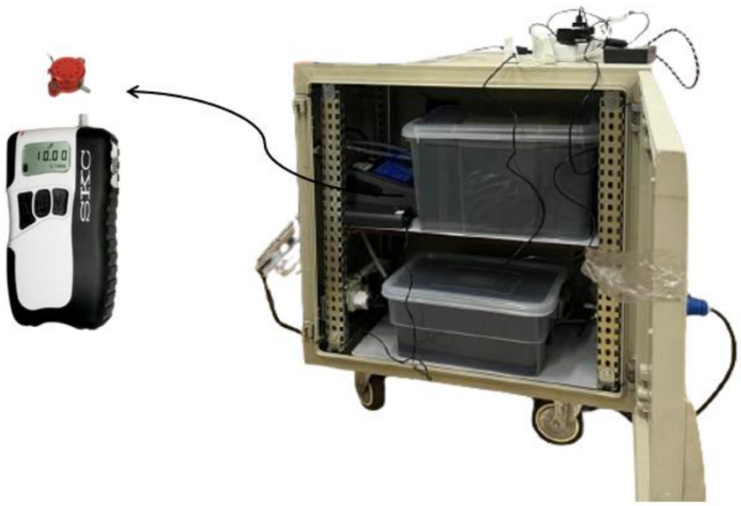

Figure 4: Sampling setup: SKC Leland Legacy pump with PEM sampler (PM 2.5, quartz filter) enclosed in a sound-insulated box. Picture provided to us. (https://inchildhealth.eu/, access: 08.January 2026)

In schools, the pump was operated at a flow rate of 10 L/min for 480 minutes per day (08:00–16:00). On Fridays, equipment was retrieved between 12:00 and 13:00, transported to the next site, and re-installed for the following Monday. In residences, the flow rate was kept at 10 L/min. Prior to sampling, quartz filters were muffled to eliminate residual impurities. Filters were stored in plastic holders in a balance room under controlled temperature (4 °C).

The Sampling campaign provided us with information on the Schools and Houses from which the air filters were placed and collected. Schools 1–5 were located in areas classified as urban traffic, while School 6 represented an urban background location. In one case, the same school was sampled in two indoor environments: the gym (School 2) and a classroom (School 3).

Houses 1–4, 6, and 7 were also classified as urban traffic, whereas House 5 was an urban background site. During the summer campaign, Houses 2 and 3 were unavailable and therefore substituted with Houses 7 and 6, respectively, both situated near the original residences.

The air sampling was conducted using SKC's Leland Legacy Pump, which is particularly suited for studies requiring consistent, long-duration indoor sampling. According to the manufacturer, the pump supports high and stable flow rates with compensated flow

control. Low operational noise was a key advantage for use in sensitive settings such as classrooms, reducing disruptions of the courses during sampling. The device's operating temperature range (0–40°C) also ensured that seasonal temperature variation (cold and warm sampling periods) remained within its functional range. (SKC Ltd. Leland Legacy Pump. Available at: https://www.skcltd.com/products2/air-sampling-pumps/leland-legacy-pump.html (Access : 12. September 2025)

3.5.2 Extraction process

The extraction process began with the preparation of an extraction buffer consisting of 0.9% NaCl and 0.05% Tween-80 solution. A 0.9% NaCl solution was prepared by dissolving 3.6 g of NaCl in 400 mL of Milli-Q water. Due to the high viscosity of Tween-80, a 10% (v/v) Tween-80 stock solution was first prepared by mixing 0.5 mL Tween-80 with 4.5 mL of 0.9% NaCl solution. For the extraction buffer (EDC), 109.45 mL of 0.9% NaCl was supplemented with 550 µL of the 10% Tween-80 solution and mixed thoroughly. Before starting the extraction, the particle concentration of the buffer was measured using a nanoparticle tracking analyzer (NTA) to ensure it was particle-free. Each air filter, with a total diameter of 47 mm, was handled under sterile conditions. From each filter, approximately three-quarters was received for analysis. Using disinfected scissors, the filter was cut into smaller pieces, and half of the received portion was placed into a pre-weighed 50 mL tube. Then 10 mL of the prepared extraction buffer were pipetted on the filter. The tubes were then shaken for 30 minutes at 250 rpm to facilitate the release of particles from the filter material. After shaking, the filter was pressed to recover as much extract as possible, transferred into a pre-weighed 15 mL tube, and weighed again to determine the residual filter mass. The resulting extract was then aliquoted into five sterile 1.5 mL tubes and stored at –20 °C, while the remaining buffer solution was kept at 4 °C. This standardized procedure ensured consistent extraction for subsequent physicochemical characterization and biological testing.

3.5.3 Screening process with A549 cells

To assess the potential cytotoxic effects of the extracted particles, an initial screening was performed using an A549 lung epithelial monoculture model. On Day 0, A549 cells were seeded (as described in chapter 3.2.2) into 96-well plates and allowed to adhere and grow. Confluency was monitored daily with the Tecan plate reader, and once cells reached the target range of 30–40%, typically by day 2 or 3, they were exposed to the extracted samples. Only frozen aliquots of the extracts were used for exposure, as these had previously demonstrated stronger biological effects compared to those stored in the cold room at 4 °C. After exposure, the cells were incubated until they reached approximately 80–100% confluency, at which point a metabolic activity assay (MTT assay) was carried out on Day 4 or 5 to determine the viability of the treated cells. This screening approach allowed for the identification of extracts with potentially significant biological impact, providing a basis for more detailed follow-up experiments.

Design of Plates:

Column 1-2	Column 3-9	Column 10-11	Column 12 (Blank)
DMEM + medium	Column 3+4 : Extraction Buffer Columns 5-9: Extracts	Column 10: EGTA 1mM Column 11: EGTA 3mM	DMEM + medium

3.5.4 Sampling Overview

Table 7. Sampling overview

Sample Number	Extract 5x1mL - 20°C	Sampling time (min)	Season	Setting	Area
1–10	School 1, School 2	253–480	winter	urban	classroom front / gym back
11–16	School 3	241–480	winter	urban	classroom back
17–22	School 4	243–480	winter	urban	classroom back
23–28	School 5	480	winter	urban background	classroom front
29–34	School 6	246–480	winter	urban background	classroom front
35–40	House 1	900–1800	winter	urban	living room
41–46	House 2	900–1800	winter	urban	living room
47–57	House 3, House 4	900–1800	winter	urban	living room
58–63	House 5	900–1800	winter	urban	living room
64–69	School 1	2–480	summer	urban	classroom front
70–77	School 2 +3	182–480	summer	urban	classroom front
78–82	School 4	480	summer	urban	classroom front
83–89	School 5	216–480	summer	urban background	classroom front
90–95	School 6	187–480	summer	urban background	school
96–100	House 1	900–1800	summer	urban	house
101–106	House 4	900–1800	summer	urban	house
107–112	House 5	900–1800	summer	urban	house
113–118	House 6	900–1800	summer	urban	house
119–124	House 7	900–1800	summer	urban	house

3.5.5 Establishment of culture conditions for A549/D3 Transwell® model

The aim of this preliminary testing was to assess how different media compositions might influence cell behavior, barrier integrity, and overall assay performance. Three different media setups, for extracts 2, 3 and 4 were compared: (1) serum free DMEM basal medium in both compartments, (2) DMEM supplemented with 10% fetal bovine serum (FBS) in the apical chamber (A549 side) but without FBS in the basolateral chamber (D3 side), and (3) DMEM supplemented with 10% FBS in both apical and basolateral chambers.

These conditions were chosen to determine the optimal environment for maintaining both cell types and to ensure reliable TEER measurements and consistent cellular responses to extracts. The results from this pilot helped to decide for a stable and reproducible platform for the subsequent exposure experiments using the selected extracts from the previous screening.

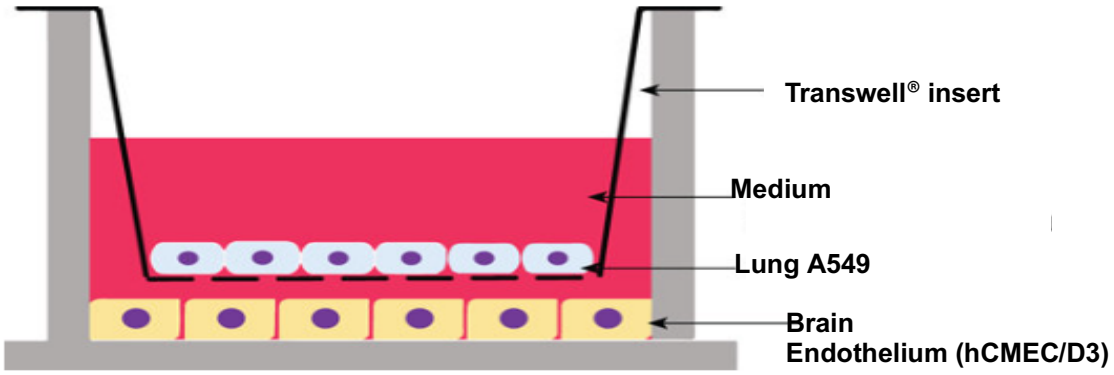

Figure 5: *Schematic representation of the Transwell co-culture system.* A549 lung epithelial cells were cultured on the apical side of the membrane insert, while human brain endothelial cells (hCMEC/D3) were seeded in the basolateral compartment (well bottom). The porous membrane allows for particle diffusion and intercellular communication. This setup was used to assess barrier integrity (TER) and cytotoxic effects upon exposure to filter-derived particle extracts.

3.5.6 Experimental procedure

To provide the two compartments required for the barrier integrity measurement, Transwell® inserts were placed into 24-well plates. In this model , the apical side (“air side”) refers to the inside of the insert (medium volume:300 µL) where cells are grown on its membrane, while basolateral side (“blood side”) corresponds to the well (medium volume: 900 µL).

First, A549 cells were seeded on 1.0 µm inserts and exposed to filtered indoor extracts refer to chapter 3.5.4 “Sampling overview”on the apical side. On Day 2 hCMEC/D3 cells were seeded in the wells with the EBM-2 medium. Additionally a medium change with 10% FBS and 1% Penstrep supplemented DMEM was done for the inserts. On Day 4, there was a medium change for both cell lines, using DMEM with 10% FBS for the inserts and EBM-2 for the wells. On Day 7, a medium change was performed again using the same medium for the inserts, while the wells received serum-reduced EBM2 (0.25% FBS instead of 5%). On Day 8, the two cell lines were combined, the A549 in the inserts with the hCMEC/D3 in the wells, and then exposed to the samples. On that same day, TER measurements were performed immediately before and after exposure. TER measurement was done using a chopstick electrode (STX2 – World Precision Instruments) and an EVOMTM volt ohm meter (World Precision Instruments).The electrode was incubated in DMEM basal medium for 40 minutes before the measurement was done. The long part of the electrode was placed inside the well, whereas the shorter part was placed inside of the insert. The blanks were measured first. When the value was stable for 10 seconds it was noted down. Between different compounds and setups, the electrode was washed in DMEM basal medium. The ensure reproducibility and comparability, the samples and electrode were equilibrated at room temperature and measurements were taken at the same position of the insert every time. After the measurements the electrode was washed in milli-Q for 1 min and again disinfected for 1-2 min in 70% EtOH. The electrode was stored dry. An additional TER measurement and an MTT assay were conducted 48 hours post-exposure.

In the preliminary testing 3 inserts were used for each extract (2-4), 3 inserts for the extraction buffer (EB), 2 inserts were used as a negative control, containing either DMEM

without FBS or with 10% FBS supplementation and 1 insert was used as a positive control, receiving EGTA 3mM. This setup was used for each media condition.

3 inserts were used as blanks, with no cells seeded on either side in 1 plate. The setup for the preliminary testing provided 3 different conditions as described in chapter 3.5.5 “Establishment of culture conditions for A549/D3 Transwell model“ and three independent experiments were conducted.

Following the preliminary testing, one condition of the three tested set-ups and 13 samples were chosen for three additional experimens. (refer to Table 8 in chapter 7.5)

The chosen condition was DMEM supplemented with 10% fetal bovine serum (FBS) in the apical chamber (A549 side), but without FBS in the basolateral chamber. Two plates were used for these three experiments and each plate had 24 wells. Each well contained a 1.0 µm insert with A549 cells, and hCMEC/D3 cells were seeded in the wells. For each plate 3 inserts were used per sample and 6 inserts for their respective extraction buffer (EB), 2 inserts were used as a negative control, containing DMEM without FBS, 1 insert was used as a postive control containing EGTA 3mM. One plate also contained three blanks (no cells seeded on either side).

4 Particle characterization

Nanoparticle tracking analysis (NTA) utilizes Brownian motion to analyze and visualize particles in the nanometer range. The speed of particle movement, which depends on the temperature and viscosity of the suspension, is related to the hydrodynamic diameter of the particles using the Stokes–Einstein equation (Filipe et al., 2010).

This technique combines laser light scattering microscopy with a CCD camera (short for charge-coupled device), which enables the imaging and recording of nanoparticles in solution (Filipe et al., 2010). Additionally, the measurement also provides the concentration of the suspension in units of particles per mL.

The NTA device also allows the determination of the zeta potential based on electrophoretic mobility. The zeta potential is a key parameter describing the electrostatic potential at the hydrodynamic shear plane of nanoparticles in suspension and serves as a measure of their colloidal stability. It is influenced by various factors including the solvent, pH, viscosity, ionic strength, conductivity, and temperature (Martin et al., 2022; Smith et al., 2017). In aqueous solutions, charged nanoparticles are surrounded by an electric double layer consisting of a firmly bound Stern layer and a more loosely associated diffuse layer. The slipping plane between these two regions defines the location at which the zeta potential is measured (Smith et al., 2017).

Using nanoparticle tracking analysis (NTA), zeta potential measurements can be performed via electrodes integrated into the sample chamber. When an electric field is applied, both the nanoparticles and the surrounding fluid are set into motion. The apparent drift velocity of each particle is a superposition of electrophoretic and electroosmotic motion, from which the electrophoretic velocity (μ_e) can be determined. The zeta potential (ζ) is then calculated using the Helmholtz–Smoluchowski equation (Griffiths et al., 2011).

Before each measurement, the NTA system was calibrated using 100 nm polystyrene calibration beads supplied by the manufacturer. The sample chamber was rinsed with 1 mL of deionized water and the absence of particles was verified on the display. The calibration beads were serially diluted in deionized water, first to 1:1,000 then to

1:250,000. Approximately 1 mL of the diluted suspension was introduced bubble-free into the device using a syringe. The software performed an auto-alignment procedure to ensure the optical system was properly centered and symmetrical, indicating readiness for measurement. For fluorescence calibration, beads matched to the 640 nm laser wavelength were diluted in deionized water similarly to 1:100,000 (via 1:1,000 and 1:100 dilutions) and calibrated using the same steps. No special alignment was necessary for zeta potential measurements.

Prior to each measurement, nanoplastic stock solutions were ultrasonicated for 10 minutes at room temperature in an ultrasonic bath to disperse potential aggregates formed during storage. For polystyrene (PS) nanoparticles, a 1 mL aliquot was transferred into 1.5 mL glass roll-neck vials and sealed with parafilm. Samples were vortexed briefly (5–6 seconds) before further dilution. Serial dilutions were prepared in MilliQ water to achieve optimal particle concentrations within the ZetaView Quatt 4 Laser System's measurement range (~10^7–10^8 particles/mL), targeting approximately 100 particles per frame for tracking analysis. After each dilution step, samples were vortexed for 2–3 seconds to ensure homogeneity and injected bubble-free into the device sample chamber using a 1 mL syringe. The sample chamber was rinsed with 1 mL deionized water before use and checked for residual particles.

Measurement parameters for size analysis of 100 nm PS particles were set at 25°C using a 520 nm laser, with camera sensitivity at 75%, shutter speed of 100, and frame rate of 15 frames per second. Fluorescence measurements were carried out with excitation at 670 nm (selected based on the absorption scan) and emission recorded from 690 to 800 nm, as well as with excitation at 620 nm and emission recorded from 640 to 800 nm. Additionally camera sensitivity was increased to 100% and minimum brightness threshold was adjusted from 30 to 100 to optimize detection. Size and fluorescence analyses were conducted at 11 positions, with means and standard deviations calculated after automatic outlier removal. Zeta potential measurements employed a 488 nm laser at 25°C, with sensitivity and shutter settings adjusted to 60 and 100 and measurements performed at two positions in either pulsed or continuous mode, depending on sample conductivity.

Throughout, media and solvent controls (MilliQ water, ethanol, DMSO) at matching dilution factors were measured to identify and exclude background noise. The viscosity of all diluted samples was assumed constant due to the high dilution in MilliQ water.

5 Assays

5.1 MTT Assay

The assay is based on the ability of mitochondrial enzymes in living cells to reduce a water-soluble yellow compound, 3-(4,5-dimethylthiazol-2-yl)-2,5-diphenyltetrazolium bromide (MTT) into purple, insoluble formazan crystals (Mosmann, 1983). The resulting color can be quantified spectrophotometrically.

The toxic MTT solid was dissolved in DPBS to yield the concentration of 12 mM (50 mg in 10 mL DPBS). The solution was stored at 4°C and covered with aluminum foil to protect it from potentially harmful UV light. For the experiments with nanoplastics and the 6ppd-quinone by the 46th incubation hour of the cells, a 96-well plate was taken out of the incubator, and 10 μL of MTT solution was added to each well containing 200 μL of medium per well. A plate was incubated for another 2 hours at 37°C, 5% CO_2, 95% air atmosphere, 95% humidity. When the incubation was completed, the plate was placed on ice, the medium was removed, and the wells were washed with 100 μL ice-cold DPBS/well. The DPBS was then removed by pipetting. Further, a 100 μL of DMSO was pipetted into wells to dissolve the formed crystals, and a plate was incubated for another 10 minutes at 37°C, 5% CO_2, 95% air atmosphere, 95% humidity. Subsequently, the absorbance of the solution in each well was measured on a plate reader (Enspire 2300) at 570 nm. Prior to measurement, the plate was shaken for 30 seconds inside of the instrument.

For the Transwell experiments, after 47 hours of incubation, the inserts were transferred to a 96 well plate, where15 μL 12 mM MTT stock solution were added to each insert (apical side). 45 μL 12 mM MTT stock solution were added to each well (basolateral side). The plates were then incubated for another hour at 37°C, 5% CO_2, 95% air atmosphere, 95% humidity. When the incubation was completed the medium was removed, and the inserts were washed with 200 μL ice-cold DPBS, and the wells with 600 μL ice-cold DPBS. The DPBS was then removed by pipetting. Further, 220 μL of DMSO was pipetted into the inserts to dissolve the formed crystals, and 600 μL of DMSO were added to the wells for the same purpose. The plates were incubated for another 10 minutes at 37°C, 5% CO_2, 95% air atmosphere, 95% humidity. After 10 minutes, 200 μL from each well and 200 μL

from each well was pipetted into a 96 well plate for the absorbance measurement. Subsequently, the absorbance of the solution in each insert and each well was measured on a plate reader (Enspire 2300) at 570 nm. Prior to measurement, the plate was shaken for 30 seconds inside of the instrument.

6 Statistical analysis

The cell experiment data were presented as mean ± standard deviation (SD) in the form of bar charts. Statistical analysis was performed using one-way ANOVA followed by the Holm- Šidák post-hoc test. Statistical significance was indicated in the diagrams as follows: * $p < 0.05$ (significant), ** $p < 0.01$ (very significant), *** $p < 0.001$ and **** $p < 0.0001$ (highly significant).

6.1 MTT Assay for cell viability

Only 6 out of 8 wells per column were taken into calculations, top and bottom row was considered faulty due to potentially increased evaporation of media on the edges of the plates, and therefore, not included in the mean value. For the Experiments with the Transwell model, all wells were taken into calculations. The average of blank (medium without cells) was subtracted from each data point. Each column was averaged. The cell viability by every condition was calculated in percentage relatively to the untreated vehicle control from the same plate, with control being either EBM-2 medium and water or EMEM medium or DMEM medium. Standard deviation in percentage relatively to untreated vehicle control was also included.

6.2 TER

To obtain the actual TER values ($\Omega\ cm^2$), the mean TER values of the wells without cells were subtracted from the individual values of the wells with cells and multiplied by the growth surface area of 0.336 cm^2. The calculated values were then normalized to the mean value of the corresponding control wells containing, depending on the experiemental setup either, EBM-2 medium and water or EMEM medium or DMEM medium. Furthermore, the resulting data were expressed as mean percentages relative to this control.

7 Results

7.1 NTA Particle characterization and fluorescence measurement of Nanoplastics

To ensure sterile conditions, all polystyrene nanoparticles (NPs) used for experiments were sterilized using UV radiation. The fluorescence signals of all particle types remained clearly detectable after sterilization, ensuring their continued applicability for tracking and analytical purposes (refer to Figure 6 and 7) .

When comparing the fluorescence spectra before and after UV sterilization, characteristic differences between the nanoparticles types became evident. The highest signal prior to sterilization was observed for PS C50, reaching values close to 200,000 at its emission maximum. After UV treatment, the fluorescence decreased, but remained at the highest level among all tested particles, with a strong fluorescence signal. PS P50 also displayed strong fluorescence before sterilization, with maximum intensities around 175,000. After UV exposure, the peak decreased to approximately 155,000. The signal didn't drop significantly and it is also comparable to the signal of PS C50 after UV sterilization.

For PS P100, the fluorescence maximum was observed at approximately 130,000 before treatment, which then decreased to around 40,000 after sterilization. A similar trend was noted for PS A100, which dropped from roughly 100,000 to 60,000. These findings indicate that both PS P100 and PS A100 experience a pronounced decrease in signal strength. PS A50 showed values of about 60,000 before UV exposure and around 30,000 after exposure. This almost halved intensity highlights a comparatively high sensitivity of this particle type to UV exposure, resulting in a substantial loss of fluorescence.

PS C100, in contrast, demonstrated fluorescence stability. The fluorescence values of around 80,000 prior to sterilization remained the same after UV treatment.

The MQ blank served as a control and surprisingly displayed comparable fluorescence signals to some of the stained nanoplastics before and after UV.

In summary, all nanoparticle types showed a reduction in fluorescence after UV sterilization, but the extent of the decrease varied considerably. PS P100 was most strongly affected, while PS C100 retained a stable fluorescence profile.

PS C50 consistently provided the highest absolute fluorescence intensities both before and after treatment, making it particularly suitable for applications where a strong signal is required. Importantly, despite the losses, all particle types maintained fluorescence levels sufficient for reliable detection.

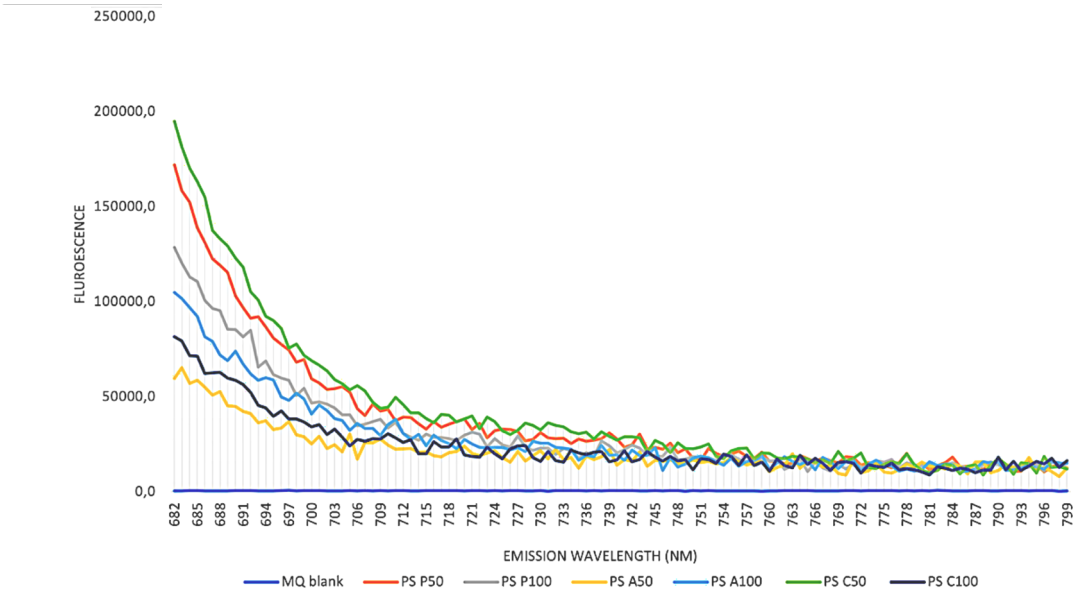

Figure 6: Polystyrene Nanoplastic, fluorescence measurement before UV sterilization was done at 620/640/800 nm with TECAN

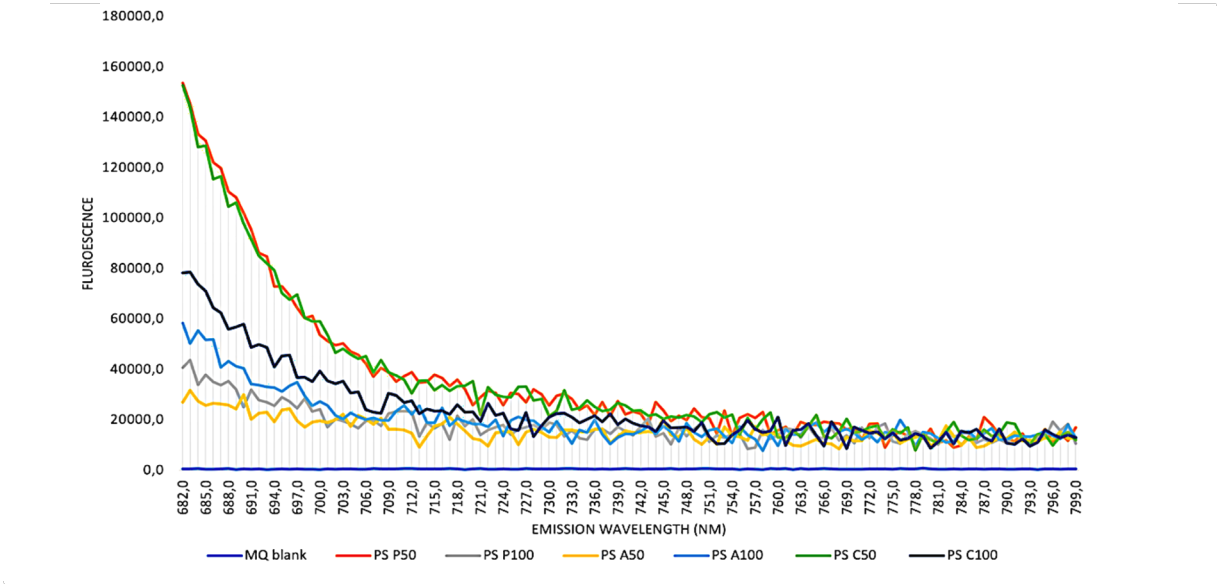

Figure 7: Polystyrene Nanoplastic, fluorescence measurement after UV sterilization was done at 620/640/800 nm with TECAN

7.2 Effects of potential environmental toxins on cell viability

7.2.1 Effects of 6ppd-Q on cell viability

This study investigated the potential toxic effects of 6ppd-Q on cells of the blood-brain barrier (BBB). hCMEC/D3 (human brain endothelial) and HMC3 (human microglial) cells were exposed to 6ppd-Q, and cell viability was assessed using MTT assays to determine potential cytotoxic and metabolic effects. Given the limited clinical research on the toxin, our study aimed to evaluate its impact on BBB cell health and viability, contributing to a better understanding of its potential (neuro)toxic effects.

Figures 8 and 9 present the results of the MTT cell viability assay performed with hCMEC/D3 (Figure 8) and HMC3 (Figure 9). The cells were seeded on 96-well plates and the 6ppd-Q was applied on the 6th day. MTT assay was performed on the following 7th day, after exposing the cells with the toxin for a duration of 24 hours.

7.2.2 6ppd-Q and hCMEC/D3 cells

All tested concentrations of the 6ppd-Q had a significant effect on viability of the hCMEC/D3 cells. The cell viability significantly decreased when exposed to higher concentrations of 6ppd-Q.

At 10,000 µg/ml; 3,000 µg/ml and 1,000 cell µg/ml viability drops significantly, with numbers being 47%, 43% and 44% respectively, indicating strong cytotoxic effects of 6ppd-Q at high concentrations. 300 µg/ml also show a significant reduced viability (lower than 55%). At 100 µg/ml, 30 µg/ml, and 10 µg/ml, cell viability increases again, nearing control levels (VC). The dose-response curve suggests a threshold where cytotoxic effects diminish.

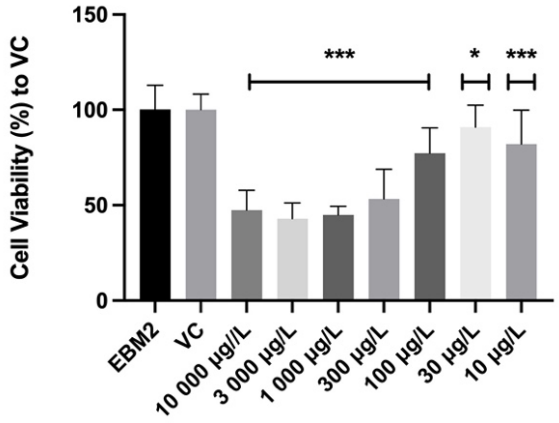

Figure 8: Effects of a 24h-treatment with 6ppd-Q on viability of hCMEC/D3 cells grown in EBM-2 medium at 37°C, 5% CO_2, 95% air atmosphere, 95% humidity, determined by MTT assay. Data were analyzed using one-way ANOVA with post hoc Holm-Sidak test. The results were represented as cell viability percentage relatively to the control (basal growth medium EBM-2) with vehicle (VC). The outliers were determined using the Grubbs test. Each column depicts a mean value ± SD from N = 18-36 individual measurements (n = 3 independent experiments) – control N = 36; otherwise N=18. The statistical significance of the data set was established via one-way ANOVA with confidence interval of 95% (*p<0.05, **p<0.005, ***p<0.001, ****p<0.0001).

7.2.3 6ppd-Q and Microglial (HMC3) cells

The exposure of HMC3 cells to all concentrations of 6ppd-Q resulted in a significant decrease in cell viability. A clear dose-dependant reduction in viability was observed, with higher concentrations of 6ppd-Q (10,000 µg/ml and 3,000 µg/ml) notably reducing cell viability. At 10,000 µg/ml cell viability drops to 70% and at 3,000 µg/ml to 66%. Even intermediate concentrations (1,000 µg/ml and 300 µg/ml) exhibited significant cytotoxic effects on the HMC3, with viability being 71% and 72%, respectively. In contrast, lower concentrations (100 µg/ml, 30 µg/ml, and 10 µg/ml) increase viability to near control levels (VC).

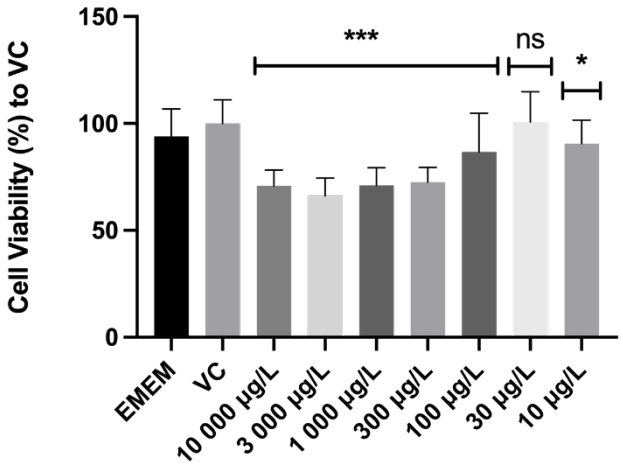

Figure 9: Effects of a 24 h-treatment with 6ppd-Q on viability of HMC3 cells grown in EMEM 5+ medium at 37°C, 5% CO_2, 95% air atmosphere, 95% humidity, determined by MTT assay. Data were analyzed using one-way ANOVA with post hoc Holm-Sidak test. The data shown are as mean ± SD. The results were represented as cell viability percentage relatively to the control (growth medium EMEM 5+) with vehicle (VC). The outliers were determined using the Grubbs test. Each column depicts a mean value ± SD from N = 18-36 individual measurements (n = 3 independent experiments) – control N = 36; otherwise N =18. The statistical significance of the data set was established via one-way ANOVA with confidence interval of 95% (*p<0.05, **p<0.005, ***p<0.001, ****p<0.0001).

7.3 Effects of stained nanoplastic particles on cell viability of hCMEC/D3

The viability study with hCMEC/D3 cells was also conducted with selected stained nano plastic particles. Given its extensive use in preliminary studies, PS pristine 100 nm was included in the analysis. PS aminated 100 nm was tested to ensure a diverse range of particle types. Additionally, PS carboxylated 50 nm was examined due to the notable cytotoxicity observed with its unstained version at high concentrations (300 µg/mL and 100 µg/mL), allowing us to determine whether staining influenced its toxic effects. The results of the MTT cell viability assays are depicted in Figures 10, 11, and 12. The cells were seeded on 96-well plates and the different types of stained nanoplastic particles were applied on the 6th day. MTT assays were performed on the 8th day, after exposing the cells with the nanoplastic for a duration of 47 hours.

The viability of hCMEC/D3 cells was significantly decreased to 72% by 100 µg/mL PS carboxylated 50 nm after 48 hours incubation compared to control with vehicle. 30 µg/mL and lower (10 µg/mL, 3 µg/mL, 1 µg/mL) showed no effects similar to the control groups.. In conclusion, stained carboxylated polystysrene nanoplastics of 50 nm exhibit dose-dependent cytotoxicity.

.

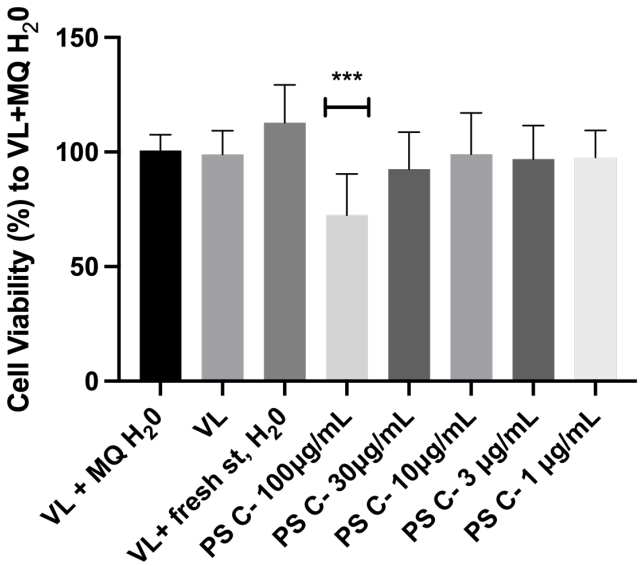

Figure 10: Effects of a 48h-treatment with stained carboxylated 50nm nanoplastics on viability of hCMEC/D3 cells grown in EBM-2 medium at 37°C, 5% CO_2, 95% air atmosphere, 95% humidity, determined by MTT assay. Data were analyzed using one-way ANOVA with post hoc Holm-Sidak test. The data shown are as mean ± SD. The results were represented as cell viability percentage relatively to the control (basal growth medium EBM-2) with vehicle. The outliers were determined using the Grubbs test. Each column depicts a mean value ± SD from N= 24-72 individual measurements (n = 3 independent experiments) – control N = 72; otherwise N=24. The statistical significance of the data set was established via one-way ANOVA with confidence interval of 95% (*p<0.05, **p<0.005, ***p<0.001, ****p<0.0001).

All tested concentrations of stained polystyrene pristine 100nm had no significant effect on viability of the hCMEC/D3 cells. H_20

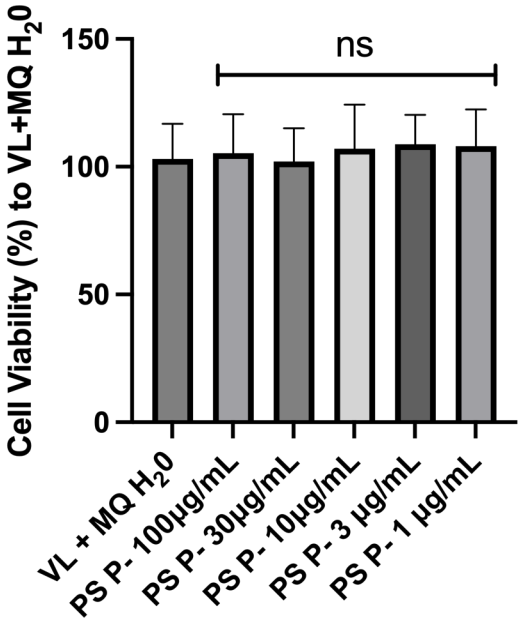

Figure 11: Effects of a 48h-treatment with stained pristine 100nm nanoplastics on viability of hCMEC/D3 cells grown in EBM-2 medium at 37°C, 5% CO_2, 95% air atmosphere, 95% humidity, determined by MTT assay. Data were analyzed using one-way ANOVA with post hoc Holm-Sidak test. The data shown are as mean ± SD. The results were represented as cell viability percentage relatively to the control (basal growth medium, EBM-2) with vehicle. The outliers were determined using the Grubbs test. Each column depicts a mean value ± SD from N = 16-18 individual measurements (n = 3 independent experiments) – control N = 18, PS P 100 µg/mL n = 16, otherwise N = 17. The statistical significance of the data set was established via one-way ANOVA with confidence interval of 95% (*p<0.05, **p<0.005, ***p<0.001, ****p<0.0001).

All tested concentrations of stained aminated polystyrene nanoplastics with 100 nm diameter had no significant effect on viability of the hCMEC/D3 cells.

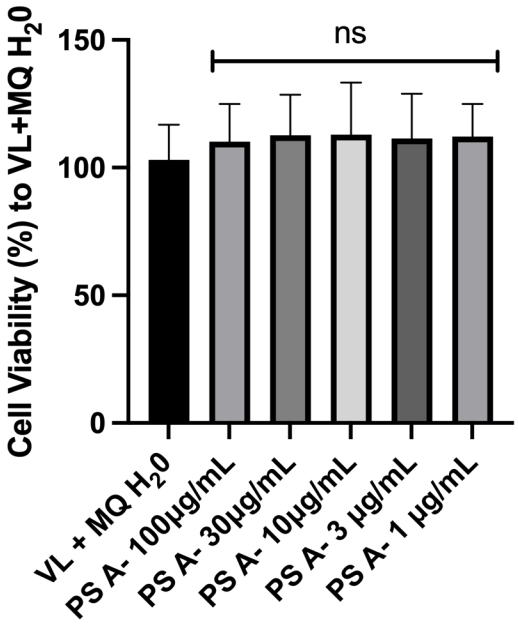

Figure 12: Effects of a 48h-treatment with stained aminated 100nm nanoplastics on viability of hCMEC/D3 cells grown in EBM-2 medium at 37°C, 5% CO_2, 95% air atmosphere, 95% humidity, determined by MTT assay. Data were analyzed using one-way ANOVA with post hoc Holm-Sidak test. The data shown are as mean ± SD. The results were represented as cell viability percentage relatively to the control (basal growth medium, EBM-2) with vehicle. The outliers were determined using the Grubbs test. Each column depicts a mean value ± SD from N = 18 individual measurements (n = 3 independent experiments) – control N = 18. The statistical significance of the data set was established via one-way ANOVA with confidence interval of 95% (*p<0.05, **p<0.005, ***p<0.001, ****p<0.0001).

7.4 Effects of unstained nanoplastics on cell viability of HMC3

With this study it was aimed to evaluate the potential toxic effects of unstained polystyrene nanoplastic types. Microglial cells HMC3 were exposed to six nanoplastic variants: polystyrene (100 nm and 50 nm), carboxylated polystyrene (100 nm and 50 nm), and aminated polystyrene (100 nm and 50 nm). Cellular viability was assessed using the MTT assay.

Figures 13-18 presented the results of the MTT cell viability assays conducted with HMC3. The cells were seeded on 96-well plates and the different nanoplastic types were applied on the 6th day. After 47 hours of exposure, the MTT assay was performed on the 8th day to evaluate cell viability.

The viability of HMC3 cells was decreased by the two highest concentration of unstained PS pristine 100 nm after 48 hours of incubation compared to control with vehicle. Cell viability was decreased by 300 µg/mL to 86% and by 100 µg/mL to 88% In contrast, lower concentrations (30 µg/mL, 10 µg/mL, 3 µg/mL and 1 µg/mL) had only minor effects on cell viability, which remained close to control levels. Cell viability was 92% at 30 µg/ml, 96% at 10 µg/ml, 95% at 3 µg/ml, and 100% at 1 µg/ml.

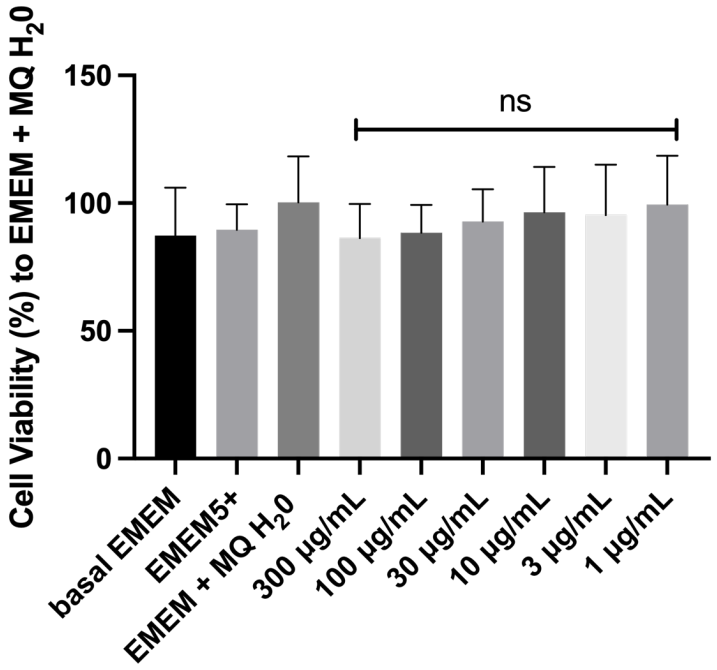

Figure 13: Effects of a 48h-treatment with unstained Polystyrene pristine 100nm nanoplastic on viability of HMC3 cells grown in EMEM 5+ medium at 37°C, 5% CO_2, 95% air atmosphere, 95% humidity, determined by MTT assay. Data were analyzed using one-way ANOVA with post hoc Holm-Sidak test. The data shown are as mean ± SD. The results were represented as cell viability percentage relatively to the control (growth medium EMEM 5+) with vehicle. The outliers were determined using the Grubbs test. Each column depicts a mean value ± SD from N =18-36 individual measurements (n = 3 independent experiments) – control N = 36. The statistical significance of the data set was established via one-way ANOVA with confidence interval of 95% (*p<0.05, **p<0.005, ***p<0.001, ****p<0.0001).

Compared to the EMEM + MQ control (normalized to 100%), no significant effects on the cell viability was observed at any tested concentration. While slight increases in viability were noted at lower concentrations (1–30 µg/mL), these changes were within the margin of variability and were not statistically nor biologically meaningful. Overall, polystyrene pristine 50 nm nanoparticles did not reduce cell viability at any concentration tested.

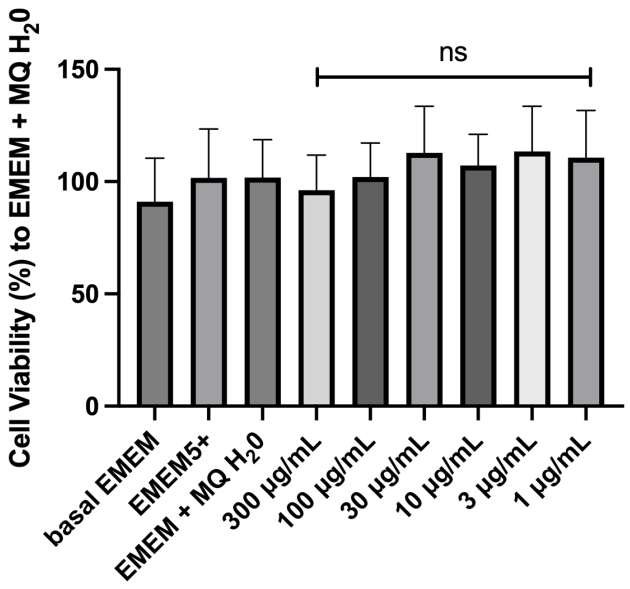

Figure 14: Effects of a 47h-treatment with unstained polystyrene pristine 50nm nanoplastic on viability of HMC3 cells grown in EMEM 5+ medium at 37°C, 5% CO_2, 95% air atmosphere, 95% humidity, determined by MTT assay. Data were analyzed using one-way ANOVA with post hoc Holm-Sidak test. The data shown are as mean ± SD. The results were represented as cell viability percentage relatively to the control (growth medium EMEM 5+) with vehicle. The outliers were determined using the Grubbs test. Each column depicts a mean value ± SD from N =18-36 individual measurements (n = 3 independent experiments) – control N = 36. The statistical significance of the data set was established via one-way ANOVA with confidence interval of 95% (*p<0.05, **p<0.005, ***p<0.001, ****p<0.0001).

At the highest concentration cell viability was reduced to 86 % by 300 µg/mL polystyrene carboxylated 100nm nanoparticles. 100 µg/mL condition reduced the cell viability to 88% and 30 µg/L to 91%.

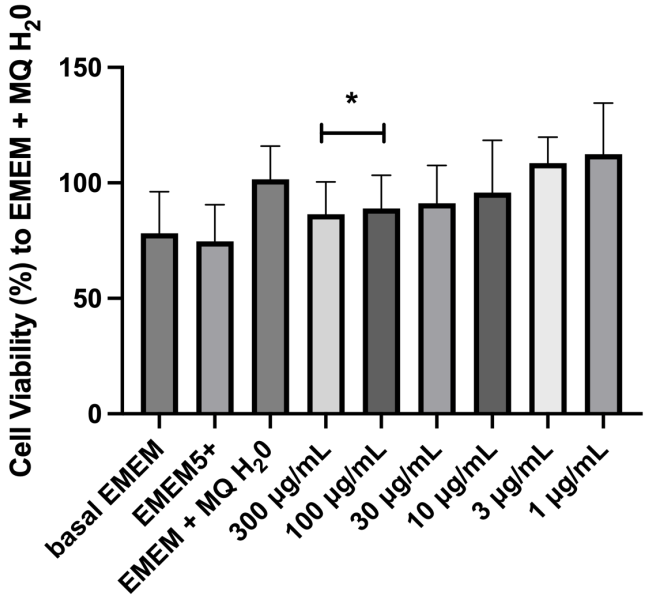

Figure 15: Effects of a 48 h-treatment with unstained Polystyrene carboxylated 100nm nanoplastic on viability of HMC3 cells grown in EMEM 5+ medium at 37°C, 5% CO_2, 95% air atmosphere, 95% humidity, determined by MTT assay. Data were analyzed using one-way ANOVA with post hoc Holm-Sidak test. The data shown are as mean ± SD. The results were represented as cell viability percentage relatively to the control (growth medium EMEM 5+) with vehicle. The outliers were determined using the Grubbs test. Each column depicts a mean value ± SD from N =18-36 individual measurements (n = 3 independent experiments) – control N = 36. The statistical significance of the data set was established via one-way ANOVA with confidence interval of 95% (*p<0.05, **p<0.005, ***p<0.001, ****p<0.0001).

As mentioned before, PS carboxylated 50 nm showed severe cytotoxicity at higher doses of 300 µg/mL and 100 µg/mL. The drop in cell viability at 300 µg/mL was 2%. 100 µg/mL reduced viability by nearly 50%, at 30 µg/mL the cell viability was reduced to 77%. Even the lower concentrations (1–10 µg/mL) seemed to reduce cell viability slightly, down to around 80–83%, but still statistically significantly.

These are by far the most pronounced effects, suggesting that C50nm PS-polystyrene nanoparticles are significantly more toxic to HMC3 cells than other polystyrene nanoplastic types.

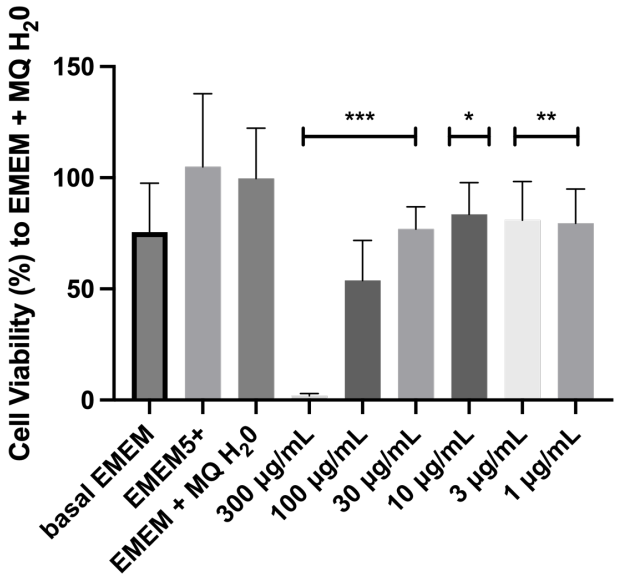

Figure 16: Effects of a 48 h-treatment with unstained Polystyrene carboxylated 50nm nanoplastic on viability of HMC3 cells grown in EMEM 5+ medium at 37°C, 5% CO_2, 95% air atmosphere, 95% humidity, determined by MTT assay. Data were analyzed using one-way ANOVA with post hoc Holm-Sidak test. The data shown are as meanc SD. The results were represented as cell viability percentage relatively to the control (growth medium EMEM 5+) with vehicle. The outliers were determined using the Grubbs test. Each column depicts a mean value ± SD from N =18-36 individual measurements (n = 3 independent experiments) – control N = 36. The statistical significance of the data set was established via one-way ANOVA with confidence interval of 95% (*p<0.05, **p<0.005, ***p<0.001, ****p<0.0001).

The viability of HMC3 cells was decreased by the highest concentration 300 µg/mL of unstained polystyrene aminated 100 nm to 88% after 48 hours of incubation compared to control with vehicle (EMEM +MQ). In contrast, lower concentrations (100 µg/ml, 30 µg/ml, 10 µg/ml, 3 µg/ml and 1 µg/ml) had only minor effects on cell viability, which remained close to or above control levels. Specifically, viability was 98% at 100 µg/ml, 100% at 30 µg/ml, 102% at 10 µg/ml, 110% at 3 µg/ml, and 118% at 1 µg/ml.

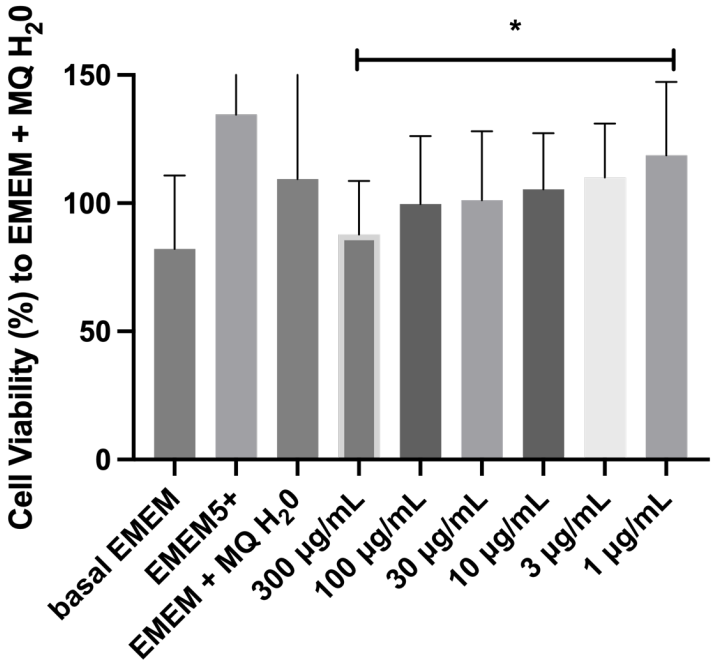

Figure 17: Effects of a 48h-treatment with unstained aminated 100nm nanoplastics on viability of HMC3 cells grown in EMEM 5+ medium at 37°C, 5% CO_2, 95% air atmosphere, 95% humidity, determined by MTT assay. Data were analyzed using one-way ANOVA with post hoc Holm-Sidak test. The data shown are as mean ± SD. The results were represented as cell viability percentage relatively to the control (basal growth medium EMEM 5+) with vehicle. The outliers were determined using the Grubbs test. Each column depicts a mean value ± SD from N = 24-48 individual measurements (n = 4 independent experiments) – control N = 48. The statistical significance of the data set was established via one-way ANOVA with confidence interval of 95% (*p<0.05, **p<0.005, ***p<0.001, ****p<0.0001).

The viability of HMC3 cells was significantly decreased by 300 µg/mL and 100 µg/mL polystyrene aminated 50 nm particles to 60% and 68% after 48 hours of incubation compared to control with vehicle (EMEM +MQ). At 30 µg/mL cell viability was reduced to 74%. Lower concentrations (1–10 µg/mL) also showed a slight reduction in viability, reaching 85% at 10 µg/mL, 84% at 3 µg/mL, and 85% at 1 µg/mL. These findings suggested a dose-dependent cytotoxic effect of PS-P A50nm nanoparticles in HMC3 cells, particularly at concentrations over 100 µg/mL.

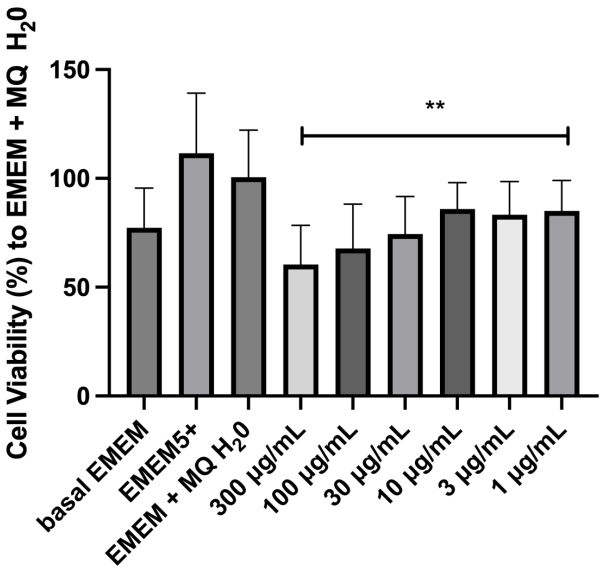

Figure 18: Effects of a 48h-treatment with unstained aminated 50nm nanoplastic on viability of HMC3 cells grown in EMEM 5+ medium at 37°C, 5% CO_2, 95% air atmosphere, 95% humidity, determined by MTT assay. Data were analyzed using one-way ANOVA with post hoc Holm-Sidak test. The data shown are as mean ± SD. The results were represented as cell viability percentage relatively to the control (growth medium EMEM 5+) with vehicle. The outliers were determined using the Grubbs test. Each column depicts a mean value ±SD from N = 18-36 individual measurements (n = 3 independent experiments) – control N = 36. The statistical significance of the data set was established via one-way ANOVA with confidence interval of 95% (*p<0.05, **p<0.005, ***p<0.001, ****p<0.0001).

7.5 Effects of Air filter dust extracts on lung cell proliferation

Following the initial screening of all 124 extracted samples using the A549 monoculture model, only those that showed a significant reduction in cell viability, specifically below 70% as determined by the MTT assay, were selected for further investigation. This pre-selection allowed to concentrate on the most promising samples. In total, 13 extracts met this criteria and were subsequently tested in a more advanced and physiologically relevant *in vitro* model: the Transwell system using a co-culture of A549 lung epithelial cells and human brain endothelial cells (D3).

This model was intentionally selected based on previous findings suggesting that nanoparticles inhaled into the lungs can translocate via the bloodstream to the brain. (Qi et al., 2022)

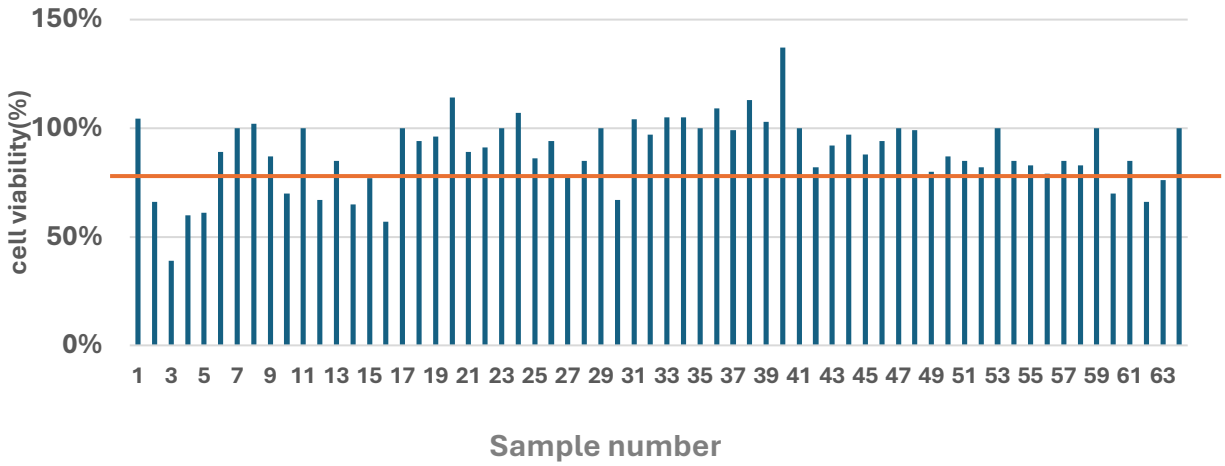

Figure 19: Summary of the cell viability data of A549 cells after exposure to samples collected from schools and houses during winter. Only the extracts that showed less than 70% cell viability were chosen for the Transwell System Model with co-culture of A549/D3.

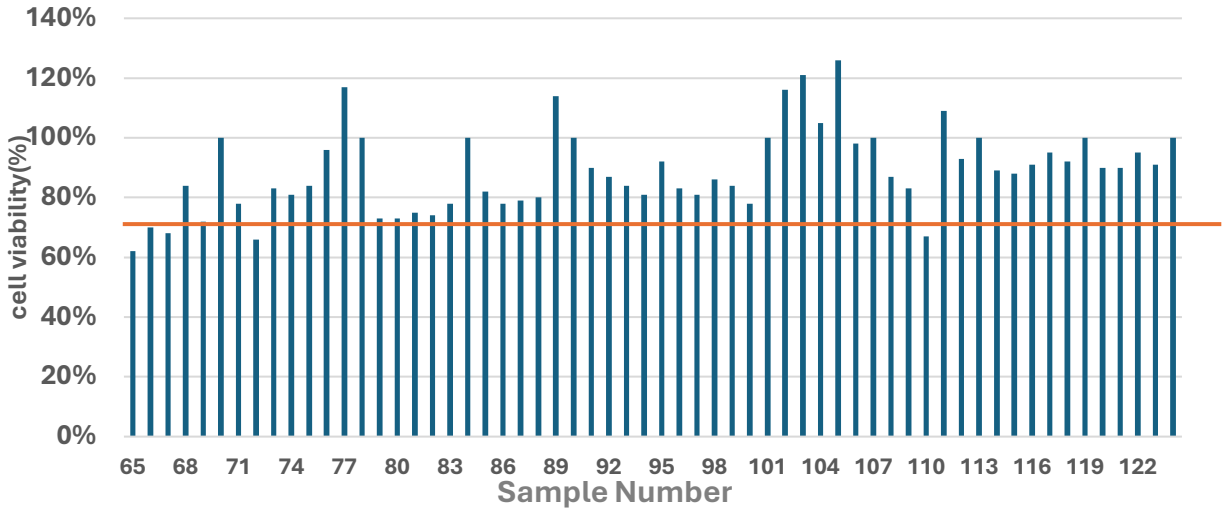

Figure 20: Summary of the cell viability data of A549 cells after exposure to samples collected from schools and houses during summer. Only the extracts that showed less than 70% cell viability were chosen for the Transwell System Model with co-culture of A549/D3.

Table 8 below showed the samples with strongest cell viability reduction after the screening and highlights the 13 samples that were selected for further experiments. The pink coloured 9 samples from the winter season and 4 samples from the summer seasonwere selected for the further studies in the Transwell model.

School 1 -Winter	**School 1 - Summer**
2A (66%)	65A (62%)
3A(39%)	66A (70%)
4A (60%)	67A (68%)
5A (61%)	69A (72%)
School 2 -Winter	**School 2 - Summer**
7A (96%)	71A (78%)
9A (87%)	72A (66%)
10A (70%)	73A (83%)
School 3 -Winter	**School 3 - Summer**
12A (67%)	74A (81%)
14A (65%)	75A (84%)
15A (78%)	76A (96%)
16A (57%)	77A (117%)
School 6 - Winter	**School 6 - Summer**
30A (67%)	92A (87%)
31A (104%)	93A (84%)
32A (97%)	94A (81%)
33A (105%)	95A (92%)
House 5 - Winter	**House 5 - Summer**
59A (70%)	108A (87%)
60A (85%)	109A (73%)
61A (66%)	110A (67%)
62A (76%)	111A (109%)
63A (76%)	112A (93%)

Table 8. Summary of the cell viability data of A549 cells after exposure to samples collected from schools and houses during winter and summer. A total of 13 samples reduced cell viability below 70% (highlighted) and were therefore selected for further analyses.

7.6 NTA data correlation to cell viability of the extract screening

Table 9 below summarizes the physicochemical properties and biological performance of the 124 samples used in the experiments, where effects of filtered indoor extracts on human lung cells (A549) were tested. Samples 1-63 were collected in the winter season, whereas samples 64-124 were collected during the summer. The table includes the median particle size (nm), zeta potential (ZP, mV), particle concentration (particles/mL), x-fold cell viability relative to a control, and the standard deviation (SD) for each measurement. This dataset allows for comparison of particle stability, surface charge, and potential cytotoxic effects across different formulations, highlighting trends between size, surface charge, concentration, and cell viability.

Table 9. NTA Data for filtered indoor particles from Spain. It includes the median particle size (nm), zeta potential (ZP, mV), particle concentration (particles/mL), x-fold cell viability relative to a control, and the standard deviation (SD) for each measurement.

Sample Number	Median size [nm]	ZP [mV]	Conc. [particles/mL]	X-Fold Viability (MW)	SD
1	106.9	-16.41	5.10E+07	1	0.131
2	121.4	-12.71	1.30E+08	0.640	0.124
3	118.3	-11.63	3.80E+08	0.421	0.063
4	109.4	-11.00	1.90E+08	0.602	0.096
5	104.2	-8.07	1.20E+08	0.703	0.115
6	120.8	-6.09	1.30E+08	0.850	0.366
7	116.7	-11.38	8.40E+07	0.965	0.077
8	116.2	-6.92	8.80E+07	1.031	0.119
9	121.5	-8.41	1.40E+08	0.873	0.073
10	137.5	-9.57	1.80E+08	0.699	0.036
11	175.4	-11.46	2.10E+08	1	0.172
12	130.3	-10.45	2.90E+08	0.667	0.172
13	142.5	-8.64	1.80E+08	0.850	0.097
14	124.3	-6.10	5.30E+08	0.652	0.084
15	121.7	-12.54	8.20E+07	0.775	0.138

16	158.0	-9.81	2.80E+08	0.570	0.127
17	132.0	-5.35	6.50E+07	1	0.153
18	126.6	-10.83	4.40E+08	0.939	0.122
19	116.8	-11.90	3.30E+08	0.965	0.160
20	126.5	-13.37	2.50E+08	1.140	0.253
21	110.6	-11.40	2.50E+08	0.890	0.136
22	118.0	-9.33	3.40E+08	0.906	0.269
23	170.0	-4.02	1.70E+08	1	0.154
24	159.3	-6.13	2.40E+08	1.071	0.165
25	124.6	-4.63	3.00E+08	0.864	0.135
26	157.5	-2.53	2.70E+08	0.940	0.149
27	147.5	-4.08	3.00E+08	0.779	0.129
28	151.5	-4.59	3.30E+08	0.853	0.107
29	117.5	-3.84	4.50E+07	1	0.195
30	117.2	-4.19	1.14E+08	0.674	0.250
31	120.2	-3.83	6.60E+07	1.042	0.203
32	116.4	-5.93	1.10E+08	0.969	0.150
33	121.9	-5.80	1.40E+08	1.050	0.190
34	118.4	-6.37	1.00E+08	1.048	0.208
35	112.9	-5.35	6.20E+07	1	0.170
36	123.2	-6.51	9.50E+07	1.089	0.174
37	136.2	-3.79	3.30E+08	0.985	0.375
38	125.0	-2.97	4.50E+08	1.134	0.231
39	132.4	-5.94	3.70E+08	1.030	0.324
40	126.2	-6.48	6.90E+08	1.369	0.586
41	130.6	-4.28	5.40E+07	1	0.210
42	139.0	-3.41	4.70E+08	0.819	0.153
43	137.0	-4.51	3.30E+08	0.918	0.172
44	135.0	-6.37	3.70E+08	0.970	0.237
45	137.1	-4.62	2.00E+08	0.885	0.267
46	134.4	-6.12	3.80E+08	0.937	0.105

47	122.5	-1.06	1.90E+07	1	0.183
48	140.0	-4.92	1.00E+08	0.989	0.113
49	132.5	-6.64	7.30E+07	0.799	0.134
50	143.0	-4.52	9.80E+07	0.873	0.173
51	128.5	-6.17	1.80E+08	0.848	0.142
52	136.1	-6.74	1.90E+08	0.822	0.101
53	114.7	-7.07	2.10E+08	0.847	0.076
54	142.9	-6.06	2.10E+08	0.831	0.045
55	142.5	-7.58	3.20E+08	0.791	0.093
56	141.2	-6.36	3.10E+08	0.851	0.077
57	117.1	-6.72	4.40E+07	0.826	0.087
58	121.2	-6.22	5.80E+07	1	0.207
59	128.3	-6.09	1.10E+08	0.703	0.068
60	130.7	-7.46	3.70E+08	0.847	0.199
61	131.2	-8.13	4.50E+08	0.663	0.080
62	111.2	-3.71	7.90E+08	0.762	0.167
63	116.8	-5.14	3.70E+08	0.759	0.098
64	108.0	-4.07	2.70E+07	1	0.209
65	133.9	-7.26	2.20E+08	0.622	0.104
66	147.9	-5.46	4.70E+08	0.703	0.389
67	135.4	-7.00	4.10E+08	0.678	0.126
68	152.8	-8.06	3.80E+08	0.844	0.108
69	153.7	-3.83	5.10E+08	0.724	0.083
70	101.2	-6.78	2.70E+06	1	0.145
71	135.4	-6.22	3.00E+07	0.782	0.105
72	125.0	-4.77	1.80E+07	0.663	0.128
73	149.6	-5.96	1.00E+07	0.830	0.121
74	136.0	-4.60	2.10E+07	0.809	0.119
75	118.9	-6.06	1.20E+07	0.835	0.099
76	128.8	-5.42	1.20E+07	0.960	0.187
77	133.2	-5.77	1.60E+07	1.169	0.196

78	119.8	-8.81	3.90E+07	1	0.110
79	135.0	-5.40	2.10E+08	0.726	0.060
80	133.9	-8.48	2.00E+08	0.729	0.206
81	131.6	-4.64	2.40E+08	0.746	0.052
82	141.4	-5.90	2.60E+08	0.741	0.064
83	130.0	-5.94	4.10E+08	0.780	0.075
84	119.8	-8.81	3.90E+07	1	0.095
85	135.0	-5.40	2.10E+08	0.816	0.080
86	133.9	-8.48	2.00E+08	0.783	0.077
87	131.6	-4.64	2.60E+08	0.791	0.047
88	141.4	-5.90	2.60E+08	0.801	0.074
89	130.0	-5.94	4.10E+08	1.138	0.812
90	105.9	-5.33	2.90E+07	1	0.094
91	125.6	-6.05	1.20E+08	0.903	0.123
92	110.4	-7.09	4.40E+08	0.870	0.165
93	117.0	-8.37	2.50E+08	0.841	0.105
94	113.5	-6.31	2.30E+08	0.813	0.176
95	121.8	-4.60	1.70E+08	0.919	0.182
96	98.2	-5.23	4.10E+06	1	0.094
97	127.8	-3.83	2.40E+07	0.981	0.127
98	131.7	-3.94	1.60E+07	1.035	0.169
99	134.0	-2.68	3.40E+07	1.014	0.124
100	134.7	-6.10	2.50E+07	0.939	0.166
101	123.1	-8.55	2.20E+07	1	0.138
102	145.8	-6.60	2.00E+08	1.155	0.162
103	126.7	-5.38	3.90E+08	1.214	0.067
104	117.4	-4.91	4.30E+08	1.051	0.154
105	105.9	-4.92	4.10E+08	1.263	0.150
106	125.9	-6.77	2.30E+08	0.984	0.051
107	178.1	-8.32	2.10E+07	1	0.248
108	163.0	-4.63	4.10E+08	0.873	0.245

109	113.0	-6.21	4.60E+08	0.733	0.250
110	136.9	-5.20	5.00E+08	0.672	0.050
111	111.0	-3.66	2.00E+08	1.093	0.099
112	194.6	-6.34	3.10E+08	0.934	0.126
113	138.6	-1.56	3.10E+07	1	0.080
114	130.3	-2.61	2.50E+08	0.886	0.093
115	124.0	-6.00	2.80E+08	0.878	0.079
116	132.5	-5.26	6.70E+08	0.914	0.162
117	98.8	-3.99	5.20E+08	0.947	0.063
118	121.8	-4.44	5.90E+08	0.921	0.103
119	165.2	-6.33	8.30E+07	1	0.098
120	139.8	-8.01	2.40E+08	0.904	0.095
121	132.2	-2.32	3.00E+08	0.900	0.118
122	116.5	-5.43	2.10E+08	0.953	0.067
123	136.5	-7.13	2.00E+08	0.914	0.076
124	120.1	-3.65	5.10E+08	0.998	0.094

No correlation was found between any particle data type with the cell viability indicating other compounds in the extracts relevant for the cell viability reductions.

7.7 Optimization of the A549/D3 co-culture Transwell® model

The results of the MTT assay for samples 2, 3 and 4 selected from the screen showed a change in A549 cell viability compared to the extraction buffer control (EB) under medium condition DMEM basal (Figure 21A) and DMEM with FBS both apically and basolaterally. (Figure 21 B) In DMEM basal medium, some variability was observed, with extract 4A showing a reduced viability around 80%. When FBS was present in both apical and basolateral compartments, sample 2A showed a tendency toward reduced viability (83%), whereas 4A displayed a slight increase of 158% relative to EB (Figure 21 B). In contrast, in the presence of 10% FBS apically without basolateral supplementation, extract-induced effects were less variable, and viability remained consistently close to EB levels. (Figure 21 C)

The cytotoxic control (EGTA, 3 mM) strongly reduced cell viability in all conditions, confirming assay sensitivity.

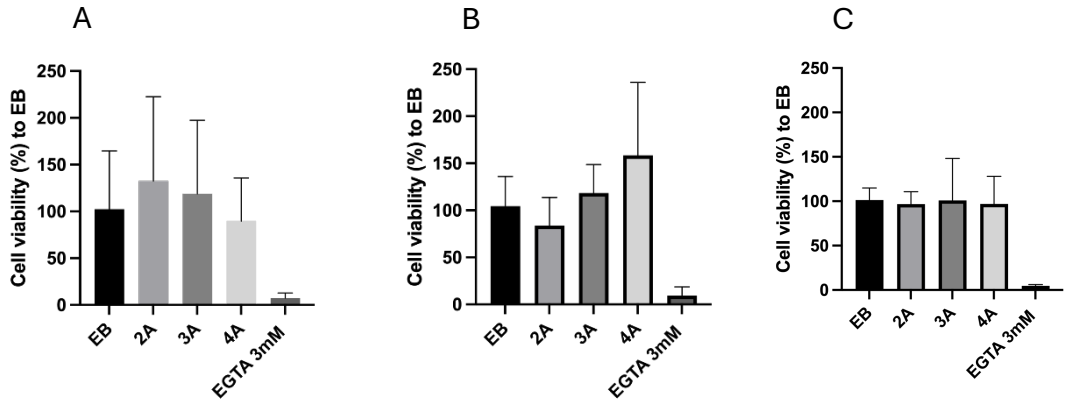

Figure 21: Cell viability of A549 cells after exposure to filter extracts (2A, 3A, 4A) compared to extraction buffer control (EB), determined by MTT assay. Cells were cultured in (A) DMEM basal medium, (B) DMEM with 10% FBS both apically and basolaterally (C) DMEM with 10% FBS apically and no FBS basolaterally. EGTA (3 mM) was used as a positive control. Each column depicts a mean value ± SD from N= 3-9 individual measurements (n = 3 independent experiments) – control N = 3 . The statistical significance of the data set was established via one-way ANOVA with confidence interval of 95% (*p<0.05, **p<0.005, ***p<0.001, ****p<0.0001).

The results of the MTT assay for samples 2, 3, and 4 revealed an increase in hCMEC/D3 cell viability under all three tested media conditions. Under DMEM basal medium cell viability increased around 127% for sample 2A, 135% for 3A and 154% for 4A (Figure 22 A). When both the basolateral and apical compartments contained DMEM with 10% FBS, the viability was around 130% for 2A and 3A and 124% for 4A (Figure 22B).

In DMEM without FBS in the basolateral compartment, but with 10% FBS on the apical side, hCMEC/D3 cells showed enhanced viability of around 180% for 2A, 165% for 3A and 130% for 4A (Figure 22C). Interestingly, even in this condition where FBS was absent from the basolateral compartment, hCMEC/D3 cells still exhibited improved viability. This pattern suggested that the absence of serum may lead to more pronounced cytotoxic effects, possibly because serum proteins can bind and sequester harmful compounds or particles, reducing their bioavailability and toxicity.

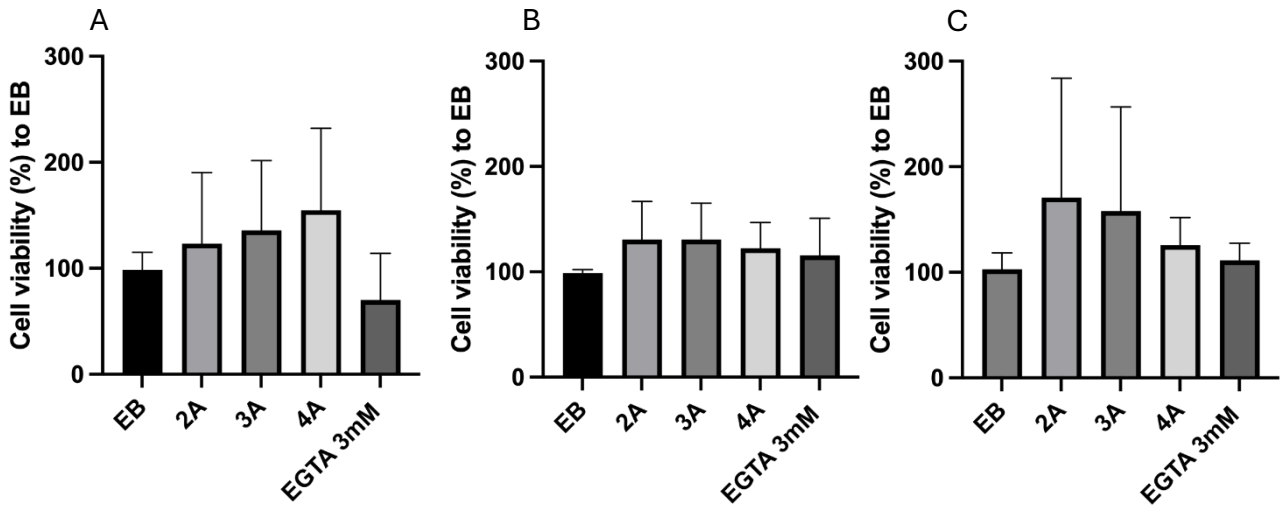

Figure 22: Cell viability of D3 cells after exposure to filter extracts (2A, 3A, 4A) compared to extraction buffer control (EB), determined by MTT assay. Cells were cultured in (A) DMEM basal medium,(B) DMEM with FBS both apically and basolaterally (C) DMEM with FBS apically and no FBS basolaterally. EGTA (3 mM) was used as a positive control. Each column depicts a mean value ± SD from N = 3-9 individual measurements (n = 3 independent experiments) – control N = 3 The statistical significance of the data set was established via one-way ANOVA with confidence interval of 95% (*p<0.05, **p<0.005, ***p<0.001, ****p<0.0001).

Figure 23A showed reductions in A549 cell viability after exposure to the tested extracts. Samples 12A,14A, 16A demonstrated cell viabilites of around 69%, 83% and 88% respectively. Sample 72A, also showed a drop in cell viability of around 80%. These values indicate a consistent but not severe cytotoxic effect across the different extracts. In comparison, the positive control EGTA (3 mM) resulted in a marked decrease in cell viability to 5.8%.

Figure 23B also demonstrated moderate reductions in A549 cell viability following exposure to the tested extracts. Samples 30A, 61A, 64A, 65A and 67A showed cell viabilities of approximately 86%,88% , 86% and 75% respectively. These values indicate a consistent but not severe cytotoxic effect across the different extracts. In comparison, the positive control EGTA (3 mM) resulted in a marked decrease in cell viability to 4%.

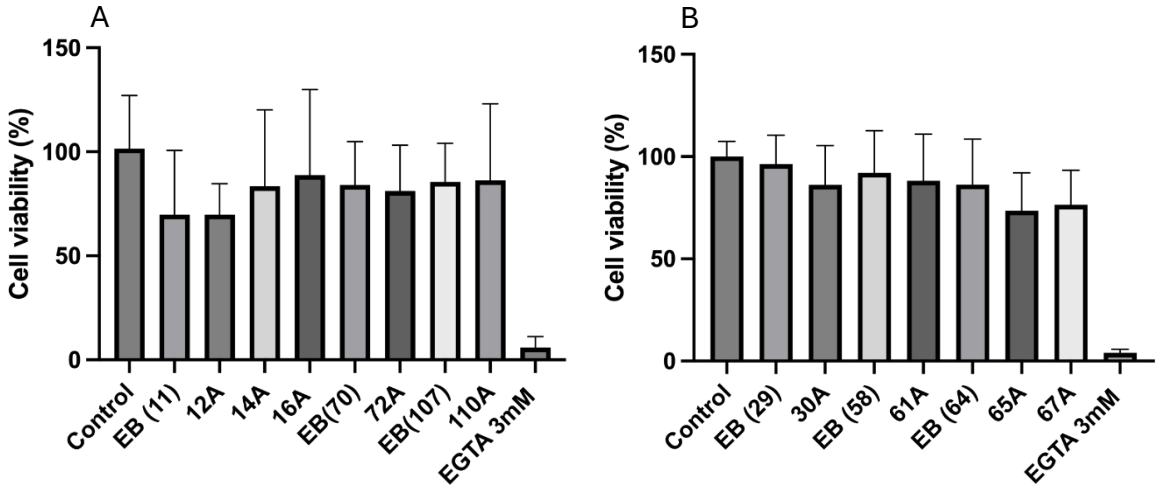

Figure 23: Cell viability of A549 cells after exposure to filter extracts compared to extraction buffer control (EB), determined by MTT assay. Cells were cultured in DMEM with FBS apically and no FBS basolaterally,. EGTA (3 mM) was used as a positive control. Each column depicts a mean value ± SD from N= 3-9 individual measurements (n = 3 independent experiments) – control N = 3 The statistical significance of the data set was established via one-way ANOVA with confidence interval of 95% (*p<0.05, **p<0.005, ***p<0.001, ****p<0.0001).

The results of the MTT assay for hCMEC/D3 cells on the basolateral side (Figure 24A) showed a general increase in metabolic activity in response to all tested extracts compared to the respective extraction buffer (EB) controls. Samples 12A,14A, and 16A exhibited viabilities of approximately 107%, 145%, and 133%, indicating a moderate but consistent elevation in cell viability. Similarly, EB(70) and 72A reached around 113% and 130%, while EB(107) and 110A showed 98.5% and 99%, respectively.

Figure 24B demonstrated a notable increase in cell viability following exposure to the tested extracts. Especially samples 30A, 61A, 65A and 67A showed a prominent increase in cell viabilities of approximately 168%, 120% ,165 % and 134% respectively.

Notably, EGTA (3 mM**)**, used as a positive control, induced a pronounced increase in MTT signal , in both Figures 24 A and B reaching**,** approximately 132% in Figure 24A and 198% in Figure 24B**.**

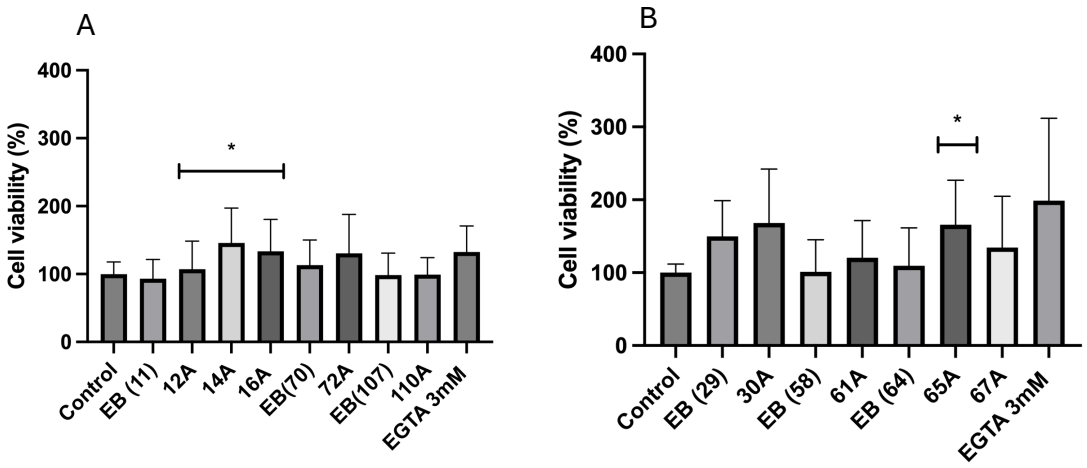

Figure 24 : Cell viability of hCMEC/D3 cells after exposure to filter extracts compared to extraction buffer control (EB), determined by MTT assay. Cells were cultured in DMEM with FBS apically and no FBS basolaterally,. EGTA (3 mM) was used as a positive control. Each column depicts a mean value ± SD from N = 3-9 individual measurements (n = 3 independent experiments) – control n = 3 . The statistical significance of the data set was established via one-way ANOVA with confidence interval of 95% (*p<0.05, **p<0.005, ***p<0.001, ****p<0.0001). In Figure 24 A, samples 12A,14A and 16A showed a statistical significance in comparison to their respective extraction buffer, EB 11. In Figure 24 B, sample 65A showed a statistical significance in comparison to its respective extraction buffer, EB 64.

7.8 TEER Results of A549/D3 Transwell® model

To evaluate the effect of extracts (samples 2, 3, and 4) on epithelial barrier integrity, transepithelial electrical resistance (TER) was measured in a Transwell model with A549 in the apical compartment and hCMEC/D3 in the basolateral compartment. The measurement was done once at 0h with the extracts and once after 48h before the MTT assay was performed. Measurements were performed for samples 2, 3, and 4 and are reported as mean ± SD (n = 3). Results indicated that the presence or absence of serum significantly influenced TER. In the absence of serum (0%/0%) in the basolateral compartment, more pronounced reductions in TEER were observed, suggesting that barrier integrity is more sensitive under serum-free conditions. Interestingly, even without serum basolaterally, hCMEC/D3 cells maintained improved viability. Overall, the most stable TEER values were obtained with the medium containing serum in the apical compartment and no serum in the basolateral compartment.

Table 10. Results of transepithelial electrical resistance (TER**)** measurement in a Transwell model with A549 in the apical compartment and hCMEC/D3 in the basolateral compartment. Measurements were performed for samples 2, 3, and 4 and are reported as mean ± SD (n = 3).

Extraxt/Sample	0% / 0%	10% / 10%	10% / 0%
Control – 0h	100 ± 3	91 ± 14	82 ± 2
EB	100 ± 7	114 ± 17	92 ± 11
2	109 ± 2	121 ± 23	88 ± 5
3	95 ± 29	128 ± 18	109 ± 14
4	109 ± 8	123 ± 1	103 ± 8
Control – 48h	84 ± 17	129 ± 1	94 ± 11
EB	104 ± 16	157 ± 9	127 ± 3
2	90 ± 16	161 ± 15	108 ± 9
3	49 ± 13	163 ± 17	105 ± 8
4	67 ± 21	143 ± 1	110 ± 7

Table 11 showed results of TER measurements performed on the 13 extracts that were selected for further experiments and are reported as mean ± SD (n = 3). The selected condition was DMEM with 10 % FBS in the apical compartment (A549) and no FBS in the basolateral compartment (hCMEC/D3). The measurement was done once at 0h with the extracts and once after 48h before the MTT assay was performed. Analysis of the TER measurements revealed no significant changes between the tested conditions.

Table 11. Results of transepithelial electrical resistance (TER) measurement in a Transwell model with A549 in the apical compartment and hCMEC/D3 in the basolateral compartment. Measurements were performed for samples EB (11), EB(70), EB(107), EB(29), EB(58), EB(64), 12, 14, 16, 72, 30, 61,65, 67, 110 and are reported as mean ± SD (n = 3). Samples 30 and 72 weren't statistically significant to their respective EB, EB(29) and EB(70).

Extraxt/Sample	10% / 0%
Control – 0h	100 ± 1
EB (11)	100 ± 2
12	100 ± 4
14	95 ± 3
16	103 ± 4
EB (70)	100 ± 3
72	85 ± 4
EB (107)	100 ± 3
110	102 ± 6
Control – 48h	100 ± 1
EB (11)	100 ± 1
12	111 ± 5
14	105 ± 3
16	107 ± 5
EB (70)	100 ± 2
72	103 ± 5
EB (107)	100 ± 1
110	102 ± 5

Extraxt/Sample	10% / 0%
Control – 0h	100± 1
EB (29)	100 ± 2
30	88 ± 3
EB (58)	100 ± 3
61	90 ± 2
EB (64)	100 ± 4
65	111 ± 14
67	99 ± 6
Control – 48h	100 ± 1
EB (29)	100 ± 2
30	100 ± 3
EB (58)	100 ± 2
61	95 ± 4
EB (64)	100 ± 1
65	98 ± 6
67	91 ± 4

8 Discussion

This thesis explored multiple aspects of nanoparticle as well as chemical and undefined air borne extract exposure on cellular models. Three main experimental components were investigated: (1) exposure of artificial polystyrene nanoparticles on cells of the human neurovascular unit, hCMEC/D3 and HMC3, (2) the effects of the environmentally relevant compound 6PPD-quinone, and (3) the impact of an undefined environmental extract containing unknown substances.

As anticipated, exposure to UV light caused a reduction in fluorescence intensity. According to Nurmukhametov *et al.,(*2007), the loss of fluorescence intensity in polystyrene based materials after UV exposure results from either a photochemical degradation or radiation-induced chemical conversions in the molecule.

8.1 Effects on cell viability

The results of the MTT cell viability assays demonstrated that exposure to 6PPD-quinone and various polystyrene nanoplastic types induced clear concentration-dependent effects of hCMEC/D3 and HMC3 cells.

For 6PPD-Q, a significant decrease in cell viability was observed at higher concentrations in both cell types. In hCMEC/D3, viability dropped to below 50% at 10,000 µg/L, 3,000 µg/L and 1,000 µg/L, indicating strong cytotoxicity at these doses. At 300 µg/L, viability remained significantly reduced (around 55%), whereas lower concentrations (100 µg/L, 30 µg/L, 10 µg/L) showed a return to values close to control levels. A similar dose-response was seen in HMC3 cells, with the highest concentrations (10,000 µg/L and 3,000 µg/L) causing viability reductions to 70% and 66%, respectively, while intermediate concentrations (1,000 µg/L and 300 µg/L) still showed significant effects (around 71–72%).

A cell type dependant response was observed with hCMEC/D3 cells showing a stronger reduction in viability at higher concentrations than HCM3 microglia. This is consistent with reports of oxidative stress responses in human cerebral endothelial cells following exposure to p-phenylenediamine-derived quinones. Xia *et al.*, (2025) reported increased reactive oxygen species and stress-related cellular responses in hCMEC/D3 cells after

exposure to PPD-quinone compounds. The ratio of PPD-Q to PPD was up to three times higher in smaller particles (0.056–0.1 µm) than in larger ones (10–18 µm), indicating that particle size plays a major role in atmospheric transformation and potential human exposure patterns (Xia *et al.*, 2025).

In the case of nanoparticle exposures, distinct patterns emerged depending on particle size and surface chemistry**.** PS C 50nm was chosen for this experiment, because this type of size and chemistry proved to be the most toxic to hCMEC/D3 (and other) cells in previous studies (cell viability and cellular uptake studies) done by other team members at AIT (Chmielewska, 2023).

For hCMEC/D3, exposure to stained carboxylated polystyrene nanoparticles (PS C50) led to a marked and statistically significant reduction in viability to around 72% at 100 µg/mL, while lower concentrations (30 µg/mL and below) were not significantly different from controls, indicating a clear dose-dependent effect. By contrast, exposure to stained plain polystyrene (P100) and aminated polystyrene (A100) did not significantly affect viability at any tested concentration, suggesting lower acute toxicity of these larger particles in endothelial cells.

These findings align with previously reported data demonstrating that smaller particles (Banerjee et al., 2021) and charged surfaces interact more strongly with cell membranes**,** leading to enhanced uptake and higher cytotoxicity (Fröhlich, 2012). The high toxicity of carboxylated 50 nm particles are related to their small size , which enhance cellular interaction and stress responses. Aminated particles, especially A50nm can also induce membrane damage and mitochondrial stress, due to their size and positive charge (Fröhlich, 2012). In line with these findings, exposure of HMC3 microglial cells to aminated A50 nanoparticles resulted in a pronounced, concentration-dependent decrease in cell viability in the present study. Cell viability was reduced to approximately 60 % and 68 % at the highest tested concentrations of 300 µg/mL and 100 µg/mL, respectively, and remained decreased to about 74 % even at 30 µg/mL. These findings suggested a dose-dependent cytotoxic effect of PS-P A50nm nanoparticles in HMC3 cells, particularly at concentrations over 100 µg/mL.

Importantly, the MTT assay measures mitochondrial metabolic activity rather than absolute cell death (Ghasemi *et al.,* 2021). A decrease in MTT signal reflects reduced

mitochondrial dehydrogenase activity, which may indicate cell death but can also reflect stress or metabolic slowdown. Therefore, the observed reductions in MTT signal at higher concentrations should be interpreted as strong mitochondrial impairment**,** likely accompanied by partial cell death at the most toxic doses.

The differential sensitivity between endothelial and microglial cells may reflect their distinct physiological roles: endothelial cells form the BBB and have robust barrier functions (Wu *et al.,* 2023) whereas microglia serve as resident immune cells that readily initiate inflammatory responses(Dello Russo *et al.,* 2018) In experimental and injury models, microglia are primary producers of key proinflammatory cytokines, such as TNF-α, IL-6, IL-1β) (Bourne *et al.*, 2025) and become activated by signals from stressed endothelial cells. Together, these data support the notion that endothelial cells are structurally and functionally geared toward a barrier role, whereas microglia are primed for immune activation under challenge. The extremely high sensitivity of HMC3 to C50nm nanoparticles supports this, suggesting microglia could act as early targets in nanoparticle-induced neurotoxicity.

Finally, the dose-dependent cytotoxic effects of 6PPD-Q observed in this study are consistent with emerging literature reporting its strong toxic potential in human cell models (Qi *et al.,* 2024).

These findings highlight that both nanoparticle properties (size, surface chemistry) and chemical pollutants like 6PPD-Q can compromise BBB-associated cells. They also emphasize the need for further mechanistic studies including ROS measurements, cytokine profiling, or extracellular vesicle analysis to complement the MTT data and better understand the pathways underlying these toxic effects.

8.2 Pilot experiment: A549 screening monoculture and A549/hCMEC/D3 co-culture Transwell® model

To explore whether a combined lung–neurovascular barrier model could provide additional insight into nanoparticle translocation and cellular effects, pilot experiments were conducted using A549 alveolar epithelial cells grown first as a monoculture, then as the apical layer in a Transwell system with hCMEC/D3 endothelial cells in the basolateral compartment. This setup aimed to mimic a simplified lung-to-brain exposure

scenario and assess its barrier characteristics (TER) and cellular mitochondrial activity (MTT) following the exposure of undefined environmental extracts.

A large-scale screening of 124 environmental extracts obtained from indoor air filters collected in schools and residential buildings revealed marked variability in their effects on A549 lung epithelial cell viability. Initial MTT assays identified 13 samples that reduced viability to below 70% compared to controls, indicating potential cytotoxicity. These samples were selected for more detailed testing in a co-culture (Transwell) system.

Pilot experiments using samples 2, 3, and 4 demonstrated moderate to pronounced effects on A549 viability depending on medium composition. In serum-free basal medium, extract 4 reduced viability of hCMEC/D3 to approximately 80%, while extracts 2 and 3 showed smaller changes. When 10% FBS was added to both apical and basolateral compartments, sample 2 produced a slight but measurable reduction in viability (~83%), whereas sample 4 led to an increase in metabolic activity (158% of control). In contrast, under conditions with 10% FBS only in the apical compartment, viability remained close to control for all three extracts, suggesting that serum proteins may bind or neutralize toxic components, thereby mitigating their cytotoxic potential.

Following the preliminary testing, one condition and 13 samples were chosen for additional experiments. The chosen condition was DMEM supplemented with 10 % FBS in the apical chamber (A549 side), but without FBS in the basolateral chamber (hCMEC/D3 side). For the apical A549 epithelial cells, several extracts (12A, 14A, 16A, and 72A) induced reduction of cell viability of approximately 69–88% relative to the control, while samples 30A, 61A, 64A, 65A, and 67A showed viabilities ranging from 75–88%. These values represent a measurable, but not severe reduction in mitochondrial activity.

On the basolateral side, hCMEC/D3 cells demonstrated an increase in metabolic activity upon exposure to most extracts (Figures 22A and 22B). Samples 12A, 14A, 16A, and 72A led to viabilities between 107–145%, whereas samples 30A, 61A, 65A, and 67A showed even more pronounced increases, up to approximately 168% of control levels. Interestingly, the positive control EGTA also induced a substantial increase in MTT signal (132–198%), consistent with cellular stress responses leading to metabolic overcompensation or increased mitochondrial activity, which may reflect either an adaptive response or assay interference rather than true proliferation.

A549 epithelial cells, positioned at the direct site of exposure, may be more prone to stress induced mitochondrial impairment, whereas endothelial cells, indirectly exposed via the basolateral compartment, may initially respond with compensatory upregulation of metabolic pathways. Another possibility is that soluble factors released from A549 cells upon exposure trigger a signalling pathway, influencing endothelial cell activity.

This suggests that factors in the extracts may have had indirect or stimulatory effects on brain endothelial metabolism or that serum diffusion from the apical side provided additional nutritional support to the basolateral cells.

Transendothelial/epithelial electrical resistance (TEER) measurements performed before and after 48 h exposure to samples 2, 3, and 4 showed no significant loss of barrier integrity under most tested conditions. TEER values remained low overall, typical for A549-based systems (Barosova et al., 2021), but were stable over 48 h, indicating that acute extract exposure did not disrupt tight junctions to a major extent**.**

Follow-up TEER measurements with the 13 selected extracts further supported this observation: no statistically significant differences were detected between samples and controls, suggesting that, despite measurable cytotoxicity in A549 cells in some conditions**,** the overall epithelial–endothelial barrier remained functionally intact during the 48 h exposure period.

8.2.1 Model limitations and future improvements

Although the combination of A549 and hCMEC/D3 in a Transwell system does not represent a standard or well-established *in vitro* model, this pilot setup provided valuable first insights into barrier behaviour and cellular responses to environmental extracts. Nevertheless, the current system has several important limitations that must be acknowledged and addressed in future work to improve its physiological relevance.

A major drawback of using A549 cells is that they express mainly type II alveolar epithelial cell markers, whereas *in vivo* the alveolar epithelium consists of type I and II cells**.** (Foster *et al.,* 1998) These type I cells play a critical role in maintaining barrier integrity by limiting fluid entry into the alveolar space (Weibel, 2015), a feature that is largely absent in A549 cultures. This structural and functional difference was reflected in the low TEER values measured in the present experiments, confirming that the A549 monolayer formed only

a weak epithelial barrier. (Barosova *et al.,* 2021) As a result, the current model does not fully replicate the tight barrier properties of the human alveolar epithelium.

To bring the model closer to *in vivo* conditions, several improvements should be considered. These include replacing A549 with more physiologically relevant cell types (e.g., primary human alveolar epithelial cells or type I–like cell lines), or creating a co-culture with additional lung cell types.

Introducing basolateral flow or shear stress could help mimic the dynamics of blood flow, as the vascular system of the lung is continuously exposed to shear stress from blood flow (Nossa *et al.*, 2021).

Moreover, the study focused primarily on TER and cell viability as endpoints, which provided only limited information on the underlying mechanisms of toxicity. To capture more subtle effects, future studies could include additional markers such as reactive oxygen species (ROS), inflammatory mediators (e.g., cytokines), or release of extracellular vesicles, which may better reflect early cellular stress responses and barrier modulation. Chemical characterization of the extracts may also help identify which components drive the observed metabolic effects.

Finally, it is also important to critically consider what actually passes through the barrier. The observed signals in the basolateral compartment may not necessarily represent intact particles, but could instead reflect secondary soluble factors released by the lung epithelial layer after exposure. Distinguishing between actual particle translocation and secondary signalling or dissolution effects will be crucial to accurately interpret transport phenomena in such model.

9 Conclusion

This research project investigated the potential health risks posed by environmental particle exposure, focusing on well characterized plastic related substances, the toxicity of 6PPD-quinone and complex airborne materials.

The results from nanoparticle exposure experiments confirmed a clear size- and surface chemistry dependent effect on cell viability. Particularly, carboxylated 50 nm polystyrene particles induced pronounced concentration-dependent reductions in cell viability, with microglial HMC3 cells showing higher sensitivity compared to hCMEC/D3 cells. These findings align with previous reports on the increased reactivity of small, negatively charged nanoplastics and underline the importance of particle characteristics in determining cellular stress responses at the brain's vascular interface.

In the case of 6PPD-quinone exposure, a strong concentration-dependent decrease in cell viability was observed in both hCMEC/D3 and HMC3 cells, with high concentrations leading to substantial cytotoxicity. Interestingly, experiments revealed a reduction in compound permeation at higher concentrations, suggesting saturation.

A major component of this thesis was the pilot testing of indoor dust extracts derived from air filters collected in schools and residential buildings. Thirteen extracts identified during initial screening were examined in an A549/D3 Transwell co-culture model. The MTT assays revealed moderate but consistent reductions in metabolic activity in A549 lung epithelial cells, with viability values typically ranging between 70–90%, while hCMEC/D3 endothelial cells on the basolateral side exhibited increased metabolic activity, in some cases up to 168%. This differential response suggests cell type specific adaptive mechanisms and emphasizes the need to interpret increases in MTT signal carefully, as they may indicate metabolic overcompensation rather than proliferation. Importantly, TER measurements remained stable throughout all exposure conditions, indicating that barrier integrity was not acutely compromised under the applied concentrations and exposure durations.

The pilot lung–neurovascular barrier model proved to be a useful screening tool, but also revealed important limitations. The use of A549 type II alveolar epithelial cells resulted in low baseline TER values, reflecting their limited barrier function compared to primary type I alveolar cells. Future optimization of the model should include more physiologically relevant lung epithelial cell types, the introduction of immune cells, and the addition of flow or shear stress to better mimic *in vivo* conditions. Furthermore, mechanistic endpoints such as oxidative stress, and inflammatory mediator release, should be integrated to provide a more comprehensive picture of biological effects.

In conclusion, the results of this research illustrate how the influence of nanoparticle properties, chemical exposures, and environmental mixtures can shape both cellular responses and barrier integrity. These insights emphasize the need for integrated and complementary *in vitro* approaches to adequately model complex exposure situations.

Bibliography

Abbott, N. J., Rönnbäck, L., & Hansson, E. (2006). Astrocyte–endothelial interactions at the blood–brain barrier. *Nature Reviews Neuroscience*, *7*(1), 41–53. https://doi.org/10.1038/nrn1824

Alvarez-Carbonell, D.; Ye, F.; Ramanath, N.; Dobrowolski, C.; Karn, J. The Glucocorticoid Receptor Is a Critical Regulator of HIV Latency in Human Microglial Cells. *J. Neuroimmune Pharmacol*. 2019, *14*, 94–109.

Appelt-Menzel, A., Cubukova, A., Günther, K., Edenhofer, F., Piontek, J., Krause, G., Stüber, T., Walles, H., Neuhaus, W., & Metzger, M. (2017). Establishment of a Human Blood-Brain Barrier Co-culture Model Mimicking the Neurovascular Unit Using Induced Pluri- and Multipotent Stem Cells. *Stem Cell Reports*, *8*(4), 894–906. https://doi.org/10.1016/j.stemcr.2017.02.021

Armulik A, Genové G, Mäe M, Nisancioglu MH, Wallgard E, Niaudet C, He L, Norlin J, Lindblom P, Strittmatter K, Johansson BR, Betsholtz C. Pericytes regulate the blood-brain barrier. Nature. 2010 Nov 25;468(7323):557-61. doi: 10.1038/nature09522. Epub 2010 Oct 13. PMID: 20944627.

Aves, A. R., Revell, L. E., Gaw, S., Ruffell, H., Schuddeboom, A., Wotherspoon, N. E., LaRue, M., & McDonald, A. J. (2022). *First evidence of microplastics in Antarctic snow*. *The Cryosphere, 16*(6), 2127–2145. https://doi.org/10.5194/tc-16-2127-2022

Bähr O, Rieger J, Duffner F, Meyermann R, Weller M, Wick W. P-glycoprotein and multidrug resistance-associated protein mediate specific patterns of multidrug resistance in malignant glioma cell lines, but not in primary glioma cells. Brain Pathol. 2003 Oct;13(4):482-94. doi: 10.1111/j.1750-3639.2003.tb00479.x. PMID: 14655754; PMCID: PMC8095903.

Banerjee, A., Billey, L. O., & Shelver, W. L. (2021). Uptake and toxicity of polystyrene micro/nanoplastics in gastric cells: Effects of particle size and surface functionalization. *PLOS ONE*, *16*(12), e0260803. https://doi.org/10.1371/journal.pone.0260803

Barron SL, Saez J, Owens RM. *In Vitro* Models for Studying Respiratory Host-Pathogen Interactions. Adv Biol (Weinh). 2021 Jun;5(6):e2000624. doi: 10.1002/adbi.202000624. Epub 2021 May 4. PMID: 33943040; PMCID: PMC8212094.

Barosova, H., Meldrum, K., Karakocak, B. B., Balog, S., Doak, S. H., Petri-Fink, A., Clift, M. J. D., & Rothen-Rutishauser, B. (2021). Inter-laboratory variability of A549 epithelial cells grown under submerged and air-liquid interface conditions. *Toxicology in Vitro*, *75*, 105178. https://doi.org/10.1016/j.tiv.2021.105178

Becker S, Soukup J, Yankaskas JR. Respiratory syncytial virus infection of human primary nasal and bronchial epithelial cell cultures and bronchoalveolar macrophages. Am J Respir Cell Mol Biol. 1992 Apr;6(4):369-74. doi: 10.1165/ajrcmb/6.4.369. PMID: 1550681.

Bergmann, M., Mützel, S., Primpke, S., Tekman, M. B., Trachsel, J., & Gerdts, G. (2019). *White and wonderful? Microplastics prevail in snow from the Alps to the Arctic*. *Science Advances, 5*(8), eaax1157. https://doi.org/10.1126/sciadv.aax1157

Bourne JH, Suthya AR, Wanrooy BJ, Wilson JL, Wen SW, Bastow CR, Zheng G, Rank M, Hickey MJ, Wong CH. Microglia are prominent producers of inflammatory cytokines during the hyperacute phase of ischemic stroke. Commun Biol. 2025 Aug 10;8(1):1193. doi: 10.1038/s42003-025-08636-1. PMID: 40783651; PMCID: PMC12335586.

Bowman PD, Ennis SR, Rarey KE, Betz AL, Goldstein GW. Brain microvessel endothelial cells in tissue culture: a model for study of blood-brain barrier permeability. Ann Neurol. 1983 Oct;14(4):396-402. doi: 10.1002/ana.410140403. PMID: 6638956.

Brachner, A., Fragouli, D., Duarte, I. F., Farias, P. M. A., Dembski, S., Ghosh, M.,Barisic, I., Zdzieblo, D., Vanoirbeek, J., Schwabl, P., & Neuhaus, W. (2020).Assessment of Human Health Risks Posed by Nano-and Microplastics Is Currently Not Feasible. International Journal of Environmental Research and Public Health,17(23), Art. 23. https://doi.org/10.3390/ijerph17238832

Chen, J., Luo, Y., Hui, H., Cai, T., Huang, H., Yang, F., Feng, J., Zhang, J., & Yan, X. (2017). CD146 coordinates brain endothelial cell–pericyte communication for blood–

brain barrier development. *Proceedings of the National Academy of Sciences of the United States of America*, *114*(36), E7622–E7631. https://doi.org/10.1073/pnas.1710848114

Chiok KR, Dahlan NA, Banerjee A, Dhar N. Establishing Air-Liquid Interface (ALI) Airway Culture Models for Infectious Disease Research. Methods Mol Biol. 2024;2813:137-144. doi: 10.1007/978-1-0716-3890-3_10. PMID: 38888776.

Chmielewska, A. (2023). Effects of Polystyrene Nanoparticles on Cells of the Neurovascular Unit. Diploma Thesis, Technische Universität Wien, reposiTUm. https://doi.org/10.34726/hss.2023.101927

Choi KG, Wu BC, Lee AH, Baquir B, Hancock REW. Utilizing Organoid and Air-Liquid Interface Models as a Screening Method in the Development of New Host Defense Peptides. Front Cell Infect Microbiol. 2020 May 20;10:228. doi: 10.3389/fcimb.2020.00228. PMID: 32509598; PMCID: PMC7251080.

Choudhary, D., Kurien, C., & Srivastava, A. K. (2020). *Microplastic contamination and life cycle assessment of bottled drinking water*. In N. Siddiqui, S. Tauseef & R. Dobhal (Eds.), *Advances in Water Pollution Monitoring and Control* (pp. 41–48). Springer Singapore. https://doi.org/10.1007/978-981-32-9956-6_4

Dawson AL, Kawaguchi S, King CK, Townsend KA, King R, Huston WM, Bengtson Nash SM. Turning microplastics into nanoplastics through digestive fragmentation by Antarctic krill. Nat Commun. 2018 Mar 8;9(1):1001. doi: 10.1038/s41467-018-03465-9. PMID: 29520086; PMCID: PMC5843626.

Dello Russo, C., Cappoli, N., Coletta, I., Mezzogori, D., Paciello, F., Pozzoli, G., Navarra,P., Battaglia, A. (2018). The human microglial HMC3 cell line: where do we stand? Asystematic literature review. Neuroinflammation,15(1), 259. https://doi.org/10.1186/s12974-018-1288-0

Dong, C.-D., Chen, C.-W., Chen, Y.-C., Chen, H.-H., Lee, J.-S., & Lin, C.-H. (2020). Polystyrene microplastic particles: *In vitro* pulmonary toxicity assessment. *Journal of Hazardous Materials*, *385*, 121575. https://doi.org/10.1016/j.jhazmat.2019.121575

Du, B., Liang, B., Li, Y., Shen, M., Liu, L.Y., Zeng, L. (2022). *First report on the occurrence of N -(1,3-Dimethylbutyl)- N '-phenyl- p - phenylenediamine (6PPD) and 6PPD-quinone as pervasive pollutants in human urine from South China*. Environmental Science & Technology Letters, 9(12), 1056–1062. https://doi.org/10.1021/acs.estlett.2c00821

Fang, L., Fang, C., Di, S., Yu, Y., Wang, C., Wang, X., Jin, Y. (2023). *Oral exposure to tire rubber-derived contaminant 6PPD and 6PPD-quinone induce hepatotoxicity in mice*. Science of The Total Environment, 869,161836. https://doi.org/10.1016/j.scitotenv.2023.161836 Fang, J., Wang, X., Cao, G., Wang, F., Ru, Y., Wang, B., Zhang, Y., Zhang, D., Yan, J.,

Fernando, A., Shahib, K., Raghu, R., Ganapathy, M. (2023). *The role of the Blood-Brain Barrier in cellular communication: A review*. World Journal of Biology Pharmacy and Health Sciences, 13, 362-381. https://doi.org/10.30574/wjbphs.2023.13.1.0027

Filipe, V., Hawe, A., and Jiskoot, W. (2010). Critical evaluation of Nanoparticle Tracking Analysis (NTA) by NanoSight for the measurement of nanoparticles and protein aggregates. *Pharmaceutical Research*, *27*, 796–810.

Forbes B, Ehrhardt C. Human respiratory epithelial cell culture for drug delivery applications. Eur J Pharm Biopharm. 2005 Jul;60(2):193-205. doi: 10.1016/j.ejpb.2005.02.010. Epub 2005 Apr 21. PMID: 15939233.

Foster KA, Oster CG, Mayer MM, Avery ML, Audus KL. Characterization of the A549 cell line as a type II pulmonary epithelial cell model for drug metabolism. Exp Cell Res. 1998 Sep 15;243(2):359-66. doi: 10.1006/excr.1998.4172. PMID: 9743595.

Franzdóttir SR, Axelsson IT, Arason AJ, Baldursson O, Gudjonsson T, Magnusson MK. Airway branching morphogenesis in three dimensional culture. Respir Res. 2010 Nov 25;11(1):162. doi: 10.1186/1465-9921-11-162. PMID: 21108827; PMCID: PMC3002372.

Fröhlich, E. (2012). The role of surface charge in cellular uptake and cytotoxicity of medical nanoparticles. *International Journal of Nanomedicine*, *7*, 5577–5591. https://doi.org/10.2147/IJN.S36111

Garcia-Mesa, Y.; Jay, T.R.; Checkley, M.A.; Luttge, B.; Dobrowolski, C.; Valadkhan, S.; Landreth, G.E.; Karn, J.; Alvarez-Carbonell, D. Immortalization of Primary Microglia: A New Platform to Study HIV Regulation in the Central Nervous System. *J. Neurovirol.* 2017, *23*, 47–66.

Garcia MM, Romero AS, Merkley SD, Meyer-Hagen JL, Forbes C, Hayek EE, Sciezka DP, Templeton R, Gonzalez-Estrella J, Jin Y, Gu H, Benavidez A, Hunter RP, Lucas S, Herbert G, Kim KJ, Cui JY, Gullapalli R, In JG, Campen MJ, Castillo EF. *In Vivo* Tissue Distribution of Microplastics and Systemic Metabolomic Alterations After Gastrointestinal Exposure. bioRxiv [Preprint]. 2023 Jun 3:2023.06.02.542598. doi: 10.1101/2023.06.02.542598. PMID: 37398080; PMCID: PMC10312509.

Geyer R, Jambeck JR, Law KL. Production, use, and fate of all plastics ever made. Sci Adv. 2017 Jul 19;3(7):e1700782. doi: 10.1126/sciadv.1700782. PMID: 28776036; PMCID: PMC5517107.

Ghasemi, M., Turnbull, T., Sebastian, S., & Kempson, I. (2021). The MTT Assay: Utility, Limitations, Pitfalls, and Interpretation in Bulk and Single-Cell Analysis. *International Journal of Molecular Sciences*, *22*(23), 12827. https://doi.org/10.3390/ijms222312827

Giard DJ, Aaronson SA, Todaro GJ, Arnstein P, Kersey JH, Dosik H, Parks WP. *In vitro* cultivation of human tumors: establishment of cell lines derived from a series of solid tumors. J Natl Cancer Inst. 1973 Nov;51(5):1417-23. doi: 10.1093/jnci/51.5.1417. PMID: 4357758.

Goßmann I, Süßmuth R, Scholz-Böttcher BM. Plastic in the air?! - Spider webs as spatial and temporal mirror for microplastics including tire wear particles in urban air. Sci Total Environ. 2022 Aug 1;832:155008. doi: 10.1016/j.scitotenv.2022.155008. Epub 2022 Apr 2. PMID: 35381237.

Greer, J.B., Dalsky, E.M., Lane, R.F., Hansen, J.D. (2023). *Tire-Derived Transformation Product 6PPD-Quinone Induces Mortality and Transcriptionally Disrupts Vascular Permeability Pathways in Developing Coho Salmon*. Environmental Science & Technology, 1;57(30),10940-10950. https://doi.org/10.1021/acs.est.3c01040

Griffiths, D. , Carr, B., Malloy, A., Smith, J. , Hole, P. , and Bernt, W. ,. (2011). Zeta potential measurement of nanoparticles by nanoparticle tracking analysis (NTA). *NSTI Nanotech*, *1*, 47.

Hassan Kazmi, S.S.U., Xu, Q., Tayyab, M., Pastorino, P., Barcelò ,D., Yaseen, Z.M., Khan, Z.H., Li, G. (2024). *Navigating the environmental dynamics, toxicity to aquatic organisms and human associated risks of an emerging tire wear contaminant 6PPD-quinone*. Environmental Pollution, 356, 124313. https://doi.org/10.1016/j.envpol.2024.124313

Helms, H.C., Abbott, N.J., Burek, M., Cecchelli, R., Couraud, P.O., Deli, M.A., Förster, C., Galla, H.J., Romero, I.A., Shusta, E.V., Stebbins, M.J., Vandenhaute, E., Weksler, B., Brodin, B. (2016). *In vitro models of the blood–brain barrier: An overview of commonly used brain endothelial cell culture models and guidelines for their use*. Journal of Cerebral Blood Flow & Metabolism, 36(5), 862-890. https://doi.org/10.1177/0271678X16630991

Janabi N, Peudenier S, Héron B, Ng KH, Tardieu M. Establishment of human microglial cell lines after transfection of primary cultures of embryonic microglial cells with the SV40 large T antigen. Neurosci Lett. 1995 Aug 4;195(2):105-8. doi: 10.1016/0304-3940(94)11792-h. PMID: 7478261.

Kannan, K., & Vimalkumar, K. (2021). A review of human exposure to microplastics and insights into microplastics as obesogens. *Frontiers in Endocrinology, 12*, 724989. https://doi.org/10.3389/fendo.2021.724989

Kosuth M, Mason SA, Wattenberg EV. Anthropogenic contamination of tap water, beer, and sea salt. PLoS One. 2018 Apr 11;13(4):e0194970. doi: 10.1371/journal.pone.0194970. PMID: 29641556; PMCID: PMC5895013.

Kuehn A, Kletting S, de Souza Carvalho-Wodarz C, Repnik U, Griffiths G, Fischer U, Meese E, Huwer H, Wirth D, May T, Schneider-Daum N, Lehr CM. Human alveolar epithelial cells expressing tight junctions to model the air-blood barrier. ALTEX. 2016;33(3):251-60. doi: 10.14573/altex.1511131. Epub 2016 Mar 17. PMID: 26985677.

Kusch-Poddar M, Drewe J, Fux I, Gutmann H. Evaluation of the immortalized human brain capillary endothelial cell line BB19 as a human cell culture model for the blood-brain barrier. Brain Res. 2005 Dec 7;1064(1-2):21-31. doi: 10.1016/j.brainres.2005.10.014. Epub 2005 Nov 14. PMID: 16289483.

Kühl L, Graichen P, von Daacke N, Mende A, Wygrecka M, Potaczek DP, Miethe S, Garn H. Human Lung Organoids-A Novel Experimental and Precision Medicine Approach. Cells. 2023 Aug 15;12(16):2067. doi: 10.3390/cells12162067. PMID: 37626876; PMCID: PMC10453737.

LeMessurier, K. S., Tiwary, M., Morin, N. P., & Samarasinghe, A. E. (2020). *Respiratory barrier as a safeguard and regulator of defense against influenza A virus and Streptococcus pneumoniae*. *Frontiers in Immunology, 11*, 3. https://doi.org/10.3389/fimmu.2020.00003

Lepiarz, I., Olajide, O. (2019). *The human microglia (HMC-3) as a cellular model of neuroinflammation*. IBRO Reports 6, Supplement, S92. https://doi.org/10.1016/j.ibror.2019.07.299

Leslie, H. A., van Velzen, M. J. M., Brandsma, S. H., Vethaak, A. D., Garcia-Vallejo, J. J., & Lamoree, M. H. (2022). Discovery and quantification of plastic particle pollution in human blood. *Environment International*, *163*, 107199. https://doi.org/10.1016/j.envint.2022.107199

Li, Y., Tao, L., Wang, Q., Wang, F., Li, G., & Song, M. (2023). Potential Health Impact of Microplastics: A Review of Environmental Distribution, Human Exposure, and Toxic Effects. *Environment & Health*, *1*(4), 249–257. https://doi.org/10.1021/envhealth.3c00052

Lieber M, Smith B, Szakal A, Nelson-Rees W, Todaro G. A continuous tumor-cell line from a human lung carcinoma with properties of type II alveolar epithelial cells. Int J Cancer. 1976 Jan 15;17(1):62-70. doi: 10.1002/ijc.2910170110. PMID: 175022.

Liu L, Xu K, Zhang B, Ye Y, Zhang Q, Jiang W. Cellular internalization and release of polystyrene microplastics and nanoplastics. Sci Total Environ. 2021 Jul 20;779:146523. doi: 10.1016/j.scitotenv.2021.146523. Epub 2021 Mar 18. PMID: 34030247.

Maeda T., Sano Y., Abe M., Shimizu F., Kashiwamura Y., Ohtsuki S., et al. (2013). Establishment and characterization of spinal cord microvascular endothelial cell lines. *Clin. Exp. Neuroimmunol.* 4 326–338. 10.1111/cen3.12045

Madorran. E., Stožer, A., Bevc, S., Maver, U. (2020). *In vitro toxicity model: Upgrades to bridge the gap between preclinical and clinical research*. Journal of the Association of Basic Medical Sciences, 20(2), 157-168. https://doi.org/10.17305/bjbms.2019.4378

Malaviya, R., Kipen, H. M., Businaro, R., Laskin, J. D., & Laskin, D. L. (2020). Pulmonary toxicants and fibrosis: Innate and adaptive immune mechanisms. *Toxicology and applied pharmacology*, *409*, 115272. https://doi.org/10.1016/j.taap.2020.115272

Martin TR, Frevert CW. Innate immunity in the lungs. Proc Am Thorac Soc. 2005;2(5):403-11. doi: 10.1513/pats.200508-090JS. PMID: 16322590; PMCID: PMC2713330.

Martin, L. M. A., Gan, N., Wang, E., Merrill, M., & Xu, W. (2022). Materials, surfaces, and interfacial phenomena in nanoplastics toxicology research. Environmental Pollution, 292, 118442. https://doi.org/10.1016/j.envpol.2021.118442

McConnell, H. L., & Mishra, A. (2022). Cells of the Blood-brain Barrier: An Overview of the Neurovascular Unit in Health and Disease. *Methods in molecular biology (Clifton, N.J.)*, *2492*, 3–24. https://doi.org/10.1007/978-1-0716-2289-6_1

Merrington, A. (2017). Recycling of plastics. In *Applied plastics engineering handbook . s.l.:William Andrew Publishing* (pp. 167–189).

Michelini, S., Mawas, S., Kurešepi, E., Barbero, F., Šimunović, K., Miremont, D., Devineau, S., Schicht, M., Ganin, V., Haugen, Ø. P., Afanou, A. K., Izabelle, C., Zienolddiny-Narui, S., Jüngert, K., Repar, N., Fenoglio, I., Šetina Batić, B., Paulsen, F., Mandić-Mulec, I., Boland, S., Erman, A., & Drobne, D. (2025). *Pulmonary hazards of nanoplastic particles: a study using polystyrene in in vitro models of the alveolar and bronchial epithelium*. Journal of Nanobiotechnology, 23, Article 388. https://doi.org/10.1186/s12951-025-03419-6

Miller AJ, Spence JR. *In Vitro* Models to Study Human Lung Development, Disease and Homeostasis. Physiology (Bethesda). 2017 May;32(3):246-260. doi: 10.1152/physiol.00041.2016. PMID: 28404740; PMCID: PMC6148341.

Mosmann, T. (1983). Rapid colorimetric assay for cellular growth and survival: Application to proliferation and cytotoxicity assays. *Journal of Immunological Methods*, *65*(1), 55–63. https://doi.org/10.1016/0022-1759(83)90303-4

Muruganandam A, Herx LM, Monette R, Durkin JP, Stanimirovic DB. Development of immortalized human cerebromicrovascular endothelial cell line as an in vitro model of the human blood-brain barrier. FASEB J. 1997 Nov;11(13):1187-97. doi: 10.1096/fasebj.11.13.9367354. PMID: 9367354.

Nagai A, Nakagawa E, Hatori K, Choi HB, McLarnon JG, Lee MA, Kim SU. Generation and characterization of immortalized human microglial cell lines: expression of cytokines and chemokines. Neurobiol Dis. 2001 Dec;8(6):1057-68. doi: 10.1006/nbdi.2001.0437. PMID: 11741401.

Nakagomi T, Kubo S, Nakano-Doi A, Sakuma R, Lu S, Narita A, Kawahara M, Taguchi A, Matsuyama T. Brain vascular pericytes following ischemia have multipotential stem cell activity to differentiate into neural and vascular lineage cells. Stem Cells. 2015 Jun;33(6):1962-74. doi: 10.1002/stem.1977. Epub 2015 Apr 23. PMID: 25694098.

Napper, I. E., Davies, B. F. R., Clifford, H., Elvin, S., Koldewey, H. J., Mayewski, P. A., Miner, K. R., Potocki, M., Elmore, A. C., Gajurel, A. P., & Thompson, R. C. (2020). *Reaching new heights in plastic pollution—Preliminary findings of microplastics on Mount Everest*. *One Earth, 3*(5), 621–630. https://doi.org/10.1016/j.oneear.2020.10.020

Narantuya D, Nagai A, Sheikh AM, Masuda J, Kobayashi S, et al. (2010) Human Microglia Transplanted in Rat Focal Ischemia Brain Induce Neuroprotection and Behavioral Improvement. PLOS ONE 5(7): e11746. https://doi.org/10.1371/journal.pone.0011746

Nkadi PO, Merritt TA, Pillers DA. An overview of pulmonary surfactant in the neonate: genetics, metabolism, and the role of surfactant in health and disease. Mol Genet

Metab. 2009 Jun;97(2):95-101. doi: 10.1016/j.ymgme.2009.01.015. Epub 2009 Feb 4. PMID: 19299177; PMCID: PMC2880575.

Nossa, R., Costa, J., Cacopardo, L., & Ahluwalia, A. (2021). Breathing *in vitro:* Designs and applications of engineered lung models. *Bioengineering & Translational Medicine, 6*(3), e10200. https://doi.org/10.1002/btm2.10200.

Oliveri Conti G, Ferrante M, Banni M, Favara C, Nicolosi I, Cristaldi A, Fiore M, Zuccarello P. Micro- and nano-plastics in edible fruit and vegetables. The first diet risks assessment for the general population. Environ Res. 2020 Aug;187:109677. doi: 10.1016/j.envres.2020.109677. Epub 2020 May 20. PMID: 32454310.

Poller, B., Gutmann, H., Krähenbühl, S., Weksler, B., Romero, I., Couraud, P.O., Tuffin, G., Drewe, J., Huwyler, J. (2008). *The human brain endothelial cell line hCMEC/D3 as a human blood-brain barrier model for drug transport studies*. Journal of Neurochemistry, 107(5),1358-68. https://doi.org/10.1111/j.1471-4159.2008.05730.x

Porotto M, Ferren M, Chen YW, Siu Y, Makhsous N, Rima B, Briese T, Greninger AL, Snoeck HW, Moscona A. Authentic Modeling of Human Respiratory Virus Infection in Human Pluripotent Stem Cell-Derived Lung Organoids. mBio. 2019 May 7;10(3):e00723-19. doi: 10.1128/mBio.00723-19. PMID: 31064833; PMCID: PMC6509192.

Prata, J. C., da Costa, J. P., Lopes, I., Duarte, A. C., & Rocha-Santos, T. (2020). Environmental exposure to microplastics: An overview on possible human health effects. *Science of The Total Environment*, *702*, 134455. https://doi.org/10.1016/j.scitotenv.2019.134455 Prata JC. Airborne microplastics: Consequences to human health? Environ Pollut. 2018 Mar;234:115-126. doi: 10.1016/j.envpol.2017.11.043. Epub 2017 Dec 21. PMID: 29172041.

Prata JC. Airborne microplastics: Consequences to human health? Environ Pollut. 2018 Mar;234:115-126. doi: 10.1016/j.envpol.2017.11.043. Epub 2017 Dec 21. PMID: 29172041.

Prudhomme JG, Sherman IW, Land KM, Moses AV, Stenglein S, Nelson JA. Studies of Plasmodium falciparum cytoadherence using immortalized human brain capillary endothelial cells. Int J Parasitol. 1996 Jun;26(6):647-55. doi: 10.1016/0020-7519(96)00027-6. PMID: 8875310.

Qi, D., Lin, H., Hu, B., Wei, Y. (2023). *A review on in vitro model of the blood-brain barrier (BBB) based on hCMEC/D3 cells*. Journal of Controlled Release, 358, 78-97. https://doi.org/10.1016/j.jconrel.2023.04.020

Qi, Y., Qiu, A., Wei, X., Huang, Y., Huang, Q., & Huang, W. (2024). Effects of 6PPD-Quinone on Human Liver Cell Lines as Revealed with Cell Viability Assay and Metabolomics Analysis. *Toxics*, *12*(6), 389. https://doi.org/10.3390/toxics12060389

Qi, Y., Wei, S., Xin, T., Huang, C., Pu, Y., Ma, J., Zhang, C., Liu, Y., Lynch, I., & Liu, S. (2022). Passage of exogeneous fine particles from the lung into the brain in humans and animals. *Proceedings of the National Academy of Sciences*, *119*(26), e2117083119. https://doi.org/10.1073/pnas.2117083119

Qian Z, Travanty EA, Oko L, Edeen K, Berglund A, Wang J, Ito Y, Holmes KV, Mason RJ. Innate immune response of human alveolar type II cells infected with severe acute respiratory syndrome-coronavirus. Am J Respir Cell Mol Biol. 2013 Jun;48(6):742-8. doi: 10.1165/rcmb.2012-0339OC. PMID: 23418343; PMCID: PMC3727876.

Reed, C. (2015). Dawn of the Plasticene age. *New Scientist*, *225*(3006), 28–32.

Rellán Álvarez, D., Vázquez Ares, D., Vázquez Brea, C., López, A. F., & Bello Bugallo, P. M. (2023). Sources, sinks and transformations of plastics in our oceans: Review, management strategies and modelling. *Science of the Total Environment, 854*, 158745. https://doi.org/10.1016/j.scitotenv.2022.158745

Rood PM, Calafat J, von dem Borne AE, Gerritsen WR, van der Schoot CE. Immortalisation of human bone marrow endothelial cells: characterisation of new cell lines. Eur J Clin Invest. 2000 Jul;30(7):618-29. doi: 10.1046/j.1365-2362.2000.00672.x. PMID: 10886302.

Samanta, A., & Medintz, I. L. (2016). Nanoparticles and DNA – a powerful and growing functional combination in bionanotechnology. *Nanoscale, 8*(16), 9037–9095. https://doi.org/10.1039/C5NR08465B

Sano Y, Shimizu F, Abe M, Maeda T, Kashiwamura Y, Ohtsuki S, Terasaki T, Obinata M, Kajiwara K, Fujii M, Suzuki M, Kanda T. Establishment of a new conditionally immortalized human brain microvascular endothelial cell line retaining an in vivo blood-brain barrier function. J Cell Physiol. 2010 Nov;225(2):519-28. doi: 10.1002/jcp.22232. PMID: 20458752.

Sato, Y., Falcone-Juengert, J., Tominaga, T., Su, H., Liu, J. (2022). *Remodeling of the Neurovascular Unit Following Cerebral Ischemia and Hemorrhage*. Cells, 11(18),2823. https://doi.org/10.3390/cells11182823

Shruti VC, Pérez-Guevara F, Elizalde-Martínez I, Kutralam-Muniasamy G. First study of its kind on the microplastic contamination of soft drinks, cold tea and energy drinks - Future research and environmental considerations. Sci Total Environ. 2020 Jul 15;726:138580. doi: 10.1016/j.scitotenv.2020.138580. Epub 2020 Apr 14. PMID: 32315857.

SKC Ltd. Leland Legacy Pump. Verfügbar unter: https://www.skcltd.com/products2/air-sampling-pumps/leland-legacy-pump.html (Zugriff: 12. September 2025)

Smith, M. C., Crist, R. M., Clogston, J. D., & McNeil, S. E. (2017). Zeta potential: A case study of cationic, anionic, and neutral liposomes. Analytical and Bioanalytical Chemistry, 409(24), 5779–5787. https://doi.org/10.1007/s00216-017-0527-z

Stins MF, Gilles F, Kim KS. Selective expression of adhesion molecules on human brain microvascular endothelial cells. J Neuroimmunol. 1997 Jun;76(1-2):81-90. doi: 10.1016/s0165-5728(97)00036-2. PMID: 9184636.

Suresh, K., & Shimoda, L. A. (2016). Lung Circulation. *Comprehensive Physiology*, *6*(2), 897–943. https://doi.org/10.1002/cphy.c140049

Tian, Z., Zhao, H., Peter, K.T., Gonzalez, M., Wetzel, J., Wu, C., Hu, X., Prat, J., Mudrock,E., Hettinger, R., Cortina, A.E., Biswas, R.G., Kock, F. V. C., Soong, R., Jenne, A., Du, B.,Hou, F., He, H., Lundeen, R., … Kolodziej, E.P. (2021). *A ubiquitous tire rubber–*

derived chemical induces acute mortality in coho salmon. Science, 371,185-189. DOI:10.1126/science.abd6951

Valavanidis A, Fiotakis K, Vlachogianni T. Airborne particulate matter and human health: toxicological assessment and importance of size and composition of particles for oxidative damage and carcinogenic mechanisms. J Environ Sci Health C Environ Carcinog Ecotoxicol Rev. 2008 Oct-Dec;26(4):339-62. doi: 10.1080/10590500802494538. PMID: 19034792.

Vareille M, Kieninger E, Edwards MR, Regamey N. The airway epithelium: soldier in the fight against respiratory viruses. Clin Microbiol Rev. 2011 Jan;24(1):210-29. doi: 10.1128/CMR.00014-10. PMID: 21233513; PMCID: PMC3021210.

Verma, R., Vinoda, K. S., Papireddy, M., & Gowda, A. N. S. (2016). Toxic Pollutants from Plastic Waste: A Review. *Procedia Environmental Sciences, 35*, 701–708. https://doi.org/10.1016/j.proenv.2016.07.069

Vethaak, A. D., & Legler, J. (2021). Microplastics and human health. *Science*, *371*(6530), 672–674. https://doi.org/10.1126/science.abe5041

Viršek MK, Lovšin MN, Koren Š, Kržan A, Peterlin M. Microplastics as a vector for the transport of the bacterial fish pathogen species Aeromonas salmonicida. Mar Pollut Bull. 2017 Dec 15;125(1-2):301-309. doi: 10.1016/j.marpolbul.2017.08.024. Epub 2017 Sep 7. PMID: 28889914.

Weibel ER. On the tricks alveolar epithelial cells play to make a good lung. Am J Respir Crit Care Med. 2015 Mar 1;191(5):504-13. doi: 10.1164/rccm.201409-1663OE. PMID: 25723823.

Weis, J., Andrews, C. J., & Dyksen, J. E., Ferrara, R. A., Gannon, J. T., Laumbach, R. J.,& Young, L. (2015). Human health impact of microplastics and nanoplastics. *NJDEP-Science Advisory Board*.

Weksler BB, Subileau EA, Perrière N, Charneau P, Holloway K, Leveque M, Tricoire-Leignel H, Nicotra A, Bourdoulous S, Turowski P, Male DK, Roux F, Greenwood J, Romero IA, Couraud PO. Blood-brain barrier-specific properties of a human adult brain

endothelial cell line. FASEB J. 2005 Nov;19(13):1872-4. doi: 10.1096/fj.04-3458fje. Epub 2005 Sep 1. PMID: 16141364.

Weksler, B., Romero, I.A., Couraud, P.O. (2013). *The hCMEC/D3 cell line as a model of the human blood brain barrier*. Fluids Barriers CNS,10(1),16. https://doi.org/10.1186/2045-8118-10-16

Wright, S. L., & Kelly, F. J. (2017). Plastic and Human Health: A Micro Issue? *Environmental Science & Technology*, *51*(12), 6634–6647. https://doi.org/10.1021/acs.est.7b00423

Wright, S. L., Thompson, R. C., & Galloway, T. S. (2013). The physical impacts of microplastics on marine organisms: A review. *Environmental Pollution*, *178*, 483–492. https://doi.org/10.1016/j.envpol.2013.02.031

Wright, S. L., Ulke, J., Font, A., Chan, K. L. A., & Kelly, F. J. (2020). Atmospheric microplastic deposition in an urban environment and an evaluation of transport. *Environment International*, *136*, 105411. https://doi.org/10.1016/j.envint.2019.105411

Wu, P., Lin, S., Cao, G., Wu, J., Jin, H., Wang, C., Wong, M. H., Yang, Z., & Cai, Z. (2022). Absorption, distribution, metabolism, excretion and toxicity of microplastics in the human body and health implications. *Journal of Hazardous Materials*, *437*, 129361. https://doi.org/10.1016/j.jhazmat.2022.129361

Wu W, Booth JL, Duggan ES, Wu S, Patel KB, Coggeshall KM, Metcalf JP. Innate immune response to H3N2 and H1N1 influenza virus infection in a human lung organ culture model. Virology. 2010 Jan 20;396(2):178-88. doi: 10.1016/j.virol.2009.10.016. Epub 2009 Nov 12. PMID: 19913271; PMCID: PMC2789846.

Xia, K., Qin, M., Han, M., Zhang, X., Wu, X., Liu, M., Liu, S., Wang, X., Liu, W., Xie, Z., Yuan, R., & Liu, Q. (2025). *Elucidating the size distribution of p-Phenylenediamine-Derived quinones in atmospheric particles*. *Environmental International, 197*, 109329. https://doi.org/10.1016/j.envint.2025.109329

Xu, M., Cao, F., & Zhang, K. (2019). A preliminary study of effects of nanoplastic particles on human lung epithelial cells. *Science of the Total Environment*, *693*, 133581. https://doi.org/10.1016/j.scitotenv.2019.133581

Xu, J., Ji, J., Ji, F., Zhou, Y., Guo, L., Li, M., Liu, W., Cai, X., Cai, Z. (2024). *6PPD-quinone exposure induces neuronal mitochondrial dysfunction to exacerbate Lewy neurites formation induced by α-synuclein preformed fibrils seeding*. Journal of Hazardous Materials, 465, 133312. https://doi.org/10.1016/j.jhazmat.2023.133312

Yi, J., Ruan, J., Yu, H., Liu, Y., & Zhang, Z. (2025). *Environmental fate, toxicity, and mitigation of 6PPD and 6PPD-Quinone: Current understanding and future directions*. *Science of the Total Environment*. https://doi.org/10.1016/j.scitotenv.2025.xxx

Yu H, Zhang W, Wang D, Shi B, Zhu Y, Hu W, He J, Hong J, Xu X, Zheng X, Chen W, Wang F, Qu F. Exposure to 6PPD-Q induces dysfunctions of ovarian granulosa cells: Its potential role in PCOS. J Hazard Mater. 2025 Mar 15;486:137037. doi: 10.1016/j.jhazmat.2024.137037. Epub 2024 Dec 31. PMID: 39764971.

Zhu, J.; Guo, R.; Jiang, S.; Wu, P.; Jin, H. Occurrence of p-phenylenediamine antioxidants (ppds) and ppds-derived quinones in indoor dust. *Sci. Total Environ.* 2024, *912*, 169325. doi: 10.1016/j.scitotenv.2023.169325. Epub 2023 Dec 14. PMID: 38101633

List of Figures

Figure 1: Schematic representation of BBB's cellular structures. Figure made using Biorender, 2026. 1

Figure 2: Laminar flow cabinet used for UV radiation of nanoplastic. 28

Figure 3: Serial dilution – concentrations of nanoparticles (adapted from Chmielewska, 2023. 28

Figure 4: Sampling setup: SKC Leland Legacy pump with PEM sampler (PM 2.5, quartz filter) enclosed in a sound-insulated box. Picture provided to us. (https://inchildhealth.eu/, access: 08.January 2026) 37

Figure 5: Schematic representation of the Transwell co-culture system. 41

Figure 6: Polystyrene Nanoplastic, fluorescence measurement before UV sterilization was done at 620/640/800 nm with TECAN 51

Figure 7: Polystyrene Nanoplastic, fluorescence measurement after UV sterilization was done at 620/640/800 nm with TECAN 52

Figure 8: Effects of a 24h-treatment with 6ppd-Q on viability of hCMEC/D3 cells grown in EBM-2 medium at 37°C, 5% CO_2, 95% air atmosphere, 95% humidity, determined by MTT assay.. 53

Figure 9: Effects of a 24 h-treatment with 6ppd-Q on viability of HMC3 cells grown in EMEM 5+ medium at 37°C, 5% CO_2, 95% air atmosphere, 95% humidity, determined by MTT assay. 54

Figure 10: Effects of a 48h-treatment with stained carboxylated 50nm nanoplastics on viability of hCMEC/D3 cells grown in EBM-2 medium at 37°C, 5% CO_2, 95% air atmosphere, 95% humidity, determined by MTT assay.. 56

Figure 11: Effects of a 48h-treatment with stained pristine 100nm nanoplastics on viability of hCMEC/D3 cells grown in EBM-2 medium at 37°C, 5% CO_2, 95% air atmosphere, 95% humidity, determined by MTT assay.. 56

Figure 12: Effects of a 48h-treatment with stained aminated 100nm nanoplastics on viability of hCMEC/D3 cells grown in EBM-2 medium at 37°C, 5% CO_2, 95% air atmosphere, 95% humidity, determined by MTT assay. 57

Figure 13: Effects of a 48h-treatment with unstained Polystyrene 100nm nanoplastic on viability of HMC3 cells grown in EMEM 5+ medium at 37°C, 5% CO_2, 95% air atmosphere, 95% humidity, determined by MTT assay. 58

Figure 14: Effects of a 47h-treatment with unstained polystyrene pristine 50nm nanoplastic on viability of HMC3 cells grown in EMEM 5+ medium at 37°C, 5% CO_2, 95% air atmosphere, 95% humidity, determined by MTT assay. 59

Figure 15: Effects of a 48 h-treatment with unstained Polystyrene carboxylated 100nm nanoplastic on viability of HMC3 cells grown in EMEM 5+ medium at 37°C, 5% CO_2, 95% air atmosphere, 95% humidity, determined by MTT assay. 60

Figure 16: Effects of a 48 h-treatment with unstained Polystyrene carboxylated 50nm nanoplastic on viability of HMC3 cells grown in EMEM 5+ medium at 37°C, 5% CO_2, 95% air atmosphere, 95% humidity, determined by MTT assay.. 61

Figure 17: Effects of a 48h-treatment with unstained aminated 100nm nanoplastics on viability of HMC3 cells grown in EMEM 5+ medium at 37°C, 5% CO_2, 95% air atmosphere, 95% humidity, determined by MTT assay.. 62

Figure 18: Effects of a 48h-treatment with unstained Aminated 50nm nanoplastic on viability of HMC3 cells grown in EMEM 5+ medium at 37°C, 5% CO_2, 95% air atmosphere, 95% humidity, determined by MTT assay.. 63

Figure 19: Summary of the cell viability data of A549 cells after exposure to samples collected from schools and houses during winter.. 64

Figure 20: Summary of the cell viability data of A549 cells after exposure to samples collected from schools and houses during summer.. 64

Figure 21: Cell viability of A549 cells after exposure to filter extracts (2A, 3A, 4A) compared to extraction buffer control (EB), determined by MTT assay..... 71

Figure 22: Cell viability of D3 cells after exposure to filter extracts (2A, 3A, 4A) compared to extraction buffer control (EB), determined by MTT assay. 72

Figure 23: Cell viability of A549 cells after exposure to filter extracts compared to extraction buffer control (EB), determined by MTT assay.. 73

Figure 24 : Cell viability of hCMEC/D3 cells after exposure to filter extracts compared to extraction buffer control (EB), determined by MTT assay.. 74

List of Tables

Table 1. Most common *in vitro* BBB models 4

Table 2. Most common *in vitro* respiratory models 9

Table 3. Polystyrene Nanoparticles 19

Table 4. Devices..... 20

Table 5. Consumables..... 21

Table 6. Chemicals 22

Table 7. Sampling overview 40

Table 8. Summary of the cell viability data of A549 cells after exposure to samples collected from schools and houses during winter and summer. 65

Table 9. NTA Data for filtered indoor particles from Spain.. 66

Table 10. Results of transepithelial electrical resistance (TER) measurement in a Transwell model with A549 in the apical compartment and hCMEC/D3 in the basolateral compartment..... 75

Table 11. Results of transepithelial electrical resistance (TER) measurement in a Transwell model with A549 in the apical compartment and hCMEC/D3 in the basolateral compartment..... 76

Abbreviations list

AIT	Austrian Institute of Technology
ANOVA	Analysis Of Variance
BBB	Blood-Brain Barrier
BDNF	Brain-Derived Neurotrophic Factor
CNS	Central Nervous System
DMEM	Dulbecco's Modified Eagle Medium
DMSO	Dimethyl Sulfoxide
DNA	Deoxyribonucleic Acid
DPBS	Dulbeco’s Phosphate Buffered Salt solution
EBM-2	Endothelial Cell Basal Medium-2
EDTA	Ethylenediaminetetraacetic acid
EMEM	Eagle’s Minimal Essential Medium
FBS	Fetal Bovine Serum
GP	GraphPad Prism
hbFGF	Human Basic Fibroblast Growth Factor
HMC3	Human Microglial Cells
hCMEC/D3	human Cerebral Microvascular Endothelial Cell Line / D3
A549	adenocarcinomic human alveolar basal epithelial cells
IL-21	Interleukin 21
MEM NEAA	Minimum Essential Medium Non Essential Amino Acids
HEPES	4-(2-hydroxyethyl)-1-piperazineethanesulfonic acid
MTT	3-(4, 5-dimethylthiazolyl-2)-2, 5-diphenyltetrazolium bromide
NF-κB	Nuclear factor kappa-light-chain-enhancer of activated B cells
NTA	Nanoparticle Tracking Analyzer
PS	Polystyrene
NP	Nanoplastics
ROS	Reactive Oxygen Species
SD	Standard Deviation
TEER	Transendothelial Electrical Resistance

VL	VascuLife
6ppd	N-(1,3-dimethylbutyl)-N'-phenyl-p-phenylenediamin